Robust Helicopter Control using Structured H_∞-based Multi-Objective Design

Application to Hingeless Rotorcraft

MSc Thesis

Tommaso Capra

Delft University of Technology

TU Delft

Robust Helicopter Control using Structured H_∞-based Multi-Objective Design

Application to Hingeless Rotorcraft

by

Tommaso Capra

Supervisor:	M. Pavel & S. Theodoulis
Project Duration:	February, 2023 - June, 2024
Faculty:	Faculty of Aerospace Engineering, Delft

Cover: AS350BA Squirrel (https://helicoptersphoto.blogspot.com/2011_09_20_archive.html)

TU Delft

Preface

At the start of my journey i knew nothing of robust control theory and helicopter dynamics. This thesis was a challenge as i learned about the robust control and helicopter dynamics discipline, improving my understanding on the subject as i went through my thesis. Completing this thesis marks the final step in finalizing my studies at the TU Delft and obtaining the degree of Master of Science in Aerospace Engineering. I look back with great pleasure at the time I spent here in Delft, where I have learned more than I could have ever expected both in this thesis and my studies. I am proud that I will be among the first students in recent years to graduate in this subject with the guidance of my supervisor Spilios Theodoulis and Marilena Pavel. This thesis lasted a little over a year at the Delft University of Technology in which i am confident more groundbreaking researches will succeed mine.

I would like to express my sincere gratitude to not only my supervisors, for masterfully guiding me through this complicated branch of control theory and helicopter control. I also would also like to thank Fedrik, Yair, Daam, and Chari, my student peers, whom supported me through out this project. Lastly, I would like to express gratitude to my family and friends as well for their emotional support and encouragement.

Thank you so much for your interest in my thesis and I hope it can inspire you to do more research on on robust control of helicopters with applications in a verity of other VTOL vehicles, because it is still an active and challenging area of research as you will soon see.

T. Capra
Delft, July 2024

Contents

Nomenclature

Abbreviations

Abbreviation	Definition
ACAH	Attitude Command Attitude Hold
AoA	Angle of Attack
CAS	Control Augmentation System
CG	Center of Gravity
DoF	Degrees of Freedom
DGM	Disk Gain Margin
HQ	Handling Qualities
I/O	input/output
MBB	Messerschmitt Bölkow Blohm
MIMO	Multiple Inputs Multiple Outputs
LOES	Lower Order Equivalent System
LMI	Linear Matrix inequality
LSPD	Loop Shaping Design Procedure
LTR	Loop Transfer Recovery
LQ	Linear Quadratic
LQR	Linear Quadratic Regulator
MTE	Mission Task Element
PI	Proportional-Integral
PIO	Pilot Induced Oscillation
RHP	Righ Hand Plane
RPM	Revolutions Per Minute
SCAS	Stability and Control Augmentation System
SSV	Structured Singular Value
SVD	Singular Value Decomposition

Symbols

Symbol	Definition	Unit
A, B, C	state-space matrices	-
a_1	longitudinal rotor flapping coefficient	-
C_D	drag coefficient	-
C_{l_α}	blade lift curve slope	-
C_T	trust coefficient	-
c	equivalent blade chord	m
DRP	disturbance rejection peak	-
DRB	disturbance rejection bandwidth	rad/s
d_i, d_o	disturbance input/output vector	-
e	model following error signal	-
F_0	Parasite drag area	m^2
F_x	body longitudinal X component of the resultant force acting on the vehicle	N
F_z	body normal Z component of the resultant force acting on the vehicle	N

Symbol	Definition	Unit
G	helicopter model	-
g	gravitational constant	-
$H_{x,y}$	hard constraint performance with index x, y	-
h	altitude	m
I_b	blade moment of inertia about flapping hinge	$kg \cdot m^2$
I_{yy}	pitch moment of interia	$kg \cdot m^2$
K	control system functions	-
L	open-loop transfer function	-
L, M	real matrices characterising complex regions	-
M, Δ	nominal and uncertain model	-
$M_u, M_w, etc.$	moment derivatives normalized by moments of inertia	-
M_y	body lateral M component of the resultant moment acting on the vehicle	$N \cdot m$
m	mass	kg
N	number of blades	-
n	measurement noise vector	-
q	body rotational pitch rate	rad/s
R	Rotor radius	m
S_i, S_o	input/output sensitivity function	-
$S_{x,y}$	soft constraint performance with index x, y	-
T_{ref}	reference model	-
T_i, T_o	input/output complementary sensitivity function	-
T_{ref}	reference model	-
$T_{x \to y}$	transfer function from x to y	-
u	input vector	-
u, w	longitudinal, normal velocities in the body frame	m/s
V	helicopter velocity	m/s
V_z	helicopter vertical velocity in the earth frame	m/s
W	weighting filter	-
X_{CG}	longitudinal center of gravity position	m
$X_u, X_w, etc.$	X force derivatives normalized by helicopter mass	-
y	measured output vector	-
Z_{CG}	vertical center of gravity position	m
$Z_u, Z_w, etc.$	Z force derivatives normalized by helicopter mass	
α	angle of attack	deg
α_c	angle of attack of the rotor disk	deg
α_{max}	size of disk margin	deg
γ	flight path angle	deg
$\gamma_{min}, \gamma_{max}$	minimum and maximum gain margins	deg
γ_l	lock number	-
ρ	air density	kg/m^3
ζ	damping ratio	-
σ	rotor solidity	-
σ	skew of the disk margin	-
$\sigma_\theta, \sigma_{V_z}$	singular value decomposition for each respective output	-
$\underline{\sigma}, \overline{\sigma}$	minimum and maximum singular values	-
τ	time constant	s
ϕ_m	phase margin	deg
$\delta_{col}, \delta_{lon}$	helicopter inputs: collective and longitudinal cyclic	deg
$\delta_{col,cmd}, \delta_{lon,cmd}$	actuator inputs: commanded collective and longitudinal cyclic	deg
θ	helicopter attitude pitch	deg

Symbol	Definition	Unit
λ	non-dimentional inflow ratio	-
$\hat{\mu}$	advance ratio	-
μ, k_m	structured singular value	-
Ω	rotor rotational speed	rad/s
ω	frequency	rad/s
ω_c	low-pass frequency	rad/s
ω_n	natural frequency	rad/s

List of Figures

List of Tables

1 Introduction

1.1. Context & Overview

The development of rotorcraft has been a long and challenging process involving simulation, analysis, and design iterations. Control systems and handling qualities have required significant attention from both designers and pilots. Due to the dynamic instability of rotorcraft during flight, artificial stability augmentation or a full authority flight control system is necessary to meet stability and handling requirements. Developments such as fly-by-wire and electronic stabilization systems have improved rotorcraft handling qualities. Several techniques have been investigated to address the controllability issues surrounding rotorcraft (Hu & Gu, 2017).

Enhancing rotorcraft handling qualities (HQ) for desirable characteristics in the time/frequency domain is specified in guidelines such as ADS-33E-PRF (Anon, 2000) and stability characteristics in the MIL documents (Anon, 2008). However, complex flow phenomena generated by rotor blades can significantly affect helicopter dynamics, such as irregular flows from vortex interaction and downwash caused by the main rotor on the tail surface (Du Val & He, 2018). The uncertainty in these unstable dynamics, particularly for agile helicopters, makes the development of flight control laws a serious technical challenge, limiting control system design solutions in terms of both handling quality performance and robustness against uncertainties.

In essence, there are many robust control methods that can account for system uncertainties by incorporating their worst-case conditions in the design phase, aiming to design a control system that remains stable with adequate stability margins and meets performance objectives (Balas, 2003). The implementation of robust control for rotorcraft vehicles varies across studies in methodology, using multivariable robust control theories such as LQG/LTR, H_∞, H_2, etc., for control law tuning in (Gribble, 1993; Kumar et al., 2008; Prempain & Postlethwaite, 2005; Silva et al., 2020; Tijani et al., 2011), which are industry standards (Balas, 2003). Which is due to the advantages these methods give, to perform trade-offs between performance, stability and robustness through the optimisation of weighted signal/transfer function norms. Recent studies have developed techniques aimed at either integrating handling requirements (Antonioli et al., 2014; Dai et al., 2014; Srinathkumar, 2015) or accounting for model uncertainty (Ji & Wu, 2011; Tijani et al., 2011) in control design for helicopter models. The most recent method accomplishing both (Authié, 2023; Biannic et al., 2017) using a 2-step optimization approach optimising model following structure and control attenuation in which the controller is robustified using a multi-model approach. Recent advances in non-smooth optimization techniques, where the non-convexity issue has been resolved and incorporated in MATLAB functions *systune()* and *hinfstruct()*, allow for multi-modal/multi-objective control design (Apkarian & Noll, 2006). By leveraging multivariable robust control theory through signal-based optimization, it is possible to achieve lower-order and simpler fixed-structure controllers optimized with multiple objectives for both HQ criteria and robustness against uncertainty, often approaching the robustness of unstructured/full-order controllers. However, controller order reduction often leads to a loss of robustness without specialized order reduction techniques, as demonstrated in (Bates & Postlethwaite, 2002; Dehkordi & Boulet, 2011; P. Apkarian, 2017; Skogestad & Postlethwaite, 2005).

1.2. Report Structure

This thesis is organized as follows. In chapter 2 shows the scientific article of the thesis in AIAA format. In chapter 3 shows the already marked bibliographic survey. In chapter 4 introduces the longitudinal helicopter model. In chapter 5 details the closed-loop controller architectures and design methodology, describing the objectives implemented with analysis of the performance of the resulting design in both the time and frequency domains. In chapter 6 looks at the robustness of the designed controller. The conclusions are presented in chapter 7.

2

Scientific Article

Multi-Objective Design of a Decentralized Structured H_∞-based Controller for Longitudinal Helicopter Flight Dynamics

T. Capra *, S. Theodoulis †,M.D. Pavel‡
Delft University of Technology, P.O Box 5058, 2600GB Delft, The Netherlands

This paper introduces a multi-objective design approach for an Attitude Command-Attitude Hold (ACAH) and vertical velocity flight control system for the MBB Bo-105 helicopter longitudinal model. The design employs a decentralized structured H_∞ dynamic controller using a PI-based and feed-forward control architecture, similar to the PID-based architecture commonly used in rotorcraft flight control design. The proposed design methodology integrates multi-objective approaches within the framework of structured H_∞ control design. The uncertain model verifies the controller's performance under different flight configurations for a helicopter at 40 kts, using μ-analysis which assesses robustness against model uncertainties. The multi-objective approach is employed in the control design process to tune parameters that balance handling qualities with robustness and stability. The performance of the resulting flight control system is investigated and evaluated against the required closed-loop time/frequency-domain criteria, as defined by ADS-33. The resulting design achieves Level 1 handling qualities, for which the advantages and limitations of the proposed methodology are discussed.

I. Nomenclature

A, B, C	=	state-space matrices
d_i, d_o	=	disturbance input/output vector
e	=	model following error signal
F_x	=	body longitudinal X component of the resultant force acting on the vehicle
F_z	=	body normal Z component of the resultant force acting on the vehicle
G	=	helicopter model
$H_{x,y}$	=	hard constraint performance with index x, y
I_{yy}	=	pitch moment of interia
K	=	control system functions
L, M	=	real matrices characterising complex regions
m	=	mass
$M_u, M_w, etc.$	=	moment derivatives normalized by moments of inertia
M_y	=	body lateral M component of the resultant moment acting on the vehicle
n	=	measurement noise vector
q	=	body rotational pitch rate
S_i, S_o	=	input/output sensitivity function
$S_{x,y}$	=	soft constraint performance with index x, y
T_i, T_o	=	input/output complementary sensitivity function
T_{ref}	=	reference model
$T_{x\rightarrow y}$	=	transfer function from x to y
u	=	input vector
V_z	=	helicopter body vertical velocity
W	=	weighting filter
X_{CG}	=	longitudinal center of gravity position
$X_u, X_w, etc.$	=	X force derivatives normalized by helicopter mass

*M.Sc., Faculty of Aerospace Engineering, Control and Simulation Division, Delft University of Technology
†Assoc. Professor, Faculty of Aerospace Engineering, Control and Simulation Division, Delft University of Technology, AIAA Assoc. Fellow
‡Assoc. Professor, Faculty of Aerospace Engineering, Control and Simulation Division, Delft University of Technology

y	=	measured output vector
Z_{CG}	=	vertical center of gravity position
$Z_u, Z_w, etc.$	=	Z force derivatives normalized by helicopter mass
ζ	=	damping ratio
$\delta_{col}, \delta_{lon}$	=	helicopter inputs: collective and longitudinal cyclic
$\delta_{col,cmd}, \delta_{lon,cmd}$	=	actuator inputs: commanded collective and longitudinal cyclic
θ	=	helicopter attitude pitch
ω_n	=	natural frequency

II. Introduction

The development of rotorcraft has been a long and challenging process involving simulation, analysis, and design iterations. Control systems and handling qualities have required significant attention from both designers and pilots. Due to the dynamic instability of rotorcraft during flight, artificial stability augmentation or a full authority flight control system is necessary to meet stability and handling requirements. Developments such as fly-by-wire and electronic stabilization systems have improved rotorcraft handling qualities. Several techniques have been investigated to address the controllability issues surrounding rotorcraft [1].

Enhancing rotorcraft handling qualities (HQ) for desirable characteristics in the time/frequency domain is specified in guidelines such as ADS-33E-PRF [2] and stability characteristics in the MIL documents [3]. However, complex flow phenomena generated by rotor blades can significantly affect helicopter dynamics, such as irregular flows from vortex interaction and downwash caused by the main rotor on the tail surface [4]. The uncertainty in these unstable dynamics, particularly for agile helicopters, makes the development of flight control laws a serious technical challenge, limiting control system design solutions in terms of both handling quality performance and robustness against uncertainties.

In essence, there are many robust control methods that can account for system uncertainties by incorporating their worst-case conditions in the design phase, aiming to design a control system that remains stable with adequate stability margins and meets performance objectives [5]. The implementation of robust control for rotorcraft vehicles varies across studies in methodology, using multivariable robust control theories such as LQG/LTR, H_∞, H_2, etc., for control law tuning in [6–10], which are industry standards [5]. Which is due to the advantages these methods give, to perform trade-offs between performance, stability and robustness through the optimisation of weighted signal/transfer function norms. Recent studies have developed techniques aimed at either integrating handling requirements [11–13] or accounting for model uncertainty [8, 14] in control design for helicopter models. The most recent method accomplishing both [15, 16] using a 2-step optimization approach optimising model following structure and control attenuation in which the controller is robustified using a multi-model approach. Recent advances in non-smooth optimization techniques, where the non-convexity issue has been resolved and incorporated in MATLAB functions *systune()* and *hinfstruct()*, allow for multi-modal/multi-objective control design [17]. By leveraging multivariable robust control theory through signal-based optimization, it is possible to achieve lower-order and simpler fixed-structure controllers optimized with multiple objectives for both HQ criteria and robustness against uncertainty, often approaching the robustness of unstructured/full-order controllers. However, controller order reduction often leads to a loss of robustness without specialized order reduction techniques, as demonstrated in [18–21].

In this paper, an Attitude Command-Attitude Hold (ACAH) and vertical velocity flight control system for the MBB Bo-105 helicopter. The paper will concentrate only on the longitudinal model was developed based on a multi-objective approach using closed-loop transfer functions to design for robustness [18, 22]. In which, reference models are used in model following methods to enforce HQ objectives, that acts as a trade-off between performance and robustness. The helicopter model utilises the bare-frame dynamics of the Bo-105 helicopter, which entails steady-state longitudinal flapping and one-dimensional inflow dynamics with actuators. The control structure used is decentralized Proportional-Integral-like (PI-like) control with a feedforward control element. This structure combines feedback control for stability and robustness against model uncertainties with feedforward control to achieve the necessary HQ objectives. Additional design objectives were established in the form of H_∞ constraints between the reference models and the actual system response, minimum disk-based stability margins, and minimization of disturbances at the input/output (I/O) to the control signal and measured output of the plant. The controller addresses flight speeds around 40 knots at sea level altitude. This approach uses robust control theory for the H_∞ constraints combined with structured singular value (SSV) analysis to assess the robustness of the design against parametric uncertainties.

This paper is organized as follows. Section III introduces the helicopter model. Section IV details the closed-loop controller architectures and design methodology, describing the objectives implemented. Section V looks at the results and analysis of the performance of the resulting design in both the time and frequency domains. The conclusions are presented in Section VII.

III. Bo105 Helicopter Model

The MBB Bo-105 longitudinal helicopter was selected due to its well-known dynamic instability, which poses challenges and limitations to robustness in the design of control laws. An analysis of the Bo-105 bare airframe dynamics [13, 23] shows that an unstable phugoid mode is present across the flight envelope. Additionally, there are local right-half-plane (RHP) zeros in the collective control channel (δ_{col}), with the presence of a global zero near the marginal stability plane at -0.015 in all of the channels when linearizing, as shown in Fig. (1). This figure shows phugoid poles in the RHP at $0.1 \pm 0.29i$, as well as the heave and pitch subsidence in the stable left-half-plane at -0.43 and -1.1, respectively. The existence of these zeros and RHP poles introduces fundamental limitations on the level of performance and robustness that can be realized in the control system's design.

The helicopter dynamics are represented in the design process by a linear time-invariant model using the standard form, which is given by Eq. (1). Here, x is the state vector and $u = [\delta_{col}\ \delta_{lon}]^T$ is the control input. The vector u comprises the collective and longitudinal inputs, in that order. A, B, and C are the stability, control, and output matrices, respectively. The measurement vector y comprises the measurements of the attitude angle θ, body-axis angular velocity q and the vertical velocity V_z. The model used is an analytical model based on [24–26], which is reduced to only the longitudinal mode. These matrices represent the 3 degrees of freedom (DoF) rigid-body dynamics (u,w,q) of the helicopter without the horizontal tail forces. The quasi-steady inflow of the main rotor is represented by a first-order model whose time constant is set to 0.1 s. This augmentation leads to a simplified 5th-order non-linear longitudinal helicopter model, which includes inflow dynamics to trim the thrust coefficient and steady-state longitudinal flapping. This model is solved for the operating equilibrium point ($\dot{x} = f(x,u) = 0$) for straight and steady horizontal flight. Linearizing the model at these points provides the state-space matrices A, B and C in Eq. (1), assuming the non-dimensional inflow remains constant. Finally, a second-order actuator dynamics model of the Bo-105 helicopter ($\omega_n = 50\,\text{rad/s}, \zeta = 0.95$) described in [27] is augmented in each of the collective and longitudinal control channels.

$$G_{AF}: \quad \dot{x} = Ax + Bu \quad y = Cx \tag{1}$$

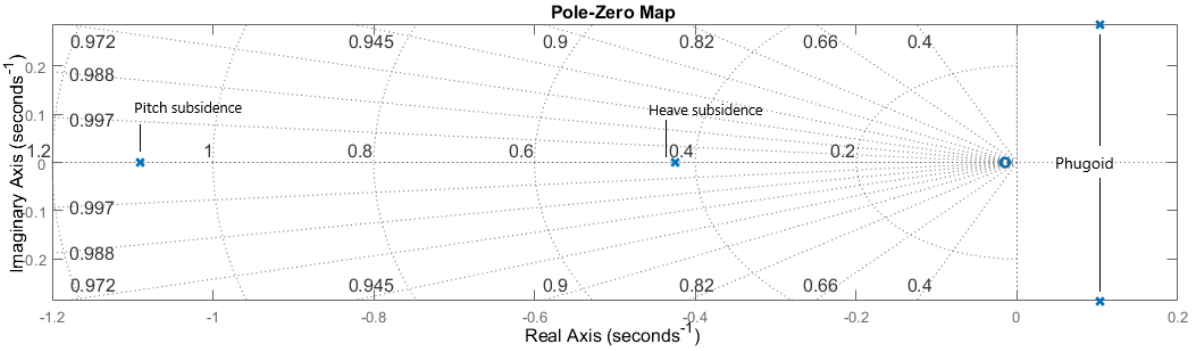

Fig. 1 Open-loop pole-zero plot of longitudinal bare-frame helicopter model at 40 kts

IV. Flight Control Design

A. Design Layout

The transfer function I/O relationships used for decentralized control design are shown in Fig. (2). The actuator model G_{act} consists of second-order transfer functions with $\omega_n = 50\,\text{rad/s}$ and $\zeta = 0.95$, applied to both input channels [27]. The two-degrees-of-freedom controller has two outputs and five inputs, since it includes both the reference and the measured signals of the controlled variables: vertical velocity, pitch rate, and pitch, respectively V_z^K, q^K, θ^K. The external signals are the disturbances at the input d_i composed of $d_{\delta_{col,cmd}}, d_{\delta_{lon,cmd}}$ and at the output d_o composed of d_{V_z}, d_q, d_θ as well as the sensor noise n composed of n_{V_z}, n_q, n_θ. Other signals involved in the controller design are the reference tracking signals $V_{z_{ref}}$ and θ_{ref}, the disturbed outputs y, composed of the measurements for V_z, q, θ and the actuator inputs, which are the commanded inputs u composed of $\delta_{col,cmd}, \delta_{lon,cmd}$ as the controller outputs.

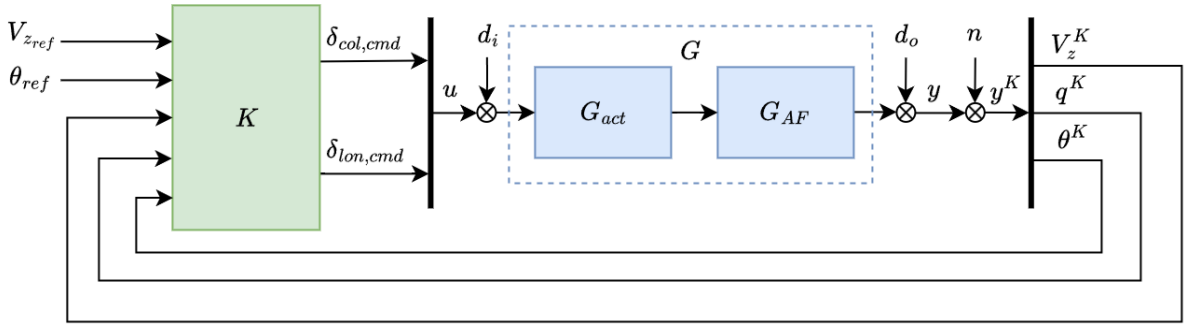

Fig. 2 Longitudinal helicopter controller I/O layout

B. Control Layout

The autopilot structure used here is decentralized as shown Fig. (3). This structure, consist of three key components. Firstly, the feed-forward injection K_{inj} using a second-order transfer functions to adjust the input signal u based on the reference signals $V_{z_{ref}}$ and θ_{ref}. The structure of K_{inj,V_z} and $K_{inj,\theta}$ is as follows:

$$K_{inj}(s) = \frac{z_1 s + z_0}{s^2 + p_1 s + p_0} \tag{2}$$

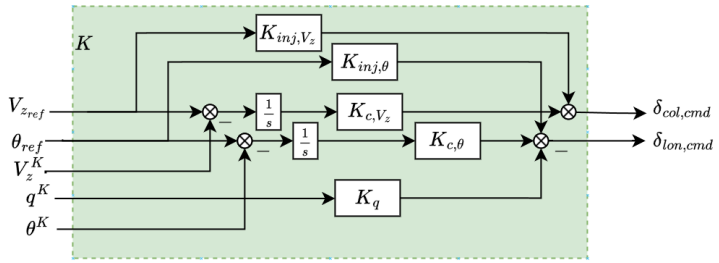

Fig. 3 Longitudinal helicopter control structure

The second components are the first-order transfer functions K_c, which act as a PI-like controllers though the integrator with a low-pass filter with frequency of ω_c. This is used for tracking the reference signals $V_{z_{ref}}$ and θ_{ref} in the autopilot loop. The structure of K_{c,V_z} and $K_{c,\theta}$ is as follows:

$$\frac{K_c(s)}{s} = \frac{K_p s + K_i}{s} \cdot \frac{\omega_c}{s + \omega_c} \tag{3}$$

Final component is the static output gain K_q which stabilizes the phugoid mode of the helicopter, improving the damping and transient response. The order of the tuned controller was determined after successive iterations in which the controller order of K_c and K_{inj} was increased incrementally. These iterations revealed that the performance of the controller increased with increased order until the robustness and handling qualities performance plateaued.

C. Design Specifications

The flight control laws for robust control in the following sections are designed to fulfill a series of hard constraints which are bounded by $\max H_{i,j} < 1$ and soft constraints which are optimised by minimising $\max S_{i,j}$ using the signals in Fig. (2) for the specified design points. The hard constraints involve the minimum necessary stability at the I/O of the plant, broken-loop-at-a-time, and pole placement constraint [28]. The soft constraints involve various I/O disturbance rejection and control attenuation shown in Eq. (4) for the vertical velocity and attitude control. Furthermore, reference tracking for the vertical velocity and attitude control described in Eq. (5). The individual transfer functions are taken from Eq. (4) and Eq. (5) matrices, which are used to separately bound the vertical velocity and attitude control loops and optimize the robustness of the controller.

$$\begin{bmatrix} y \\ u \end{bmatrix} = \begin{bmatrix} S_o & S_o G \\ K S_o & T_i \end{bmatrix} \cdot \begin{bmatrix} d_o \\ d_i \end{bmatrix} \tag{4}$$

$$\begin{bmatrix} e_{V_z} \\ e_\theta \end{bmatrix} = (T_o - T_{ref}) \cdot \begin{bmatrix} V_{z_{ref}} \\ \theta_{ref} \end{bmatrix} \tag{5}$$

1. Hard Constraints

For the stability margin requirement, minimum robust disk-based stability margins are applied at each of the actuator inputs u for commanded collective $\delta_{col,cmd}$ and commanded longitudinal $\delta_{lon,cmd}$, and at each of the helicopter outputs y for vertical velocity V_z, pitch rate q, and pitch θ, broken loop-at-a-time. The margins can be assessed by breaking the loop at set points in the control loop to guarantee robustness to simultaneous gain and phase variations, unlike classical gain and phase margins [29]. These constraints can be written in terms of the open-loop transfer functions L associated with each of the five channels computed at each input or outputs. To define the symmetric disk-based stability margins, the constraint for i^{th} input/output is written as:

$$H_{1,i} = \frac{\alpha_{max}}{2} \left\| \frac{I - L}{I + L} \right\|_\infty \leq 1 \tag{6}$$

Given the parameters α_{max} which is the disk size for the guaranteed minimum gain $[\gamma_{min}, \gamma_{max}]$ and phase margins $[\phi_{min}, \phi_{max}]$ written as [29]:

$$[\gamma_{min}, \gamma_{max}] = \left[\frac{2 - \alpha_{max}}{2 + \alpha_{max}}, \frac{2 + \alpha_{max}}{2 - \alpha_{max}} \right] \tag{7}$$

$$[\phi_{min}, \phi_{max}] = \left[-\arccos\left(\frac{1 + \gamma_{min}\gamma_{max}}{\gamma_{min} + \gamma_{max}} \right), \arccos\left(\frac{1 + \gamma_{min}\gamma_{max}}{\gamma_{min} + \gamma_{max}} \right) \right] \tag{8}$$

The minimum required classical margins of ±6 dB/±45 deg from a MIL document in [3] which are used as a standard for stability margins in flight control system design. With the minimum phase margins being the limiting parameter for the size of the disk $\alpha_{max} = 0.82$ in systematic case which results in ±7.6 dB/±45 deg for the constraint.

For the pole-placement requirement described in the HQ criteria for low speed flight and longitudinal modes, in terms of stability is a reasonable demand that the system's closed poles lie in a particular subset of the complex plane $\mathcal{D}$ for the design point at 40 kts. This guarantees certain criteria, such as sufficient damping and stable RHP-poles. The damping ratio is set to 0.35, with a minimum decay rate of 0, to meet HQ objectives defined using the ADS-33 criteria [2]. The maximum frequency of 100 rad/s for the poles is bounded in the region of the complex plane to avoid dynamics faster than the sampling rate, which is assumed to be 100 Hz. Here, $L = L^T$ and M are real matrices that can characterize a variety of regions on the complex plane [30]. Such a region is defined as:

$$H_{2,1} : \mathcal{D} = \{ z \in \mathbb{C} : f_{\mathcal{D}}(z) = L + zM + \bar{z}M^T < 0 \} \tag{9}$$

2. Soft Constraints

The disturbance rejection requirements involve rejecting plant I/O disturbances toward the measured output. The output disturbance rejection is defined by the output sensitivity transfer function S_o from the output disturbance d_o to the measured output y. These constraints are established based on the analysis in [31] which uses HQ criteria and through experimentation establishing recommend guidelines for the output disturbance sensitivity. The disturbance rejection peak DRP and disturbance rejection bandwidth DRB are used to evaluate the handling and hold characteristics for each output channel. These parameters are defined as follows:

$$\omega\left(S_o = -3\,\text{dB}\right) = DRB\ \text{rad/s}, \quad ||S_o||_\infty = DRP\ \text{dB} \tag{10}$$

The specifications on disturbance rejection are defined and enforced with the weighting function W_{S_o}. The transfer functions from $T_{d_{V_z}\to V_z}$ and $T_{d_\theta\to\theta}$ are subject to the required specifications for the vertical velocity and attitude channels, shown in Table 1 for the hold characteristics. The low-frequency gain must be reduced to reject disturbances

Table 1 Disturbance rejection guidelines [31]

	Pitch (θ)	Vertical velocity (V_z)
DRB rad/s $\geq$	0.5	1.0
DRP dB $\leq$	5.0	5.0

in this range for the respective hold modes and to limit signal amplification. Therefore, the inverted weighting function $W_{S_o}^{-1}$ is chosen such that the low-frequency attenuation converges to -40 dB. The constraints are written as:

$$S_{1,1} = \left\|W_{S_{V_z}} T_{d_{V_z}\to V_z}\right\|_\infty \tag{11}$$

$$S_{1,2} = \left\|W_{S_\theta} T_{d_\theta\to\theta}\right\|_\infty \tag{12}$$

The input disturbance rejection is defined as S_oG, the transfer function from the input disturbance d_i to the measured output y. Similarly, control signal attenuation is defined as the transfer function from the output disturbance d_o to the control output u. To align the system's I/O relationships across different operating points, the system's plant can be re-scaled, allowing the functions S_oG and KS_o to be normalized. The re-scaling of the direct control (DC) gains in the open-loop system leads to specific results for the KS_o functions, ensuring that the transfer functions $T_{d_{V_z}\to\delta_{col,cmd}}$ and $T_{d_\theta\to\delta_{lon,cmd}}$ maintain a consistent value of 0 dB at a frequency of 0 rad/s, as mentioned in [18]. For input disturbance rejection, the re-scaling is inverted as the I/O relationships are reversed. Additionally, due to normalization, similar weights can be applied for the input and output disturbance rejection. Although, for W'_{S_θ}, the roll-off is altered compared to W_{S_θ} to match the slope of the re-scaled S_oG function. The constraints are written as:

$$S_{2,1} = \left\|W_{S_{V_z}} T_{d_{\delta_{col,cmd}}\to V_z}\right\|_\infty \tag{13}$$

$$S_{2,2} = \left\|W'_{S_\theta} T_{d_{\delta_{lon,cmd}}\to\theta}\right\|_\infty \tag{14}$$

For the control signal attenuation for the feedback loop is defined as KS_o, represented by $T_{d_{V_z}\to\delta_{col,cmd}}$ and $T_{d_\theta\to\delta_{lon,cmd}}$, the inverted weighting filters are adjusted so that the transfer functions are bounded, limiting the peak values and high frequency gains. The low frequencies are limited by gains of 10 dB for both channels to provide robustness to output multiplicative uncertainty for output related the corresponding disturbance input. With sufficient roll-off at frequencies of 10 rad/s and 20 rad/s for the control signal attenuation of the vertical velocity and attitude control channels, respectively. Furthermore, high-frequency gains are attenuated at -40 dB in order to ensure reduced control effort at high frequencies limiting the effect of sensor noise on the controller. The following constraints are written as:

$$S_{3,1} = \left\|W_{KS_{V_z}} T_{d_{V_z}\to\delta_{col,cmd}}\right\|_\infty \tag{15}$$

$$S_{3,2} = \left\|W_{KS_\theta} T_{d_\theta\to\delta_{lon,cmd}}\right\|_\infty \tag{16}$$

The input tracking is defined as T_i, the transfer function from input disturbance d_i to the controller output u. These transfer functions, represented by $T_{d_{\delta_{col,cmd}}\to\delta_{col,cmd}}$ and $T_{d_{\delta_{lon,cmd}}\to\delta_{lon,cmd}}$, are constrained to enforce low-frequency

input open-loop crossover. The weighting functions limit the input tracking to provide robustness against uncertainties at the actuator input. For the weighting functions in the $\delta_{col,cmd}$ channel are 3 rad/s and for the $\delta_{lon,cmd}$ channel 15 rad/s are limited to 0 dB. With high-frequency gains of −40 dB in order to ensure a good attenuation of control disturbances at high frequencies at the input. The following constraints are written as:

$$S_{4,1} = \left\| W_{T_{\delta_{col,cmd}}} T_{d_{\delta_{col,cmd}} \to \delta_{col,cmd}} \right\|_{\infty} \tag{17}$$

$$S_{4,2} = \left\| W_{T_{\delta_{lon,cmd}}} T_{d_{\delta_{lon,cmd}} \to \delta_{lon,cmd}} \right\|_{\infty} \tag{18}$$

The model following method is used to focus on time-domain transient responses. In which, a lower-order equivalent system (LOES) for the collective to height rate response from the HQ criteria is used to evaluate the vertical velocity response characteristics for desirable reference tracking performance, written as:

$$T_{ref,V_z} = \frac{K e^{-\tau_{V_{zeq}} s}}{T_{V_{zeq}} s + 1} \tag{19}$$

The parameters which relate directly to meet the level 1 HQ criteria for the LOES for vertical velocity response are shown in Table 2 using the model following structure.

Table 2 Parameters for the model following of T_{ref,V_z}

Parameter	Description	Value
$\tau_{V_{zeq}}$	Time delay	5 ms
$T_{V_{zeq}}$	Time constant	1.0 s

The pitch control (ACAH) has reference following requirements for rise time and closed-loop shaping for level 1 handling qualities for T_o, the signal for the reference tracking performance. The LOES is formulated based on approximations seen in [32], written as:

$$T_{ref,\theta} = \frac{\omega_n^2 e^{-\tau_{\theta_{eq}} s}}{s^2 + 2\zeta\omega_n s + \omega_n^2} \tag{20}$$

The parameters which meet the level 1 HQ criteria are described in Table 3 using the model following structure, where the quickness requirement is the limiting constraint and the delay bounds phase-lag in the closed-loop bandwidth of the handling requirements. The targeted HQ criteria for the phase delay τ_{p_θ} is 0.05 s with a bandwidth ω_{BW_θ} of 6.3 rad/s

Table 3 Parameters for the model following of $T_{ref,\theta}$

Parameter	Description	Value
$\tau_{\theta_{eq}}$	Time delay	7.5 ms
ζ	Damping ratio	1
ω_n	Natural frequency	4.5 rad/s

and the response speed $\frac{q_{pk}}{\theta_{pk}}$ of 1.6 s^{-1}. The delay's for both channels can be linearized using a first-order approximation for the constraint. To ensure compliance with HQ criteria, low steady-state error is achieved through limiting the H_∞ norm of the weighted reference error signal at low frequencies, bounding the transfer functions $T_{V_{z_{ref}} \to V_z}$ and $T_{\theta_{ref} \to \theta}$. Furthermore, to ensure that the frequency domain response are followed at low to mid-frequencies, attenuation is required of −40 dB at 1 rad/s applied to both channels with a roll-off relaxing the constraint at higher frequencies where matching is less critical. The following constraints are written as:

$$S_{5,1} = \left\| W_{T_{V_z}} (T_{V_{z_{ref}} \to V_z} - T_{ref,V_z}) \right\|_{\infty} \tag{21}$$

$$S_{5,2} = \left\| W_{T_\theta} (T_{\theta_{ref} \to \theta} - T_{ref,\theta}) \right\|_{\infty} \tag{22}$$

V. Results & Analysis

The synthesised controller after tuning the five control gains $K_{inj,V_z}, K_{inj,\theta}, K_{c,V_z}, K_{c,\theta}, K_q$ against the soft and hard design specifications described above. The solution was obtained using the *systune()* function in the MATLAB Control Design Toolbox, which can handle multi-objective design problems [17, 33, 34]. In this approach, the soft design constraints $S_{i,j}$ are minimized under the condition that the hard constraints $H_{i,j}$ are satisfied, as detailed in [16, 22]. In addition to the controller gains, the function returns two scalar values, denoted by $\max(H_{i,j}) = 1$ and $\max(S_{i,j}) = 0.9$, which indicate whether the constraints are satisfied by the controller. The synthesized structured H_∞ controller are written as follows:

$$\begin{aligned} K_{inj,V_z} &= \frac{0.056s - 0.30}{s^2 + 12.24s + 54.04} \quad K_{inj,\theta} = \frac{-46.87s + 26.46}{s^2 + 11.36s + 46.16} \\ K_{c,V_z} &= \frac{0.064s + 0.066}{s + 5.45} \quad K_{c,\theta} = \frac{-11.09s - 5.67}{s + 4.87} \quad K_q = -1.97 \end{aligned} \tag{23}$$

A. Stability Requirements

In Fig. (4) and (5), the disk-based gain and phase margins as functions of frequency are shown for each of the helicopter inputs and outputs. The minimum classical gain margins are approximately ±12 dB or greater for all inputs and outputs, which is well above the 6 dB objective. In contrast, the minimum classical phase margins are ±45 deg or greater that are on target, as the hard constraint only guarantees ±7.6 dB and ±45 deg of classical margins. As shown in the figure the exclusion regions are highlighted in which the broken open-loop transfer functions are avoided indicating robustness against perturbations for combinations of phase and gain margins, meeting the disk based stability requirements set. Additionally, Fig. (6) shows the hard requirement on the pole-location for $\mathcal{D}$-stability, ensuring that all poles in the closed-loop system are stable left-hand plane with sufficient damping in accordance with the HQ criteria. The same can be said for the zero locations which indicate minimum-phase behaviors and no RHP cancellations. Although, their are poles close to the marginal plane which have an impact the robustness of the controller design elaborated further in the analysis.

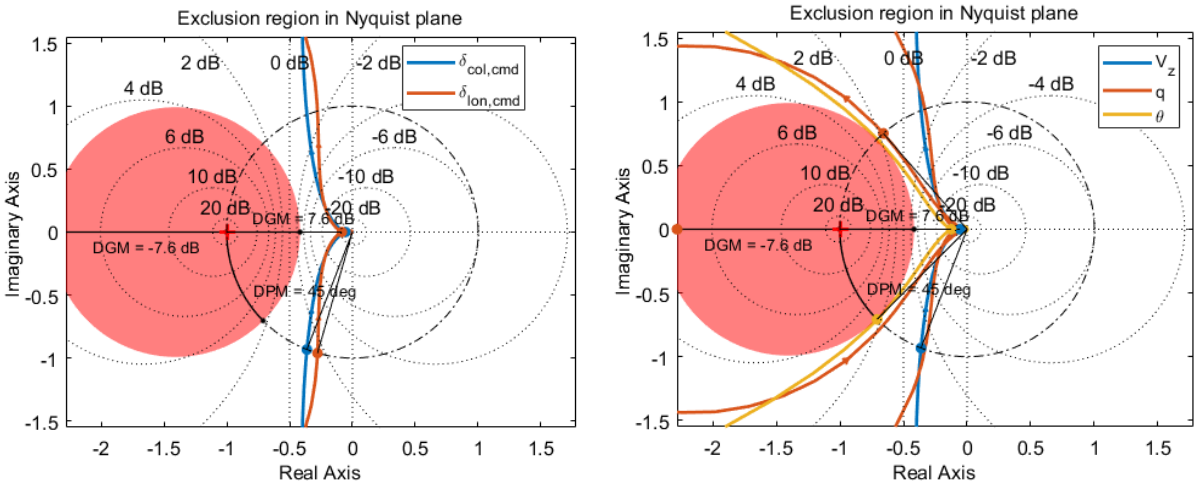

(a) Nyquist stability region for inputs (loop-at-a-time) **(b) Nyquist stability region for outputs (loop-at-a-time)**

Fig. 4 Nyquist plots with symmetric stability regions for the inputs/outputs (loop-at-a-time) of open loops for the design point at 40 kts

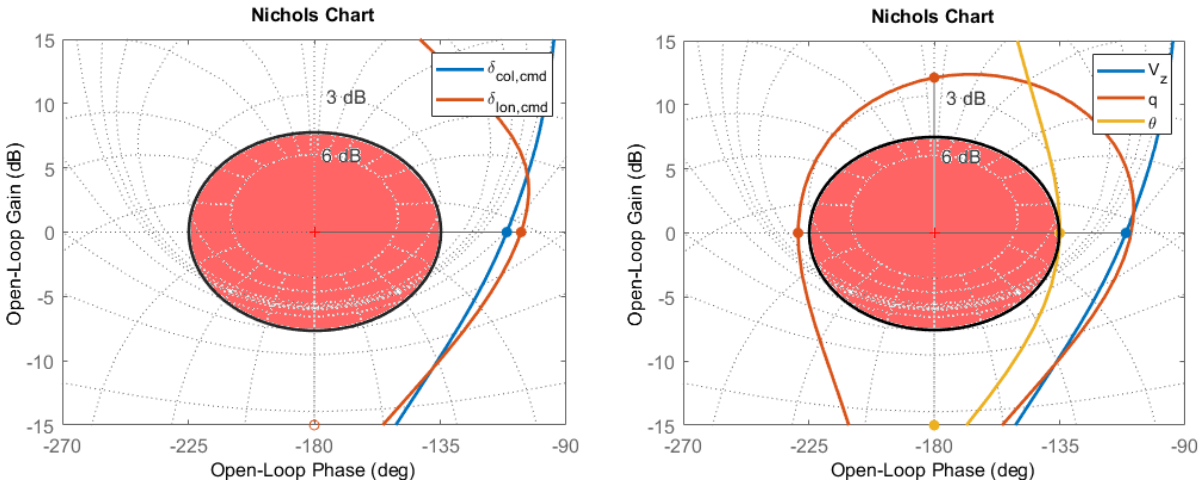

(a) Nichols stability region for inputs (loop-at-a-time) **(b) Nichols stability region for outputs (loop-at-a-time)**

Fig. 5 Nichols plots with symmetric stability regions for the inputs/outputs (loop-at-a-time) of open loops for the design point at 40 kts

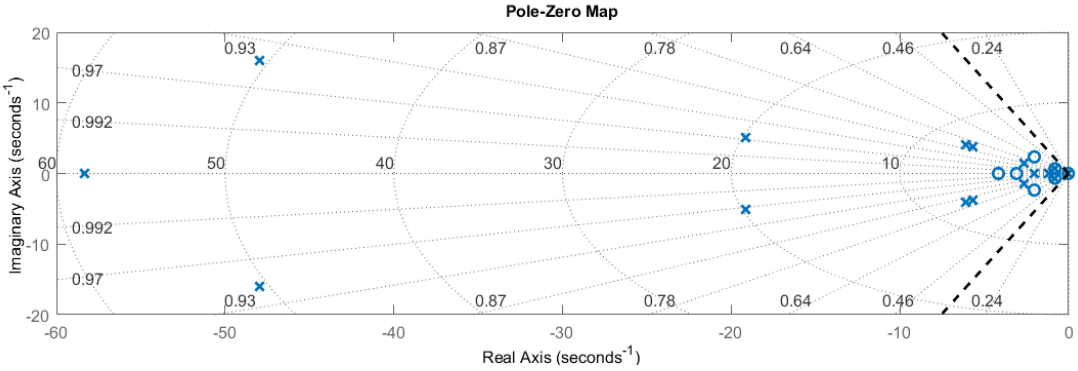

Fig. 6 Closed-loop pole-zero plot for the design point at 40 kts

B. Closed-loop Transfer Functions

The five different closed-loop transfer functions that are constrained to assess the frequency-domain characteristics of the closed-loop system are shown in Fig. (7) for the 2-DoF controller. To attenuate I/O disturbances acting on both the plant input and output, S_o and S_oG signals are minimized at low frequencies. Furthermore, it can be seen that the KS_o, T_i and T_o signals have adequate roll-off at high frequencies to attenuate the high frequency measurement noise.

The closed-loop transfer functions of the 2-DoF controller design are shown in Fig. (8). It can be seen that $T_o - T_{ref}$ has a high peak in the mid-frequency range and is low in the low-frequency which results in low steady-state error from sufficient integral action of the controller. This peak is reshaped with the feedforward controller, leading to the controlled system requiring more control effort in this frequency range without affecting the robustness of the feedback control. Furthermore, bounding the $T_o - T_{ref}$ function in Fig. (8) to be small at lower frequencies will reduce the error between the reference model and the output of the system at lower to mid-frequencies. A trade-off takes place where the peak of $T_o - T_{ref}$ is limited as much as possible in the mid-frequency range, while minimizing functions KS_o the required control effort in the from the reference tracking and T_i the input tracking so the signals have adequate roll-off at higher frequencies.

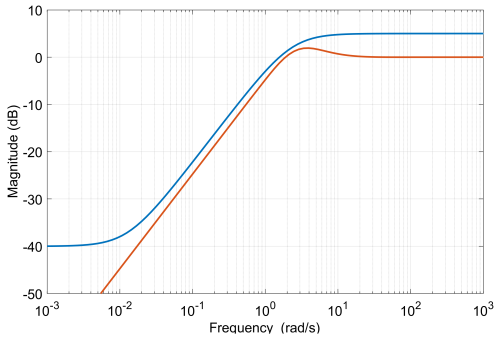

(a) Soft constraint on $T_{d_{V_z} \to V_z}$ (output disturbance sensitivity on V_z)

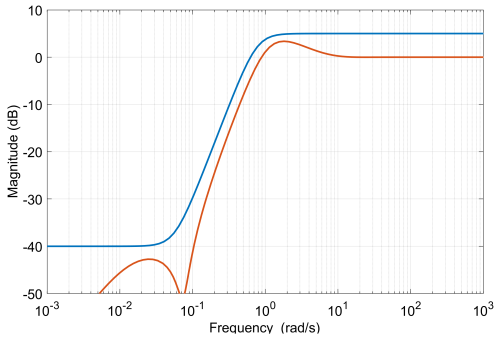

(b) Soft constraint on $T_{d_\theta \to \theta}$ (output disturbance sensitivity on θ)

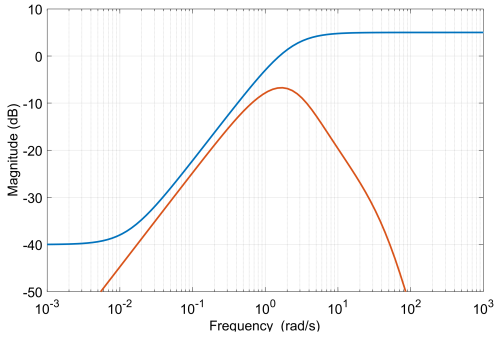

(c) Soft constraint on $T_{d_{\delta_{col,cmd}} \to V_z}$ (input disturbance sensitivity on V_z)

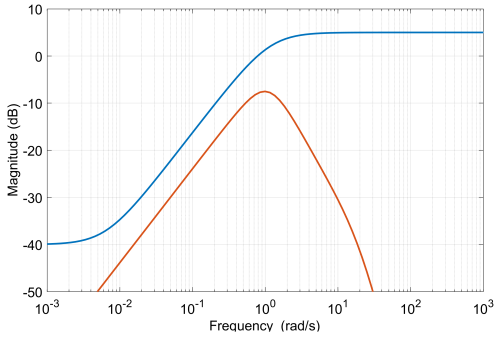

(d) Soft constraint on $T_{d_{\delta_{lon,cmd}} \to \theta}$ (input disturbance sensitivity on θ)

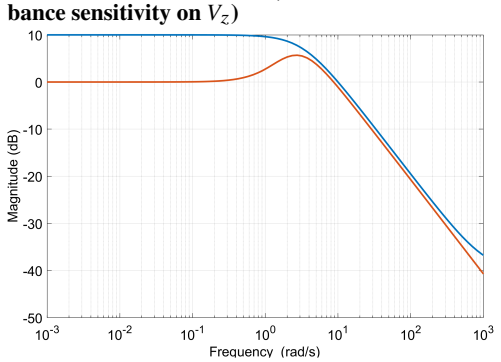

(e) Soft constraint on $T_{d_{V_z} \to \delta_{col,cmd}}$ (output disturbance sensitivity on $\delta_{col,cmd}$)

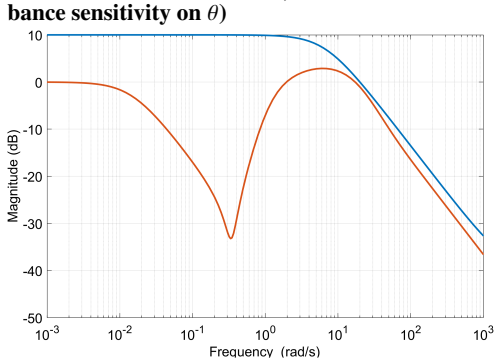

(f) Soft constraint on $T_{d_\theta \to \delta_{lon,cmd}}$ (output disturbance sensitivity on $\delta_{lon,cmd}$)

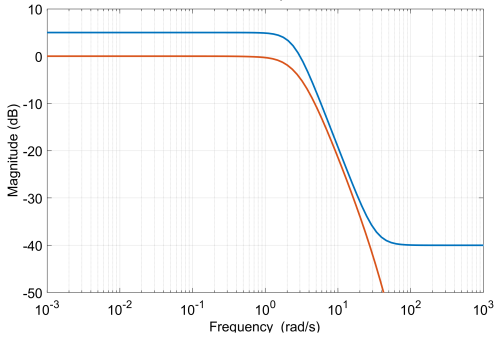

(g) Soft constraint on $T_{d_{\delta_{col,cmd}} \to \delta_{col,cmd}}$ (input disturbance sensitivity on $\delta_{col,cmd}$)

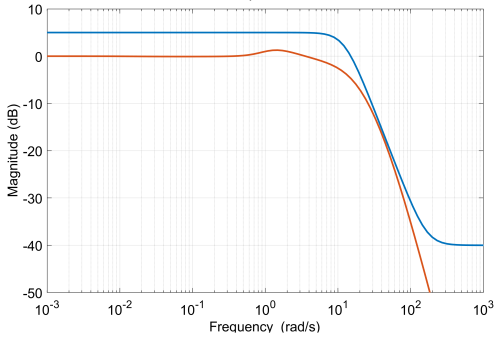

(h) Soft constraint on $T_{d_{\delta_{lon,cmd}} \to \delta_{lon,cmd}}$ (input disturbance sensitivity on $\delta_{lon,cmd}$)

Fig. 7 Overview of the designs of soft constraints related to disturbance rejection and signal attenuation frequency responses for the design point at 40 kts (blue: inverted weights W^{-1}, red: designed solution)

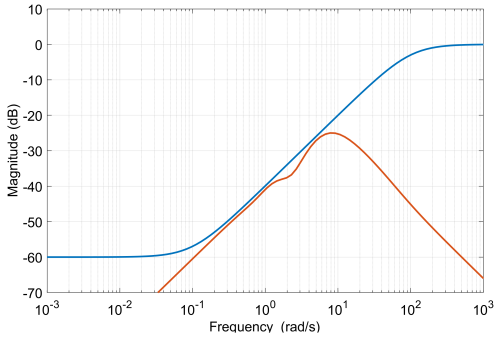

(a) Soft constraint on $T_{V_{z_{ref}} \to V_z} - T_{ref,V_z}$ (reference tracking)

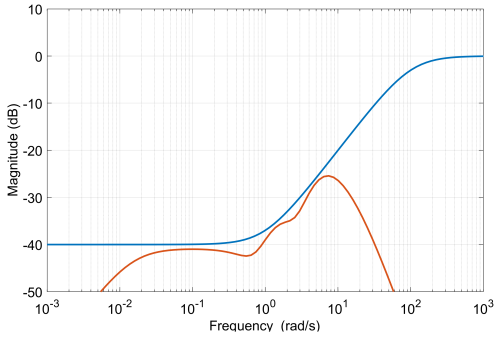

(b) Soft constraint on $T_{\theta_{ref} \to \theta} - T_{ref,\theta}$ (reference tracking)

Fig. 8 Overview of the designs of soft constraints related model following frequency responses for the design point at 40 kts **(blue: inverted weights W^{-1}, red: designed solution)**

C. Handling Quality Requirements

The performance of the resulting design is evaluated against the quickness and bandwidth of the attitude response which are the requirements that are enforced using a model following approach for the longitudinal helicopter model. The quickness criterion, defined by ADS-33, uses amplitude step inputs to assess the rate at which the controller converges to the target attitude while minimising overshoot using the peaks as metrics $\frac{q_{pk}}{\theta_{pk}}$. Fig. (9) shows the results obtained using the designed system in the time domain, which can be compared with the theoretical performance of the reference model. As can be seen, responses remain close to the targets defined by the reference models. This indicates that the combination of the reference model tracking approach leads to a consistent response of the flight control system solution in the time domain. Furthermore, the responses exhibit inter-axis decoupling between the channels, despite the absence of constraints directly associated with decoupling requirements. However, the risk of actuator saturation remains, which is a problem for the attitude quickness requirement. As shown in Fig. (9b), the attitude command quickness is $\frac{q_{pk}}{\theta_{pk}} = 1.8\,\mathrm{s}^{-1}$ meeting level 1 required for mission task elements (MTE) and attitude target acquisition ($> 1.6\,\mathrm{s}^{-1}$) requirement for 1 deg attitude changes.

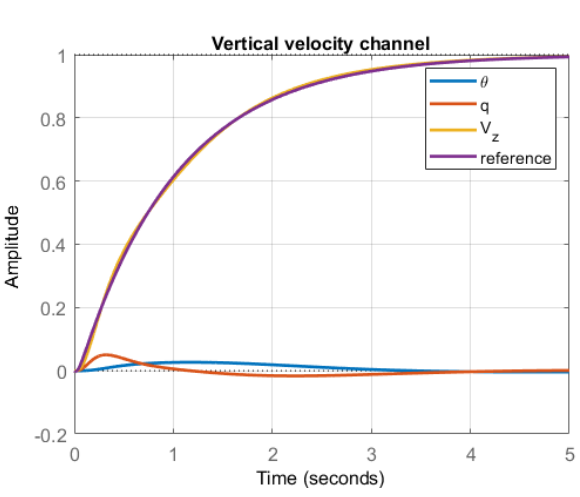

(a) 1.0 m/s **step response of $V_{z_{ref}}$**

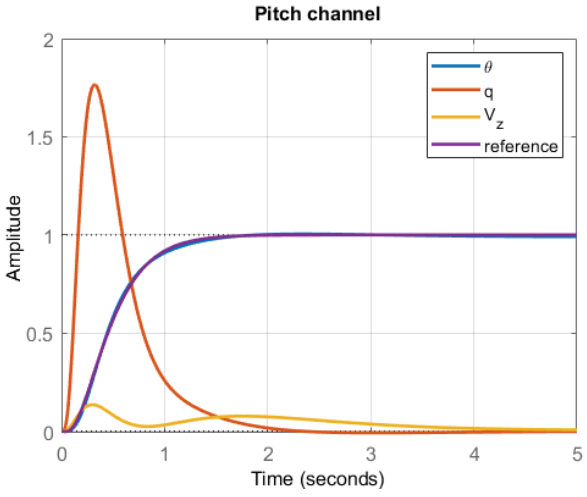

(b) 1.0 deg **step response of θ_{ref}**

Fig. 9 Step responses in the time domain

The bandwidth handling criteria assess the accuracy of the reference tracking in the frequency domain using two parameters: the phase delay τ_{p_θ} and bandwidth ω_{BW_θ}. The bandwidth of the ACAH response types is the minimum between the frequency at which the phase is at -135 deg and the frequency at which the gain is 6 dB greater than at the crossover frequency ω_{180}. The phase delay τ_{p_θ} is defined according to Eq. (24) in terms of the crossover frequency ω_{180} and the phase shift at twice the crossover frequency $\Delta\phi_{2\omega_{180}}$. The application of this criterion to the designed flight control system from reference models is shown in Fig. (10), meeting level 1 handling requirements and closely matching the reference point [2].

$$\tau_{p_\theta} = \frac{\Delta\phi_{2\omega_{180}}}{57.3(2\omega_{180})} \tag{24}$$

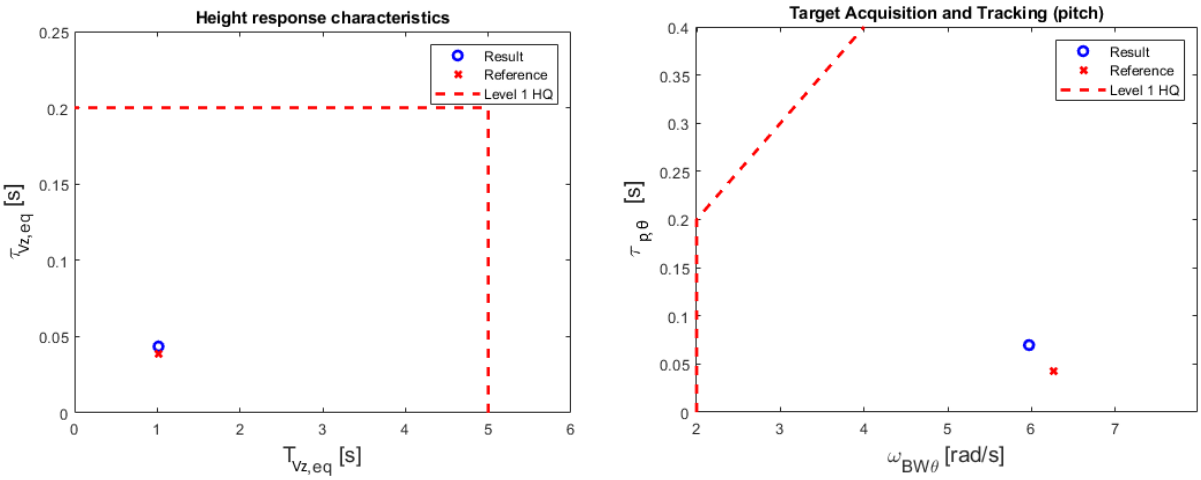

(a) Vertical velocity LOES response requirements **(b) Bandwidth requirements for small-amplitude attitude**

Fig. 10 Model following frequency domain HQ requirement

D. Robustness Analysis

To investigate robustness against uncertainties, an uncertain model of the helicopter was derived from the design model by defining a ±20 % uncertainty for all stability and control derivatives in matrices A and B of Eq. (1), with a breakdown of the uncertain derivatives with the most significant contributions. The robustness of the resulting controller is assessed using an SSV or μ analysis, as shown in Fig. (11) [19].

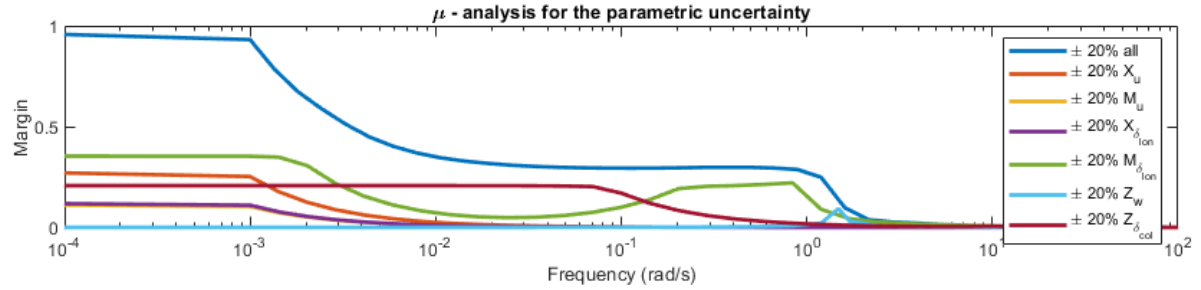

Fig. 11 Structured singular value analysis for the design point at 40 kts **(stability and control derivatives)**

The upper bound peak value is equal to 0.9988 at a critical frequency of 0 rad/s at the design velocity when all of the uncertainty is applied, indicating that robust stability for the uncertainty is guaranteed. This corresponds to the controller being capable of handling $100/(0.9988) = 100.12$ % of the uncertainty. Therefore, for values less than 1, the controller is robustly stable against the specified parametric uncertainty.

The uncertainty in the longitudinal X and moment M derivatives significantly affect the phugoid dynamics, which are the major contributing factors towards the robustness limitations at 0 rad/s. In contrast, the normal Z derivatives affecting the heave subsidence, which is already stable in the open loop and has a less significant cumulative contribution to robust stability.

Furthermore, parametric uncertainties can be added directly into the nonlinear model using MATLAB's *ureal()* and linearized using *ulinearize()* to obtain an uncertain linear model for variations in mass and moment of inertia ($m \pm 10\,\%$, $I_{yy} \pm 10\,\%$) combined with variations in the center of gravity position both normally and longitudinally ($Z_{CG}, X_{CG} \pm 0.05$ m) from the nominal model. Additionally, multiplicative uncertainties in the aerodynamic forces and moments were added ($F_x \pm 20\,\%$, $F_z \pm 20\,\%$, $M_y \pm 20\,\%$). This introduces uncertainties in the force/moment derivatives and operating points, which allows for the robustness of the resulting controller to be assessed at various flight configurations. The μ analysis, shown in Fig. (12), demonstrating that the system is robustly stable against the parametric changes in the configuration and the uncertainty in the aerodynamic forces and moments, with a tolerance up to $100/(0.238) = 420\,\%$. This results shows that the controller is robustly stable against shifts in centre of gravity positions, uncertainty in the forces X, Z and moment M as well as the changes in the mass and moment of inertia. This indicates that the limitation to the robustness of the autopilot are stability and control derivatives which significantly affect the phugoid dynamics of the helicopter.

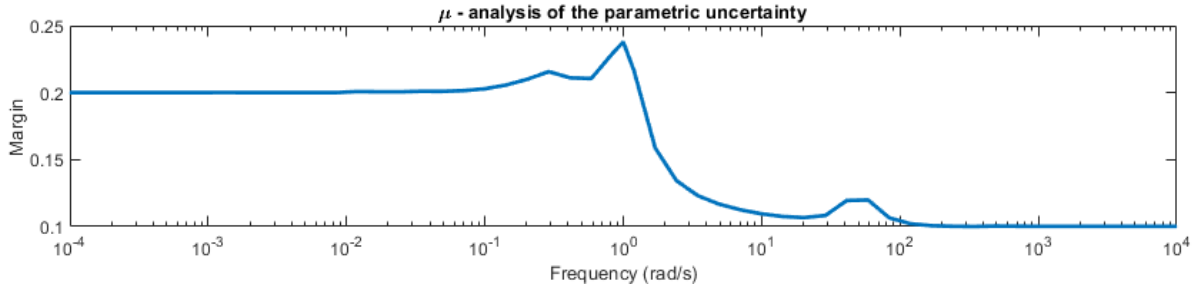

Fig. 12 Structured singular value analysis for the design point at 40 kts **(configuration and forces/moments)**

VI. Non-linear simulations

To showcase the robustness of the controller, nonlinear Monte Carlo simulations were performed, as shown in Fig. (13), by varying uncertain parameters used for Fig. (12), which corresponds to the μ analysis. The following simulations use a series of step-wise reference signals where the altitude is $h = 0$ m to assess the non-linear performance. The reference signal profiles allow for flight coverage around the design point. In the simulation, uncertainties in the force/moment derivatives and operating points were introduced in the nonlinear 3-DoF longitudinal helicopter model. The commanded maneuvers were designed to stay within the limitations of actuators for the nominal model.

It can be seen that even for large vertical velocity changes and pitch angles, the control effort is small, and the response accurately follows the reference signal. This is evident in the first 25 seconds when the step functions were individually applied. Both steps converge to the reference signal, but as seen, the parametric uncertainty introduces notable variations in the vertical velocity response in terms of overshoot, with consistent rise times. Although, the ACAH response remains consistent throughout the simulation, including the uncertainty. Furthermore, although uncertainties influence the response, the controller is still able to accurately track the reference signal with a noticeable degradation in performance as uncertainty increases. This degradation is primarily seen in the vertical velocity control during simultaneous reference commands with the pitch channel for 5 deg steps. The steady-state error is approximately around the order of 0.1 m/s, which is a relatively small steady-state error. However, due to the non-linear coupling dynamics, greater levels of variation are introduced in the final 30 seconds of the simulation for 15 deg steps reference inputs.

To conclude, the simulation verified in the time domain the results of the μ analysis performed, given that changes in the stability of the model are assumed to be negligible as a function of velocity.

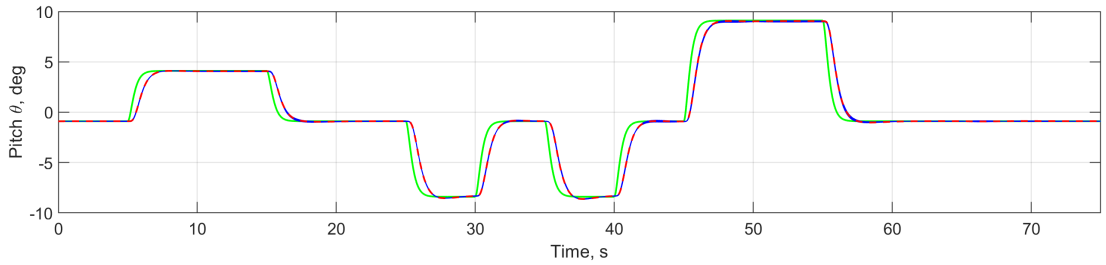

(a) Tracked output signal θ (pitch attitude)

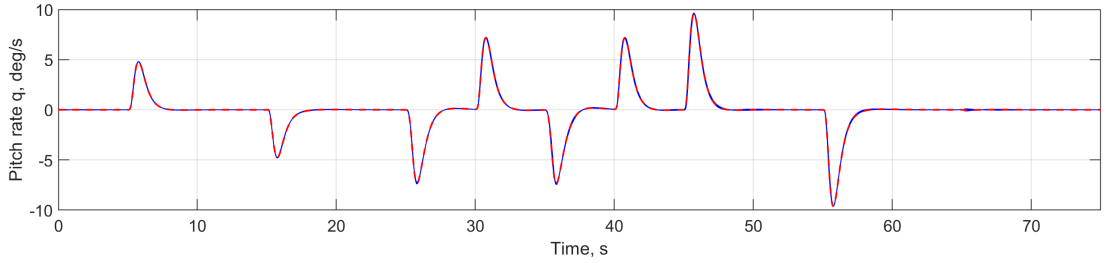

(b) State output signal q (pitch rate)

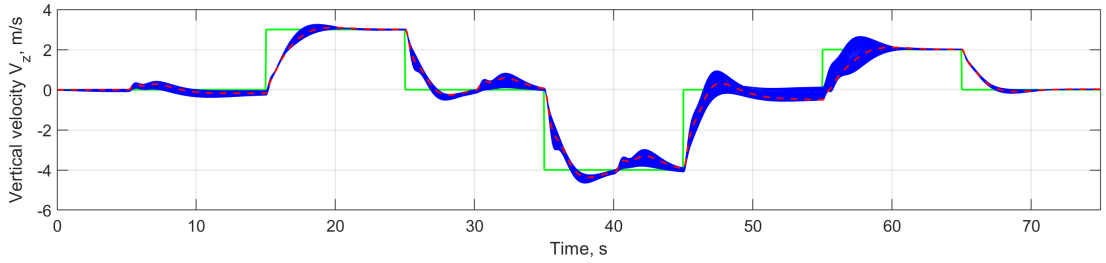

(c) Tracked output signal V_z (vertical velocity)

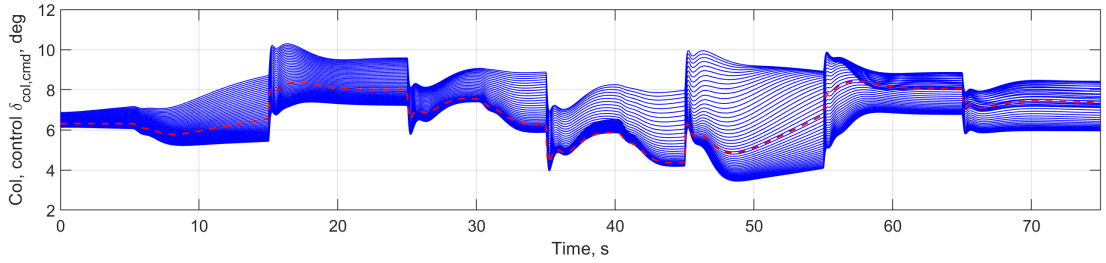

(d) Control signal $\delta_{col,cmd}$ (desired collective)

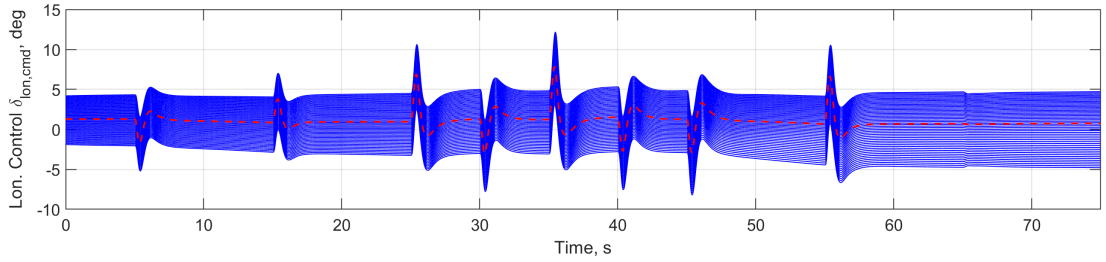

(e) Control signal $\delta_{lon,cmd}$ (desired longitudinal)

Fig. 13 Nonlinear simulation (green: reference, red: nominal parameter run, blue: 50 uncertain parameter runs)

VII. Conclusion

This paper introduced a flight control architecture combining robust control theory as a method for tuning controllers to meet HQ requirements. The design methodology adopts a multi-objective approach to balance trade-offs between robustness and performance in the controller design using the frequency domain. The proposed methodology uses simple structured controllers that can be gain-scheduled and/or applied in multi-modal methods to obtain robust controllers. Various soft and hard constraints were systematically applied, resulting in a 2-DoF longitudinal controller with desired properties for reference tracking, disturbance rejection at the plant inputs and outputs, sensor noise attenuation, control signal attenuation, and disk-based stability margins. Additionally, μ analysis verified the robustness of the controller against various parametric uncertainties.

This methodology is limited by the designer's experience in handling the trade-offs between robustness and performance to meet HQ requirements and ensure the constraint parameters are properly tuned. Despite this limitation, the methodology simplifies the design process. Future work could focus on better understanding the connection between helicopter design limitations and control law design in terms of robustness and performance in meeting HQ requirements.

The next steps include testing the methodology on a higher fidelity nonlinear model of the helicopter to confirm the results obtained by applying the selected ADS-33 and stability criteria to the linear model. As a gain-scheduled controller and/or multi-model approaches can be used to account for nonlinear phenomena across the flight envelope. In addition, to development of the control architecture to take into account higher-order rotor dynamics, rotor flow state aerodynamics and aero-elasticity. Furthermore, robust control design under the constraints of actuator authority limits using anti-windup schemes also needs investigation.

References

[1] Hu, J., and Gu, H., "Survey on Flight Control Technology for Large-Scale Helicopter," *International Journal of Aerospace Engineering*, Vol. 2017, 2017, p. 1–14. https://doi.org/10.1155/2017/5309403, URL https://dx.doi.org/10.1155/2017/5309403.

[2] Anon, "ADS-33E-PRF-Handling Qualities Requirements for Military Rotorcraft," , 2000. URL https://www.roberttheffley.com/docs/HQs/ADS-33E-PRF.pdf.

[3] Anon, "Detailed specification: Flight systems—Design, installation, and test of piloted aircraft, general specification for MIL-DTL-9490E," , 2008. URL http://everyspec.com/MIL-SPECS/MIL-SPECS-MIL-DTL/MIL-DTL-9490E_10979/.

[4] Du Val, R. W., and He, C., "Validation of the FLIGHTLAB virtual engineering toolset," *The Aeronautical Journal*, Vol. 122, No. 1250, 2018, pp. 519–555. https://doi.org/10.1017/aer.2018.12, URL https://dx.doi.org/10.1017/aer.2018.12.

[5] Balas, G. J., "Flight Control Law Design: An Industry Perspective," *European Journal of Control*, Vol. 9, No. 2, 2003, pp. 207–226. https://doi.org/https://doi.org/10.3166/ejc.9.207-226, URL https://www.sciencedirect.com/science/article/pii/S0947358003702763.

[6] Kumar, M. V., Sampath, P., Suresh, S., Omkar, S., and Ganguli, R., "Design of a stability augmentation system for a helicopter using LQR control and ADS-33 handling qualities specifications," *Aircraft Engineering and Aerospace Technology*, Vol. 80, No. 2, 2008, pp. 111–123.

[7] Gribble, J. J., "Linear quadratic Gaussian/loop transfer recovery design for a helicopter in low-speed flight," *Journal of Guidance, Control, and Dynamics*, Vol. 16, No. 4, 1993, pp. 754–761.

[8] Tijani, I. B., Akmeliawati, R., Legowo, A., Budiyono, A., and Abdul Muthalif, A. G., "robust controller for autonomous helicopter hovering control," *Aircraft Engineering and Aerospace Technology*, Vol. 83, No. 6, 2011, pp. 363–374. https://doi.org/10.1108/00022661111173243, URL https://doi.org/10.1108/00022661111173243.

[9] Silva, L. R. T. d., Campos, V. A. F. d., and Potts, A. S., "Robust Control for Helicopters Performance Improvement: an LMI Approach," *Journal of Aerospace Technology and Management*, Vol. 12, 2020. https://doi.org/10.5028/jatm.v12.1179.

[10] Prempain, E., and Postlethwaite, I., "Static H loop shaping control of a fly-by-wire helicopter," *Automatica*, Vol. 41, No. 9, 2005, pp. 1517–1528. https://doi.org/https://doi.org/10.1016/j.automatica.2005.04.001, URL https://www.sciencedirect.com/science/article/pii/S000510980500141X.

[11] Antonioli, J.-C., Taghizad, A., Rakotomamonjy, T., and Ouladsine, M., "Towards the development of a methodology for designing helicopter flight control laws by integrating handling qualities requirements from the first stage of tuning," *40th European Rotorcraft Forum (ERF 2014)*, 2014.

[12] Dai, J., Ying, J., and Tan, C., "A novel particle swarm optimization based robust H-infinity control for rotorcrafts," *Engineering Computations*, Vol. 31, No. 4, 2014, pp. 726–741. https://doi.org/10.1108/ec-07-2012-0148, URL https://dx.doi.org/10.1108/ec-07-2012-0148.

[13] Srinathkumar, S., "Eigenstructure Control: A Rotorcraft Handling Qualities Engineering Tool," *Journal of the American Helicopter Society*, Vol. 60, 2015. https://doi.org/10.4050/JAHS.60.022010.

[14] Ji, S., and Wu, A., "Study on dual-loop controller of helicopter based on the robust H-infinite loop shaping and mixed sensitivity," *2011 International Conference on Electrical and Control Engineering*, 2011, pp. 1291–1294. https://doi.org/10.1109/ICECENG.2011.6057783.

[15] Biannic, J.-M., Taghizad, A., Dujols, L., and Perozzi, G., "A multi-objective H design framework for helicopter PID control tuning with handling qualities requirements," *7th European Conference for Aeronautics and Space Science (EUCASS), Milan, Italy*, 2017, p. 89.

[16] Authié, P., "A multi-model and multi-objective approach to the design of helicopter flight control laws," *CEAS Aeronautical Journal*, 2023, pp. 1–15.

[17] Apkarian, P., and Noll, D., "Nonsmooth H Synthesis," *IEEE Transactions on Automatic Control*, Vol. 51, No. 1, 2006, pp. 71–86. https://doi.org/10.1109/TAC.2005.860290.

[18] Skogestad, S., and Postlethwaite, I., *Multivariable feedback control: analysis and design*, john Wiley & sons, 2005.

[19] Bates, D., and Postlethwaite, I., *Robust multivariable control of aerospace systems*, Series 03: Control and simulation, 1566-7987 ; 08, DUP Science, Delft, 2002.

[20] P. Apkarian, D. N., "The H Control Problem is Solved," *AerospaceLab*, , No. 13, 2017. https://doi.org/10.12762/2017.al13-01, URL https://dx.doi.org/10.12762/2017.al13-01.

[21] Dehkordi, V. R., and Boulet, B., "Robust controller order reduction," *International journal of control*, Vol. 84, No. 5, 2011, pp. 985–997.

[22] Theodoulis, S., and Proff, M., *Robust Flight Control Tuning for Highly Agile Missiles*, 2021. https://doi.org/10.2514/6.2021-1568, URL https://arc.aiaa.org/doi/abs/10.2514/6.2021-1568.

[23] Srinathkumar, S., "Rotorcraft Precision Hover Control in Atmospheric Turbulence via Eigenstructure Assignment," *Journal of the American Helicopter Society*, Vol. 64, No. 1, 2019, pp. 1–12. https://doi.org/10.4050/JAHS.64.012005, URL https://www.ingentaconnect.com/content/ahs/jahs/2019/00000064/00000001/art00005https://doi.org/10.4050/JAHS.64.012005.

[24] Pavel, M. D., *Six degrees of freedom linear model for helicopter trim and stability calculation*, Delft University of Technology, Faculty of Aerospace Engineering, 1996.

[25] Simplicio, P., Pavel, M., van Kampen, E., and Chu, Q., "An acceleration measurements-based approach for helicopter nonlinear flight control using Incremental Nonlinear Dynamic Inversion," *Control Engineering Practice*, Vol. 21, No. 8, 2013, pp. 1065–1077.

[26] Vicente Melo E Carvalho Marques, M., "Investigation of L1 Adaptive Control as an Augmentation Loop," 2017.

[27] Bouwer, G., and Hilbert, K. B., "A Piloted Simulation of a Model Following Control System," *Journal of the American Helicopter Society*, Vol. 31, No. 2, 1986, pp. 27–32.

[28] Apkarian, P., and Noll, D., "Nonsmooth optimization for multiband frequency domain control design," *Automatica*, Vol. 43, No. 4, 2007, pp. 724–731. https://doi.org/https://doi.org/10.1016/j.automatica.2006.08.031, URL https://www.sciencedirect.com/science/article/pii/S0005109806004559.

[29] Seiler, P., Packard, A., and Gahinet, P., "An Introduction to Disk Margins [Lecture Notes]," *IEEE Control Systems Magazine*, Vol. 40, No. 5, 2020, pp. 78–95. https://doi.org/10.1109/MCS.2020.3005277.

[30] Chilali, M., Gahinet, P., and Apkarian, P., "Robust pole placement in LMI regions," *IEEE Transactions on Automatic Control*, Vol. 44, No. 12, Apkarian, pp. 2257–2270. https://doi.org/10.1109/9.811208.

[31] Berger, T., Ivler, C., Berrios, M. G., Tischler, M. B., and Miller, D., "Disturbance rejection handling qualities criteria for rotorcraft," *72nd Annual Forum of the American Helicopter Society, West Palm Beach, USA*, 2016.

[32] Tischler, M. B., Berger, T., Ivler, C. M., Mansur, M. H., Cheung, K. K., and Soong, J. Y., *Practical Methods for Aircraft and Rotorcraft Flight Control Design: An Optimization-Based Approach*, ARC, 2017.

[33] Apkarian, P., "Tuning controllers against multiple design requirements," *2013 American Control Conference*, 2013, pp. 3888–3893. https://doi.org/10.1109/ACC.2013.6580433.

[34] Apkarian, P., Gahinet, P., and Buhr, C., "Multi-model, multi-objective tuning of fixed-structure controllers," *2014 European Control Conference (ECC)*, 2014, pp. 856–861. https://doi.org/10.1109/ECC.2014.6862200.

3

Bibliographic Survey

3.1. Helicopter Handling Qualities

There are requirements which assesses helicopter control systems handling qualities to make the helicopter controllable for the pilot. This is because controlling a helicopter manually using the cyclic input requires training due to acting like a double integrator system which is difficult for a human pilot to control. To alleviate the problem, stability augmentation and flight control systems are implemented which need to adhere to the requirements specified in the ADS-33E-PRF document to ensure the proper level of stability and control for the pilot (Anon, 2000).

3.1.1. Definition

The concept of flight performance is subjective and complex, as it depends on the interactions between humans and machines. Flying qualities refer to ”the stability and control characteristics that have an important bearing on the safety of flight and on the pilots” (Phillips & H., 1949). Handling qualities, on the other hand, governs ”the stability and control characteristics that have an important bearing on the safety of flight and on the pilots' impressions of the ease of flying an aeroplane in steady flight and in manoeuvres” (Cooper & Harper, 1969). While flying qualities describe the aircraft's static and dynamic stability, handling qualities incorporate the human element into the stability and control of the aircraft. Due to the inherent difficulty of flying helicopters, handling requirements are established to guide the design of helicopters and control laws, taking into account human-in-the-loop stability. These requirements dictate desirable flight behaviour in terms of technical specifications using pole-zero locations as shown in Figure 5.5, which characterizes desirable oscillatory pole locations, and response characteristics in both the time and frequency domains shown in Figure 3.1c and Figure 3.1b, respectively, which define key parameters of both domains.

3.1.2. Handling Quality Rating

The requirements are formulated using Cooper-Harper Handling Qualities Rating Scale which is a subjective way to measure the ease of controlling an aircraft (Anon, 2000). This rating scale is used to this date as a reference to measure the handling qualities of helicopters. As shown in Figure 3.2, the rating scale is a subjective quantification of deficiencies within the control of a system. This scale has 3 main levels or categories to assess the handling quality. Level 1 indicates by a pilot rating of 1 to 3 which shows the minimal workload of the pilot to perform manoeuvres and maintain control of the vehicle. Level 2 with a pilot rating of 4 to 6 describes an increase in the workload of the pilot due to minor deficiencies in the control system present which requires compensation from the pilot to maintain control. Level 3 with a pilot rating of 7 to 9 indicates undesirable control properties which require an extensive workload from the pilot to control the system with major deficiencies affecting the overall performance of the human-machine system. The 'ADS-33 Aeronautical design standard performance specification: handling qualities requirements for military rotorcraft was established in 1985 and last updated in 2000 as a mission-oriented way of quantifying handling qualities for military rotorcraft using the Cooper-Harper Handling Qualities Rating Scale (Anon, 2000). This document specifies the Mission Task Elements (MTE) to provide guidelines for designing a helicopter with the corresponding

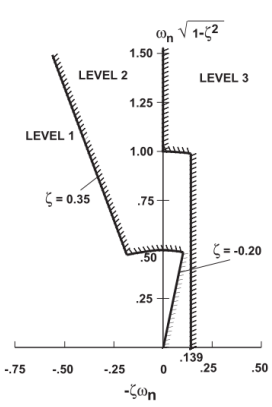

(a) Limits on the pitch (roll) oscillations at hover and low speed (Anon, 2000)

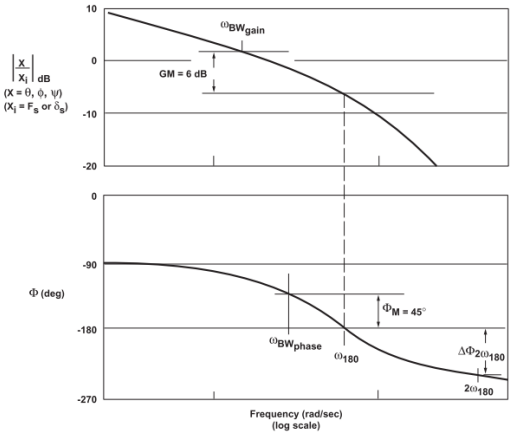

(b) Key frequency domain parameters used to compute bandwidth and time delay (Anon, 2000)

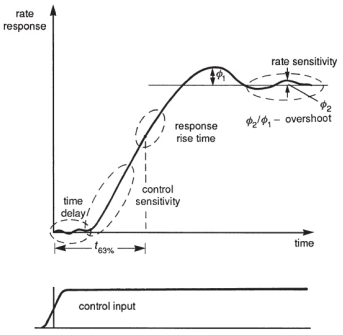

(c) Handling qualities parameters from step response (G. Padfield & Safari, 2018)

Figure 3.1: Definition of response and frequency characteristics described in the handling quality requirements (Anon, 2000)

control system, depending on the type of helicopter and environmental conditions. The MTEs are a set of manoeuvres and control system response elements used for measurements of the control and manoeuvrability requirements shown in Figure 3.1.

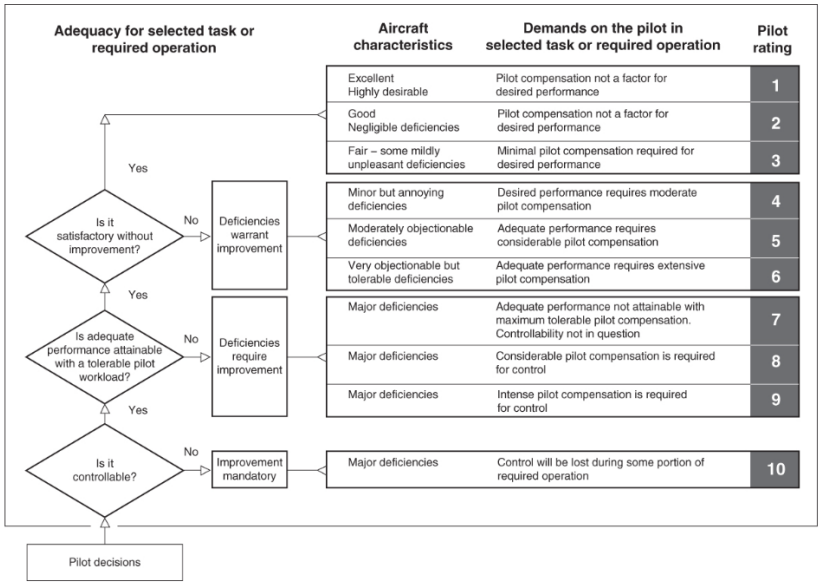

Figure 3.2: The Cooper-Harper Handling Qualities Rating Scale (Cooper & Harper, 1969)

3.1.3. Handling Requirements

As explained in subsection 3.1.2, helicopters have undesirable handling dynamics that make them difficult to control. Therefore, when designing the control system, the handling quality requirements are used as soft requirements, with stability requirements taking priority as hard requirements which will be explained in section 3.4 (Anon, 2008; SAE, 2008). In addition to the technical handling requirements, suggested signal disturbance rejection requirements and pilot-induced oscillation (PIO) avoidance requirements are also considered when designing the control system of helicopters (Berger, Ivler, Berrios, et al., 2016) (Tischler et al., 2017).

In the literature associated with control system design for helicopters, only key sets of requirements are considered in the scope of research on the control system, with handling quality parameters optimized as design objectives. The common requirements seen are attitude bandwidth and phase delay,

which look at frequency-domain response characteristics indicating the responsiveness of the system, calculated using Figure 3.1b (Srinathkumar, 2015). Another common requirement used in helicopter control research is the dynamic handling stability requirement, which requires the control system pole-zero to be located at level 1, as seen in Figure 5.5 (Jeong et al., 2012). Furthermore, there are also handling requirements in the time-domain response for both small and large-step attitude response characteristics described in Figure 3.1c, which show the agility of the system (Biannic et al., 2017). Most of the requirements seen in robust control of helicopters are taken from a subset of the ADS-33E-PRF (Anon, 2000).

Research also focuses on cross-coupling and turbulence disturbance rejection requirements, which based on the requirements in ADS-33E-PRF (Srinathkumar, 2015, 2019). Although, there are no criteria within the ADS-33E-PRF that measure turbulence disturbance rejection. There are studies which make control system design suggestions, which are provided in terms of turbulence rejection requirements (Berger, Ivler, Berrios, et al., 2016) (Tischler et al., 2017). The cross-coupling requirements are mentioned in the ADS-33E-PRF, which uses rates and attitudes signal ratios to assess the magnitude of the coupling.

3.2. H_∞ Based Robust Control Methods

Robust control is an approach to system control design that explicitly deals with uncertainty. However, methods within robust control are described as robust against uncertainty but depend on the definition of uncertainty. This is because there are various ways to define the model and analyse uncertainty to assess the robustness of the controller, which correspond to the methods used to obtain a measure of the range of variation of model parameters that the controller is guaranteed to work within. H_∞ control is known for its guaranteed performance and robustness, as linear controllers are synthesized by optimizing using the H_∞ norm of a set of transfer functions from the system. Depending on the uncertainty, control and plant structure, the method used to synthesize the controller with the control objectives used can vary, and in this section, we will discuss the known H_∞ methods applied to helicopters.

In H_∞ control, the general formulation of the problem is shown by the set of transfer functions determined by which input w and output z signals in Figure 3.7 can be freely chosen and derived using Equation 3.1. This is the general setup of any H_∞ optimization problem, as described in Equation 3.2 in which after synthesising the controller its robustness is analysed using unstructured and/or structured shown in Figure 3.3c from the uncertainties caused by the plant variations Δ.

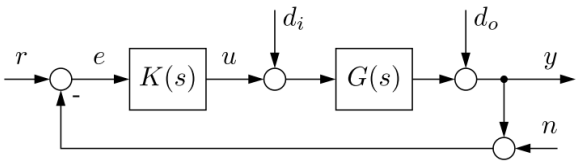

(a) Standard closed loop system structure

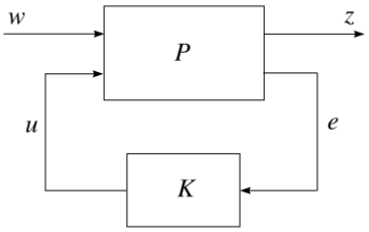

(b) Standard H_∞ optimization problem

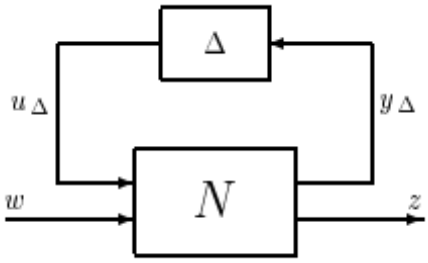

(c) $N\Delta$ structure for robust performance analysis

Figure 3.3: Set-up of the H_∞ optimization and robust performance analysis (Skogestad & Postlethwaite, 2005)

$$T_{w\to z}(P,K) = P_{11} + P_{12}K(I - P_{22}K)^{-1}P_{21} = \frac{z}{w} \quad \begin{bmatrix} z \\ e \end{bmatrix} = \begin{bmatrix} P_{11} & P_{12} \\ P_{21} & P_{22} \end{bmatrix} \begin{bmatrix} w \\ u \end{bmatrix} \tag{3.1}$$

$$\text{minimise } ||T_{w\to z}(P,K)||_\infty \text{ subject to } K \text{ stabilises } P \text{ internally for } K \in \kappa \tag{3.2}$$

3.2.1. Mixed Sensitivity

The mixed sensitivity method is a method in which a set of the transfer functions H_∞ norm are minimised using the controller K using the sensitivity functions S. In mixed sensitivity, the signals within the input w and output z signals are weighted in the frequency domain to provide a trade-off between contradicting optimisation objectives. The approach varies depending on the signals w and z, weighting functions W, and control structure with the optimization method which determines the robust stability performance of the method.

z/w	r	d_i	d_o	n
e	S_o	$-S_oG$	$-S_o$	$-S_o$
y	T_o	S_oG	S_o	$-T_o$
u	KS_o	$-KS_oG$	$-KS_o$	$-KS_o$
$y - y_d$	$T_o - W_{ref}$	S_oG	S_o	$-T_o$

Table 3.1: H_∞ mixed-sensitivity optimisation functions for different combinations of z/w signals

Several variations of methods have been applied to helicopter control, which alters these factors. A basic one is the S/KS mixed sensitivity, which minimizes Equation 3.3. Minimizing $||S_o||_\infty$ gives attenuation towards output disturbance signals, defining the disturbance rejection criteria. Minimizing $||KS_o||_\infty$ gives attenuation towards disturbances at the output and avoidance of large control signals due to reference demands, with increasing robust stability to additive unstructured uncertainty (Bates & Postlethwaite, 2002). Both transfer functions can be seen in Table 3.1, minimizing the effects of r onto e and d_o onto y for S_o with r onto u for KS_o. The weighting transfer functions W are used to allow trade-offs in the frequency domain for the chosen optimization functions. This can be observed when implementing the synthesized multivariable controller on the helicopter, which is robust against incorrect scaling of the actuator response (D. Walker, 2003).

$$T_{w\to z} : [d_o] \to \begin{bmatrix} z_1 \\ z_2 \end{bmatrix} = \begin{bmatrix} -W_1 e \\ -W_2 u \end{bmatrix} \quad K = \arg\min \left\| \begin{bmatrix} W_1 S_o \\ W_2 K S_o \end{bmatrix} \right\|_\infty \tag{3.3}$$

The mixed sensitivity method can be extended to S/T/KS to introduce the complementary sensitivity $||T_o||_\infty$ in the vector, which reduces the sensitivity to noise with increasing robustness against output multiplicative uncertainty (Bates & Postlethwaite, 2002). This optimization method is used to provide further robustness against plant uncertainties by minimizing the effect r has on y for T_o. The mixed sensitivity method is used due to its optimization of controllers that have noise and disturbance rejection, in which the closed-loop response can be tuned using the weighting functions that trade-off between robustness and performance to meet handling requirements (Luo et al., 2003). There are also variants of mixed sensitivity which introduce the model following signals called the signal-based approach. The signal-based method is a method in which a set of the transfer functions H_∞ norm are minimised using the controller K using the sensitivity functions S and the reference model W_{ref}. In signal based H_∞ control, both the input w and output z signals are weighted in the frequency domain to provide the trade-off between contradicting optimisation objectives to meet requirements. This approach differs from as it introduces the optimisation of $||W_e(T_o - W_{ref})W_i||_\infty$ signal seen in Figure 3.4 (Skogestad & Postlethwaite, 2005). This signal is the difference between the ideal and real closed loop system which is used to optimise for the desired performance of the system within the frequency domain (Gu et al., 2013). This allows for shaping responses within the time and frequency domain within the closed-loop system which can be used to obtain the desired handling qualities and time response characteristics (Biannic et al., 2017). In addition, obtaining a robust controller by constraining S_oG,T_i for input disturbance rejection and S_o,KS_o for output disturbance rejection as well as managing stability constraints thought the sensitivity S_i,S_o and co-sensitivity T_i,T_o for the inputs and output respectively (Jeong et al., 2012; Seiler et al., 2020) The limitation of mixed sensitivity is that it only provides robustness guarantees at

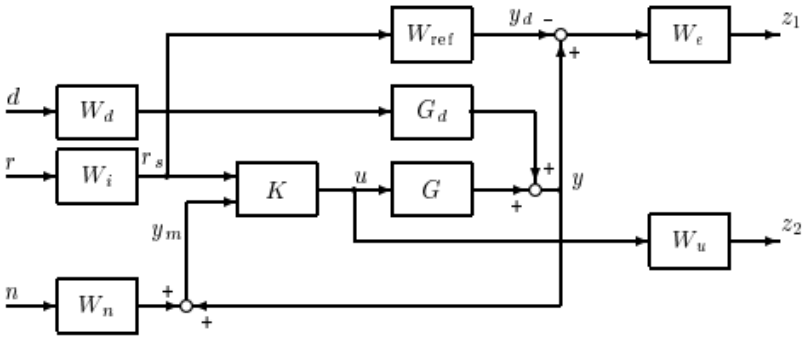

Figure 3.4: A signal-based H_∞ control design (Skogestad & Postlethwaite, 2005)

the plant input or output using standard methods for K/KS, S/T/KS and model following H_∞ optimisation. In addition, to a skewed robustness at the plant input or output which causing problems with a lightly damped oscillatory behaviour like the phugoid mode for helicopters. The optimisation exploits the fact that there is no disturbance at the plant input which can excite plant poles which tries to cancel the feedback path from the output disturbance to the plant input with zero. This can be a problem when the optimisation of the controller performs pole-zero cancellation, the cancellation results in poor robust stability properties (Bates & Postlethwaite, 2002). Although, a more balanced optimisation using the 4-block mixed sensitivity method using signals $w = \begin{bmatrix} d_i^T & d_o^T \end{bmatrix}^T$ to obtain Equation 3.4 which is shown in subsection 3.2.2 which prevents pole-zero cancellation within the optimisation of controller K seen in H_∞ loop shaping designs.

$$T_{w\to z} : \begin{bmatrix} d_o \\ d_i \end{bmatrix} \to \begin{bmatrix} z_1 \\ z_2 \end{bmatrix} = \begin{bmatrix} -W_1 e \\ -W_2 u \end{bmatrix} \quad K = \arg\min \left\| \begin{bmatrix} W_1 S_o & W_1 S_o G \\ W_2 K S_o & W_2 K S_o G \end{bmatrix} \right\|_\infty \tag{3.4}$$

3.2.2. Loop Shaping Design Procedure

The Loop Shaping Design Procedure (LSDP) is a method that uses the same principles as mixed sensitivity, where the controller K minimizes the H_∞ norm for signals w to z. The approach varies depending on the signals w and z, weighting functions W, and control structure through the optimization method. The main difference between the two methods is that the mixed sensitivity method tunes the closed-loop behaviour, while LSDP tunes the open-loop behaviour. This is achieved by using the sensitivity transfer functions $S_o = (I - GK)^{-1}$ and $T_o = (I - S_o)$. The LSDP involves two main steps:

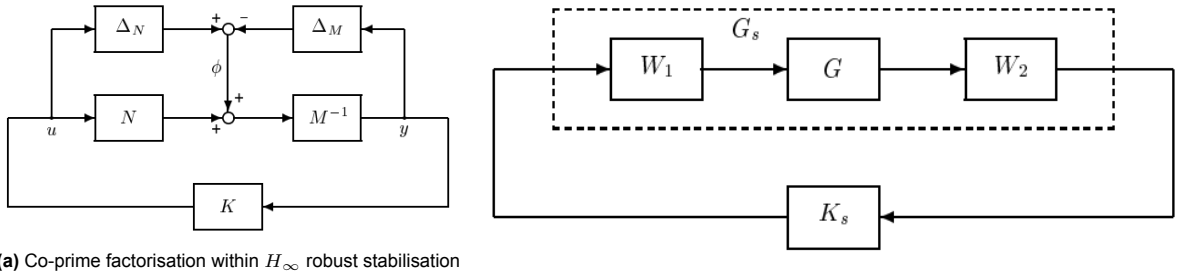

(a) Co-prime factorisation within H_∞ robust stabilisation problem

(b) The shaped plant and controller

Figure 3.5: H_∞ optimization using the loop shaping design procedure (Skogestad & Postlethwaite, 2005)

open-loop shaping using pre/post-compensators W_1 and W_2, and the K_s H_∞ controller synthesis for G_s. The open loop is dynamically shaped using W_1. The loop shaping uses $\overline{\sigma}(GK)$ and $\underline{\sigma}(GK)$ as the upper and lower bounds of singular values, where the pre-compensator is treated as part of the controller $K = W_1$, as shown in Figure 3.6. The open-loop shape of GW_1 is designed using integral action and high gain at low frequencies of singular values of $\underline{\sigma}(GK)$ achieved by using a proportional-integral weight (Toscano, 2013). The $\underline{\sigma}(GK) >> 1$ at low frequencies provides attenuation towards output disturbance signals at the plant output for good reference tracking (Bates & Postlethwaite, 2002). In addition, robust stability to additive output uncertainty also requires $\frac{1}{\underline{\sigma}(G)} << 1$ to be small at those

frequencies which can not be set by the designer and is limited by the design of the vehicle its self. At the cross-over frequencies, phase advancing is used to reduce roll-off rates of about 20 dB/decade for a desired bandwidth achieved through a lead-lag filter. At high frequencies, low gain is required for noise rejection and insensitivity to neglected fast dynamics, achieved using a low-pass filter, resulting in $\overline{\sigma}(GK) << 1$. This provides robust stability to output multiplicative uncertainty at higher frequencies. The same can be done when shaping $\sigma(KG)$ for corresponding robust stability to input uncertainty so that $\underline{\sigma}(KG) >> 1$ at low frequencies and $\overline{\sigma}(KG) << 1$ at high frequencies. These functions are the components used to shape the open-loop system for W_1. Furthermore, within this shaping procedure, pole-zero cancellations can be avoided when designing W_1 (Skogestad & Postlethwaite, 2005). W_2 is chosen reflecting the relative importance of the output channels as a diagonal matrix.

$$G_s = W_2 G W_1 = M_s^{-1} N_s \tag{3.5}$$

$$\gamma_{min} = \frac{1}{\sqrt{1 - || \begin{bmatrix} N_s & M_s \end{bmatrix} ||_H^2}} < \gamma = \left\| \begin{bmatrix} K_s \\ I \end{bmatrix} (I - G_s K_s)^{-1} M_s^{-1} \right\|_\infty = \left\| \begin{bmatrix} K_s S_s & K_s G_s S_s \\ S_s & G_s S_s \end{bmatrix} \right\|_\infty = \left\| [\phi] \rightarrow \begin{bmatrix} u_s \\ y \end{bmatrix} \right\|_\infty \tag{3.6}$$

Before moving towards the controller synthesis step, the minimum achievable robustness margin can be calculated for the controller to be synthesised for K_s using Equation 3.6 for the coprime factor singular value robustness γ derived from the robustness analysis. This optimisation function is similar to the 4-block mixed sensitivity when optimising for $w = \begin{bmatrix} d_i^T & d_o^T \end{bmatrix}^T$ instead of $w = \begin{bmatrix} \phi \end{bmatrix}$ in the LSDP in which the weighting function is integrated into the open-loop transfer function instead of the closed-loop. As seen this method allows for the level of robustness to be predicted with no γ iteration seen in mixed-sensitivity methods to find the control solution. After, γ_{min} meets the robustness requirements which are derived using robust analysis of uncertainty within the system. The controller K_s is synthesised using the H_∞ norm for signals w to z with the control structure as shown in Figure 3.6 with a command filter $K_s(0)W_2(0)$ ensures a steady state gain of 1 between r and y. The variations of the method

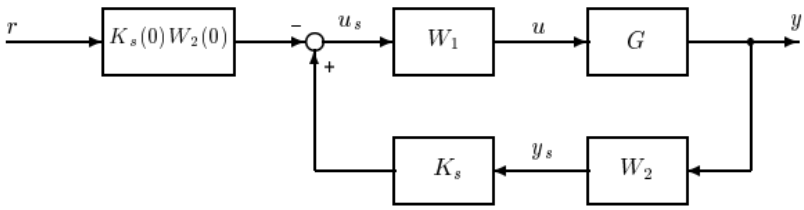

Figure 3.6: Implementation of H_∞ loop-shaping controller (Skogestad & Postlethwaite, 2005)

include 2 DoF and observer-based loop shaping controllers. In the 2 DoF case the LSDP is extended with the model following which is added to allow optimisation between the ideal response T_{ref} and the real system response using $w = \begin{bmatrix} r^T & \phi^T \end{bmatrix}^T$ and $z = \begin{bmatrix} u_s^T & y^T & e^T \end{bmatrix}^T$. As shown in Figure 3.7a and Equation 3.7, the scalar value ρ is used to weigh the performance of the ideal response over the robustness. This allows for shaping responses within the time and frequency domain within the closed-loop system which can be used to obtain the desired handling qualities and time response characteristics (D. J. Walker & Postlethwaite, 1996). Furthermore, reducing $\rho \rightarrow 0$, simplifies the H_∞ control problem to a standard LSDP as seen in Equation 3.6. The same steps of the LSDP are used with the addition of tuning the ideal closed-loop response T_{ref} and its constant diagonal weight matrix ρI. The $W_i = (W_o(I - G_s(0)K_2(0))^{-1} G_s(0) K_1(0))^{-1} T_{ref}(0)$ is to make the closed-loop transfer function from r to the controlled outputs $W_o y$ match the desired model T_{ref} at steady state with $W_o = I$ if there are no extra feedback measurements which need to be controlled (Skogestad & Postlethwaite, 2005).

$$\gamma_{min} < \gamma = \left\| \begin{bmatrix} \rho(I - K_2 G_s)^{-1} K_1 & K_2 (I - G_s K_2)^{-1} M_s^{-1} \\ \rho(I - G_s K_2)^{-1} G_s K_1 & (I - G_s K_2)^{-1} M_s^{-1} \\ \rho^2((I - G_s K_2)^{-1} G_s K_1 - T_{ref}) & \rho(I - G_s K_2)^{-1} M_s^{-1} \end{bmatrix} \right\|_\infty \tag{3.7}$$

The control structure can also be extended using a linearised plant observer as part of the control structure when synthesising the H_∞ controller. This observer-based control structure allows for state

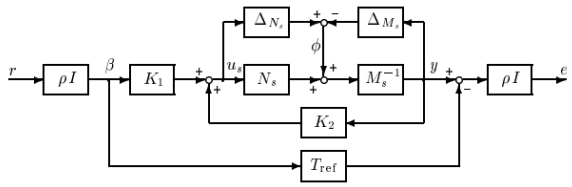

(a) Two degrees of freedom H_∞ loop shaping design problem

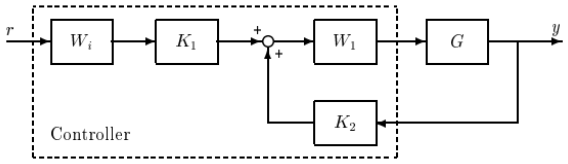

(b) Two degrees of freedom H_∞ loop shaping controller

Figure 3.7: Control architecture for the synthesised H_∞ loop shaping controller (Skogestad & Postlethwaite, 2005)

feedback control of the shaped plant as shown in Figure 3.8 for both degrees of freedom controllers. In addition, this control scheme has advantages when implemented using gain-scheduling as the derived gain H_s and K_s or F_s & F_r which are the solutions to the H_∞ control problem that smoothly varies with the operating point and the stability margin γ for the plant G_s (Bates & Postlethwaite, 2002). This is because although plant G may vary with scheduled variables at different operating, the open-loop can be shaped to achieve similar G_s which results in consistent performance and robustness when gain-scheduling synthesised H_∞ controllers (Civita et al., 2003).

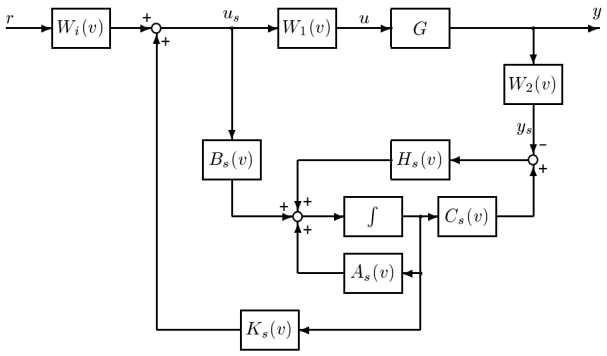

(a) An implementation of an H_∞ loop shaping controller for use when gain scheduling against a variable v

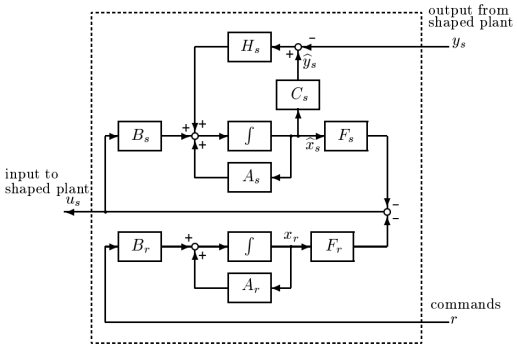

(b) Structure of the two degrees of freedom H_∞ loop shaping controller

Figure 3.8: H_∞ loop shaping controller with an observer-based control structure (Skogestad & Postlethwaite, 2005)

3.2.3. μ Synthesis

The μ controller synthesis method is used to minimize a set of transfer functions H_∞ norm using the controller K and combining it with μ synthesis, a robust analysis method. This is done for signals w to z and weighing functions W. The key difference between the μ controller synthesis and other H_∞ methods is that it uses the μ analysis to optimize for plant structured uncertainty expressed in Figure 3.9, and to optimize for unstructured uncertainty using the sensitivity functions in $T_{w\to z}$. The control synthesis method iterates between two different optimizations, the mixed sensitivity controller optimization K, and the optimization of the D scales which minimize the μ value as seen in Equation 3.8.

$$K = \arg\min ||DT_{w\to z}D^{-1}||\infty \quad D = \arg\min ||DTw \to zD^{-1}||_\infty \tag{3.8}$$

$$\mu(M) = \frac{1}{\min(k_m | \det(I - k_m M\Delta) = 0 \text{ for structured } \Delta, \overline{\sigma}(\Delta) < 0)} \quad \mu(T_{w\to z}) \leq \min_{D\in\mathcal{D}} \overline{\sigma}(DT_{w\to z}D^{-1}) \tag{3.9}$$

The D scales are transfer function diagonal matrices that are invertible and transform the nominal model M, which is the system in Figure 3.7. The transformation allows for the optimization of the singular structured value μ shown in Equation 3.9 (Skogestad & Postlethwaite, 2005). This method of synthesizing a μ-based controller is called the DK-iteration and is performed as follows:

1. **K-step.** Synthesize an H_∞ controller for the scaled problem $K = \arg\min ||DT_{w\to z}D^{-1}||_\infty$ with fixed $D(s)$.

2. **D-step.** Find $D(j\omega)$ to minimize at each frequency $\overline{\sigma}(DT_{w\to z}D^{-1})$ with fixed $T_{w\to z}$.
3. Fit the magnitude of each element of $D(j\omega)$ to a stable and minimum-phase transfer function $D(s)$ and go to Step 1 when iterating.

The μ controller is used to synthesize controllers for helicopters in research to account for variations in parameters, through structured uncertainty analysis. This allows for robust controllers to be synthesized that are robust against varying flight conditions using the multi-model design approach. In this approach, the structured uncertainty is used to vary the nominal model, and the controller is designed for the worst-case condition shown in Figure 3.3c. In addition, the model following transfer functions in $T_{w\to z}$ can be optimized through the K-step to obtain desired time and frequency domain response characteristics and other mixed sensitivity transfer functions shown in Table 3.1 to optimize for other factors included in the previous H_∞ methods H_∞ methods (Ma et al., 2015).

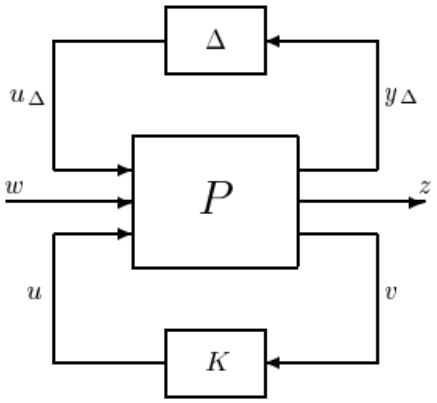

Figure 3.9: General control configuration for controller synthesis and uncertainly analysis (Skogestad & Postlethwaite, 2005)

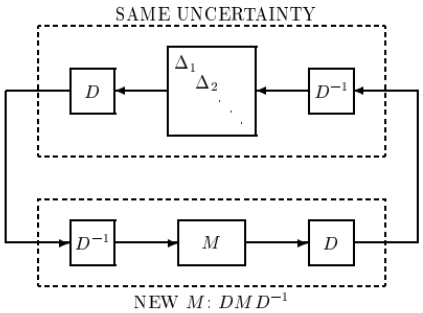

Figure 3.10: Use of block-diagonal scalings $\Delta D = D\Delta$ (Skogestad & Postlethwaite, 2005)

3.3. Other Robust Control Methods

Although H_∞ control is known for its guaranteed performance and robustness, there are other methods and variations that can also be robust. Unlike standard H_∞ control, which optimizes robustness through structured and unstructured uncertainty, there are other methods that can establish similar trade-offs between robustness and performance. These methods may not be as straightforward in terms of optimization as they introduce other norms and constraints, but they offer certain benefits in control system design for implementation on helicopters. Additionally, there are H_2 optimization methods that use the H_2 norm, as shown in Equation 3.10, to optimize the transfer function $T_{w\to z}$ in terms of a white noise input $w(t)$. The H_2 optimization methods minimize the root-mean-square of the z/w signals.

$$||T_{w\to z}||_2 = \sqrt{E(w(t)w(t)^T)} \tag{3.10}$$

$$\mathcal{J} = \frac{1}{2}\int_0^\infty (x^T Q x + u^T R u)dt \quad R = R^T > 0 \quad Q = Q^T > 0 \tag{3.11}$$

Furthermore, the H_2 norm is used in linear quadratic (LQ) control of helicopters to meet handling requirements using Equation 3.11 (Kumar et al., 2008). This approach requires access to the states of the system, which are estimated using a Kalman filter or a state observer. Although LQ control can be made robust to model uncertainty, noise, and disturbances through design iteration of R and Q using loop transfer recovery (LTR) procedures required to recover the robustness in the output when introducing the Kalman filter, it may be limited by the presence of non-minimum phase zeros or lightly damped systems (Skogestad & Postlethwaite, 2005). These limitations can affect the performance and robustness of the LQ controller design. The result is a design procedure that indirectly shapes KG or GK and can be used to optimize for robustness against plant input or output uncertainty.

The optimization of the set of transfer functions $T_{w\to z}$ can be divided into individual transfer functions $T_{w_i\to z_i}$. These individual stacked transfer functions can then be optimized separately using a combination of H_2 and H_∞ norms. This approach can be used to perform multi-objective control synthesis designs on helicopters, in which transfer functions have separate requirements that need to be optimized (Marantos et al., 2013). This variation of the mixed sensitivity method is called robust mixed H_2/H_∞ control.

The methods which use linear matrix inequality (LMI) based approaches can similarly be used to perform multi-objective control synthesis by adding constraints onto the LMI during optimization. The constraints can be formulated to constrain the pole-zero location and controller structure (Silva et al., 2020). The main benefit of this approach is that the pole-placement requirements can be defined as part of the optimisation.

3.4. Previous Research & Literature

When designing and performing research on helicopter control systems, it is important to consider practical aspects and account for system control requirements. The driving control requirements must be incorporated into the preliminary design of control systems for helicopters, which are subjected to model uncertainty due to varying flight conditions and unknown complex aerodynamics. The research on robust control of helicopters focuses on its implementation using small UAVs and test benches, with stability requirements and model uncertainty being the core subjects within the literature. Additionally, data is available on existing helicopter designs to model and test different controller designs, with handling qualities requirements being added to show the feasibility of implementation. Depending on the fidelity of the helicopter model, design objectives for the controller, and control architecture, the resulting controller design within the literature may differ. An overview of the literature to be discussed is shown in Table 3.2.

Table 3.2: Overview and key information of papers which apply robust control methodology on to helicopters

Reference (Author,year)	Method	Analysed Uncertainties	Tracked Responce
(Marantos et al., 2013)	mixed H_2/H_∞	· wind velocity	· Position control · Attitude control
(Kumar et al., 2008)	LQR	-	· Attitude control
(Ma et al., 2015)	μ systhesis	· Actuator output	· Attitude control
(Civita et al., 2003)	LSDP	-	· Attitude control · Velocity control
(D. J. Walker & Postlethwaite, 1996)	LSDP	-	· Attitude control
(Luo et al., 2003)	Mixed Sensitivity & LQR/H_2	-	· Attitude control
(Ayush et al., 2020)	Mixed Sensitivity	-	· Attitude control
(Khalid et al., 2017)	LSDP	-	· Atttude control
(Guarnizo et al., 2010)	μ systhesis	· Multiplicative plant output	· Attitude control

(D. Walker, 2003)	Mixed Sensitivity	-	· Attitude control
(Ji & Wu, 2011)	Mixed senitivity & LSDP	-	· Velocity control · Attitude control
(Trentini & Pieper, 2001)	mixed H_2/H_∞ & LQR/H_2	· High/Low frequency plant mismatch · actuator dynamics · rotor mast flex mode · Sensor dynamics	· Attitude control
(Biannic et al., 2017)	LMI	· Velocity · Mass · Centre of Gravity locations	· Attitude control
(Panza & Lovera, 2014)	LMI	· Multiplicative plant output · Flight envelope (altitude/velocity)	· Attitude control
(Horn et al., 2012)	LQR/H_2	-	· Attitude control
(Jeong et al., 2012)	Mixed Sensitivity	· Additive plant input	· Attitude control
(Horn et al., 2012)	LQR/H_2	-	· Attitude control
(Takahashi, 1994)	Mixed Sensitivity	-	· Attitude control
(Saetti & Horn, 2017)	LQR/H_2	-	· Attitude control

3.4.1. Model Fidelity

The model fidelity used in this literature can be as simple as 2 or 3 degrees of freedom motion tested using test benches that simulate the gyroscopic and coupling effects of helicopters (Ayush et al., 2020; Guarnizo et al., 2010; Khalid et al., 2017). These models test the practical implementation aspects of the control method when subjected to uncertainties within the hardware. These models neglect the translational body and rotor dynamics but are used in research to test the feasibility of implementation in terms of attitude control. This model does not resemble the dynamics of the entire helicopter but only simulates one of the contributing factors that impact helicopter control. The model can be extended to 6 degrees of motion for translational and rotational control, which linearizes the stability derivatives for a quasi-steady flow (Biannic et al., 2017; Trentini & Pieper, 2001). The 6 degrees of motion fidelity models are the minimum used to assess the handling quality requirements used to research the feasibility of implementing H_∞ controllers on helicopters. This is done primarily through system-identified models of existing helicopters and incorporating structured uncertainties to analyze controller robustness against model mismatches. These mismatches are caused by neglecting the flapping motion and changes in the inflow on the rotor. The high-fidelity models include multiple degrees of motion, which extends the model further into the rotor dynamics and airflow around the rotor. This is done for 9 DoF state models which have the rotor states and can go up to 67 states, including the actuator, mast flexing, and corrected high/low frequency obtained through experimental results. In addition to changes in the dynamics due to inflow and blade flapping (D. Walker, 2003) (Ji & Wu, 2011). These additional states can also be utilized by the H_∞ controller using rotor state feedback control to increase the margins for the trade-off between robustness and performance (Horn et al., 2012; Panza & Lovera, 2014).

3.4.2. Control Objectives

The objectives of the helicopter controller vary with the available tools and models, depending on the research topic. The minimal motion models for helicopters using test benches primarily focus on stability objectives and control methods that stabilize the non-linear rotational coupling of twin rotor systems. The objectives are measured through response characteristics, although the benchmark against which performance is assessed through this is open to interpretation. The focus of literature that uses 2-3 degrees of freedom models of motion is to implement the robust controller using the model design, controller in continuous time, and the physical setup to test practical aspects. This introduces problems related to discretization/sampling with uncertainty within the hardware. This approach is also seen in the

literature that uses small unmanned aerial vehicles with helicopter configurations. In addition to stability, handling quality requirements are also used to assess performance in terms of the ADS-33 (Jeong et al., 2012). However, only key handling quality requirements are chosen based on their relevance to the research on a case-by-case basis. These requirements are considered in the preliminary phases of the control system design of helicopters due to their importance to the pilot's controllability of the system (Tischler et al., 2017). Furthermore, existing models of the helicopter can be used to design robust controllers, verifying them using non-linear models, and experimentally validating their performance to research the feasibility of designing a robust controller (D. Walker, 2003).

The main objective of the research in the literature is to design an attitude control system and/or SCAS for helicopters, which can be extended to include velocity and position tracking controllers. This can be achieved through a variety of control architectures. The elements of the control architecture for helicopters can also go through design iterations, including notch filters to avoid signal amplification at set frequencies, command modeling to smooth out control inputs, and decoupling controllers to decouple the dynamics of the helicopter (Tischler et al., 2017). This structure is also designed on a case-by-case basis depending on the research and the fidelity of the model used. An example of this is rotor state feedback used on helicopters, which use a model-following structure to incorporate the rotor states (Horn et al., 2012; Takahashi, 1994). This structure uses an inverted plant to decouple dynamics in which the controller is used as a robust compensator, as shown in Figure 3.11. This structure is used for rotor load alleviation controller design and is used in conventional helicopter control system design (Saetti & Horn, 2017; Tischler et al., 2017). However, research using mixed sensitivity and LSPD uses straightforward control structures with different degrees of controller centralization, as the control problem can be split from a single MIMO system into smaller ones by looking at signal-based control (D. Walker, 2003). Another control structure used in conventional helicopter control is a cascaded control structure that uses attitude to control velocity and velocity to control position. These control structures are more transparent and simple than complex centralized full-order controllers, but these structures also limit the performance by decoupling the control systems (Tischler et al., 2017).

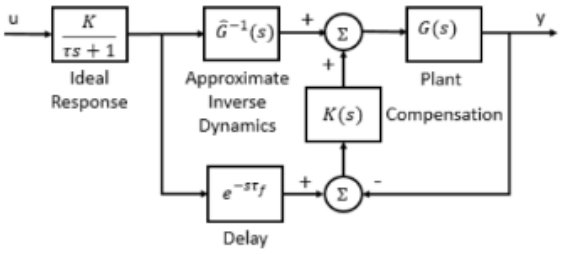

Figure 3.11: Explicit Model Following (Saetti & Horn, 2017)

The nominal models can be analysed through structured uncertainty in which parameters and signals can vary in the real system. This allows the controller to be assessed regarding robustness to certain variations. The robustness analysis used in the literature is signal and parametric uncertainty. The signal uncertainty which describes plant input and output signal uncertainty can represent mismatches between the actual and real signals. This is done to take into account unknown actuator dynamics at the input and disturbances/biases at the output (Panza & Lovera, 2014) (Jeong et al., 2012). Parametric uncertainty is used to schedule individual controllers over the flight envelope to make the controller robust against a bounded range of velocities and altitude. In addition, to check whether the controller synthesised is robust against plant uncertainty and changes in flight conditions (Panza & Lovera, 2014). This analysis is limited by the number of varying flight conditions analysis which is correlated to the complexity of the control problem and the fidelity of the model.

3.4.3. Conclusion

The literature review summarizes the basic concepts and previous research on robust control of helicopters. The controller are asses through handling quality and stability requirements standardized using the ADS-33 specifications for military rotorcraft. Robust control methods, including H_∞ based methods, can optimize the controller to meet the requirements under the uncertainty of the model. The three primary methods discussed for helicopters are mixed sensitivity, loop shaping design procedure,

and μ synthesis. Other methods, such as linear quadratic control and mixed norm methods, also use H_2 optimization. More complex methods can directly solve the controller with the requirements by incorporating the constraints into the Linear Matrix Inequality (LMI) optimization. The primary difference is that H_∞ methods minimize the H_∞ norm, while H_2 methods minimize the root-mean-square of the signal.

The literature provides limited information on the completion of handling requirements used as benchmarks for designing a control system for helicopters. Factors such as model fidelity, control structure, and requirements used impact the performance of the controller and the complexity of the control problem that needs to be solved. Finally, the uncertainty analysis of the nominal model for the helicopter in the literature is limited by the number of uncertain variables and the fidelity of the model used. Due to this, papers show limited use of structured uncertainty analysis and its effect on the control system design in terms of control architecture and model fidelity limitations.

3.4.4. Research Gap and Contribution

The literature discussed provides handling requirements as benchmarks for designing a control system for helicopters (Antonioli et al., 2014; Dai et al., 2014; Srinathkumar, 2019). Additionally, accounting for model uncertainty (Ji & Wu, 2011; Tijani et al., 2011) in control design for helicopter models is another criterion considered in the literature. Furthermore, the model fidelity, control structure, and requirements discussed impact the performance of the controller and the complexity of the control problem that needs to be solved. Finally, the uncertainty analysis of the nominal model for the helicopter in the literature is limited by the number of uncertain variables and the fidelity of the model used. Due to this, papers show limited use of structured uncertainty analysis and their effect on control system design in conjunction with the completion of other objectives, like the handling quality requirements, using multi-objective approaches.

For these reasons, this study introduces a methodology based on a multi-objective approach using closed-loop transfer functions to design for robustness (Skogestad & Postlethwaite, 2005). Reference models are used to enforce HQ objectives. In this approach, a structured control design combines feedback control for stability and robustness against uncertainties with feedforward control to achieve the necessary HQ objectives. The design method is applied to an agile helicopter vehicle (MBB Bo-105) known for its unstable dynamics, posing a challenging control problem. This study addresses the limitations imposed by handling quality requirements combined with robustness against uncertainty, offering additional insights into the robust control of open-loop unstable helicopter vehicles. Structured control is used, allowing the method to be applied using a variety of control architectures. This approach reduces manual intervention and implementation difficulty while meeting control objectives. To achieve this, design objectives leverage the properties of the H_∞ norm in the constraints between the reference models and the actual system response, minimum disk-based stability margins, and minimization of disturbances at the input/output (I/O) to the control signal and measured output of the plant.

To obtain a clear purpose and define the structure of the research, the research objective and its research questions are formulated as follows:

Research Objective

To investigate the effects of uncertainties in the rotor dynamics onto longitudinal helicopter dynamics and control by explicitly modelling the model uncertainty of the rotor dynamics on the helicopter model and analysing the robustness of the synthesised controller.

Research Questions

- **RQ-1:** How can the uncertainties within the rotor dynamics be modelled?
  - **RQ-1.1:** Which parameters within the rotor dynamics are uncertain?
  - **RQ-1.2:** What is the uncertainty bound of these parameters?
  - **RQ-1.3:** How does the uncertainty in the rotor dynamics affect the helicopter dynamics?
- **RQ-2:** Does the uncertain rotor dynamics affect the robustness and performance of the synthesised robust controller?
  - **RQ-2.1:** Which elements of the controller are affected by the uncertain rotor dynamics?
  - **RQ-2.2:** How do the uncertain rotor dynamics affect the handling qualities of the helicopter?
  - **RQ-2.3:** How do the uncertain rotor dynamics affect the robustness of the controller?

4

Longitudinal Helicopter Model

The non-linear analytical helicopter vehicle model used in this study is provided and validated by (Pavel, 1996), with the results being utilized throughout the research. The helicopter vehicle's dynamics are described by a nonlinear 3-degree-of-freedom model, operating at a fixed altitude and subsonic air speeds. This model is defined by a set of analytical nonlinear equations, as shown in section 4.1, where the assumptions underlying the model are also discussed, along with an approximation of the actuator dynamics. Subsequently, the non-linear set of equations is trimmed and linearized to match the Bo-105 specifications detailed in the Appendix A (Pavel, 1996). The properties of the open-loop dynamics, are discussed in terms of stability and controllability in section 4.2.

4.1. Non-linear flight dynamics

The non-linear model consists of symmetrical non-linear airframe dynamics and a linear second-order actuator model. These models are valid for a flight envelope defined by airspeed and altitudes, approximately ranging from $0 \leq V \leq 70\,\mathrm{m/s}$ and $0 \leq h \leq 5000\,\mathrm{m}$ (Heffley, 1979; Pavel, 1996). The equations for the airframe are modeled with respect to the states in the body coordinate frame shown in Figure 4.1. To obtain the angle of attack (AoA) α and airspeed V.

$$\alpha = \arctan\left(\frac{w}{u}\right) \quad V = \sqrt{u^2 + w^2} \quad \gamma = \theta - \alpha \tag{4.1}$$

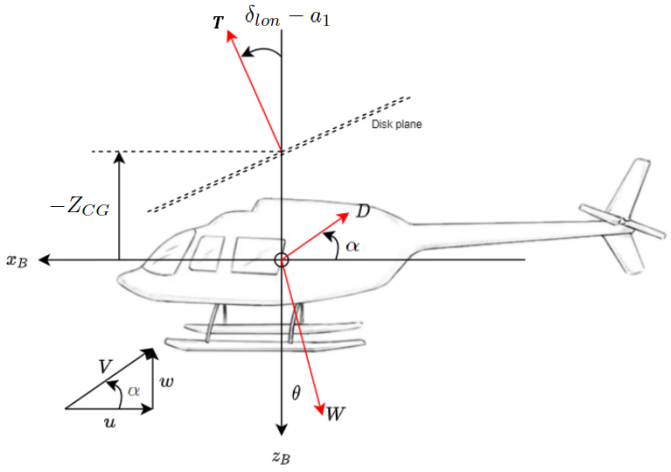

Figure 4.1: Diagram of 3-DoF longitudinal helicopter in body frame (Maurer, 2023)

Assuming that the main rotor is the primary significant contributor to helicopter controls, the angle of attack (AoA) of the rotor disk and the non-dimensional velocities can be computed with respect to the rotor disk.

$$\alpha_c = \delta_{lon} - \alpha \quad \lambda_c = \frac{V}{\Omega R}\sin(\alpha_c) \quad \hat{\mu} = \frac{V}{\Omega R}\cos(\alpha_c); \tag{4.2}$$

For this simple helicopter model, only approximations of the contributions to the longitudinal rotor flapping a_1 are modeled in steady state (Pavel, 1996). In this model, the rotor blades are assumed to be stiff and free to rotate around the rotor hub. This neglects contributions from blade bending and other rotor disk flapping modes, although the longitudinal flapping mode is the key contributor to the longitudinal helicopter dynamics.

$$a_1 = \frac{\frac{8}{3}\hat{\mu}\delta_{col} - 2\hat{\mu}(\lambda_c + \lambda_i) - \frac{16q}{\gamma_l \Omega}}{1 - \frac{1}{2}\hat{\mu}^2} \quad \gamma_l = \frac{\rho C_{l_\alpha} c R^4}{I_b} \tag{4.3}$$

Similarly, using element blade theory and the Glauert method, an approximation of the thrust coefficient C_T can be made. This is done by trimming and solving for the inflow state, which can be denoted as λ_i, so that both Equation 4.4 and 4.5 are equal. Equation 4.5 assumes that the flow conditions to the rotor is around hover with minimal flow contributions perpendicular to the rotor plane. In addition, to Equation 4.4 with is an approximation assumes no blade twist and a linear relationship between lift force and AoA for the rotating rotor blade.

$$C_T^{elem} = \frac{C_{l_\alpha}\sigma}{4}\left[\frac{2}{3}\delta_{col}(1 + \frac{3}{2}\hat{\mu}^2) - (\lambda_c + \lambda_i)\right] \tag{4.4}$$

$$C_T^{glau} = 2\lambda_i\sqrt{\left[\frac{V}{\Omega R}\cos(\alpha_c - a_1)\right]^2 + \left[\frac{V}{\Omega R}\sin(\alpha_c - a_1) + \lambda_i\right]^2} \tag{4.5}$$

The thrust force of the rotor and the drag of the main airframe are assumed to be the two primary forces that dictate the helicopter dynamics. This assumption ignores the rotor hub drag force and the aerodynamic tail forces.

$$T = C_T^{elem}\rho(\Omega R)^2\pi R^2 \tag{4.6}$$

$$D = \frac{1}{2}\rho V^2 C_D S \quad C_D S = F_0 \tag{4.7}$$

This results in the sum of forces in the body reference frame shown in Figure 4.2b, for the forces in Equation 4.8.

$$\begin{bmatrix} X \\ Z \\ M \end{bmatrix} = \begin{bmatrix} -D\cos(\alpha) + T\sin(\delta_{lon} - a_1) \\ -D\sin(\alpha) - T\cos(\delta_{lon} - a_1) \\ T(-Z_{CG}\sin(\delta_{lon} - a_1) + X_{CG}\cos(\delta_{lon} - a_1)) \end{bmatrix} \tag{4.8}$$

Using the three degree-of-freedom equations in addition to the trim condition of the inflow parameter gives the non-linear Equation 4.9 in the form $\dot{x} = f(x, u)$.

$$\begin{bmatrix} \dot{u} \\ \dot{w} \\ \dot{q} \\ \dot{\theta} \\ \dot{\lambda}_i \end{bmatrix} = \begin{bmatrix} \frac{X}{m} - g\sin(\theta) - qw \\ \frac{Z}{m} + g\cos(\theta) + qu \\ \frac{M}{Iyy} \\ q \\ \frac{C_T^{elem} - C_T^{glau}}{\tau_{\lambda_i}} \end{bmatrix} \tag{4.9}$$

The actuator system has been characterised by second-order models as approximations the limited control bandwidth in the frequency domain. The swash plate connects the main rotor controls to the actuator as shown in Figure 4.2a. Due to this all inputs use the same set of actuators using the swash-plate. (Bouwer & Hilbert, 1986) approximated the actuators for the Bo-105 as a second-order model $\frac{2526.6}{s^2+95.5s+2526.6}$ using $\omega_n = 50.265$ and $\zeta = 0.95$.

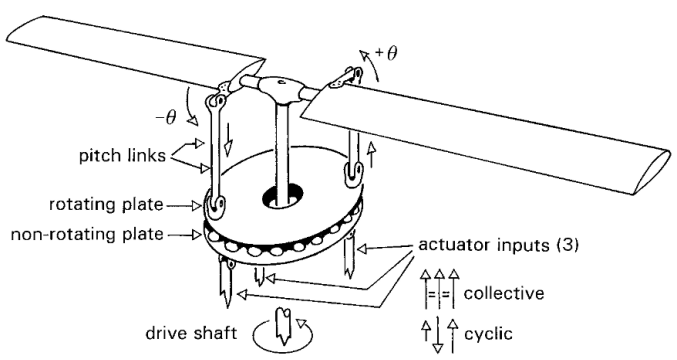

(a) Helicopter control using the swashplate (G. D. Padfield, 2008)

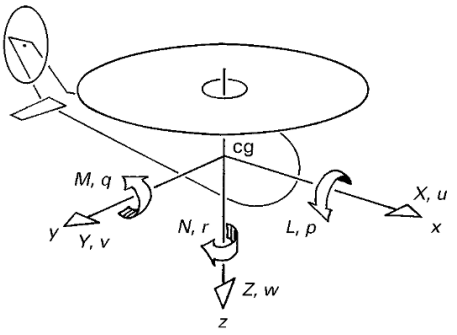

(b) Illustration of the body reference system (G. Padfield & Safari, 2018)

Figure 4.2: Illustration of the body reference system and helicopter controls

The following control allocation scheme used in Equation 4.10 with the following approximation of the saturation limits described in Table 4.1 taken from (Voskuijl et al., 2010).

$$G_{act}: \quad \begin{bmatrix} \delta_{col} \\ \delta_{lon} \end{bmatrix} = \begin{bmatrix} \frac{2526.6}{s^2+95.5s+2526.6} & 0 \\ 0 & \frac{2526.6}{s^2+95.5s+2526.6} \end{bmatrix} \begin{bmatrix} \delta_{col,cmd} \\ \delta_{lon,cmd} \end{bmatrix} \tag{4.10}$$

Table 4.1: Actuator Saturation Limits

States	δ_{max}	δ_{min}	$\pm\dot{\delta}_{max}$
δ_{col}	15.0	−0.2	16.0
δ_{lon}	11.0	−6.0	28.8

4.2. Linearized flight dynamics

The model can be analyzed by linearising the non-linear helicopter model using classic Jacobian numerical linearization methods for simplicity. This approach has implications for linear analysis on a point-by-point basis. The linearization method is constrained by steady-state equilibrium points, necessitating stability of the states at operating points. In trimming the longitudinal helicopter model, we assume steady-state horizontal flight to simplify the process and ensure stability in finding the operating point. The unknown states described in Table A.1 are then solved for.

Table 4.2: Linearization and operating point determination for steady-state horizontal flight

States	Known	Steady-state	Set to zero	Sol. at $h = 0\,\mathrm{m}, V = 20\,\mathrm{m/s}$
h	✓	✓	-	$0\,\mathrm{m}$
V	✓	✓	-	$20\,\mathrm{m/s}$
α		✓		$-0.8970\,^\circ$
γ	✓	✓	✓	$0\,^\circ$
u		✓		$20.6\,\mathrm{m/s}$
w		✓		$-0.3\,\mathrm{m/s}$
q	✓	✓	✓	$0\,^\circ/\mathrm{s}$
θ		✓		$-0.8970\,^\circ$
λ_i		✓		0.025
δ_{col}		✓		$6.3\,^\circ$
δ_{lon}		✓		$1.3\,^\circ$
$\dot{\delta}_{col}$	✓	✓	✓	$0\,^\circ/\mathrm{s}$
$\dot{\delta}_{lon}$	✓	✓	✓	$0\,^\circ/\mathrm{s}$

To verify the model for the longitudinal helicopter, the trim conditions can be reproduced from model validation in (Pavel, 1996). The trim results from the model inputs shown in Figure 4.3 for the steady-state swashplate configuration. For the unknown states in steady state, which are an output of the trimming procedure done using the $findop()$ function in MATLAB.

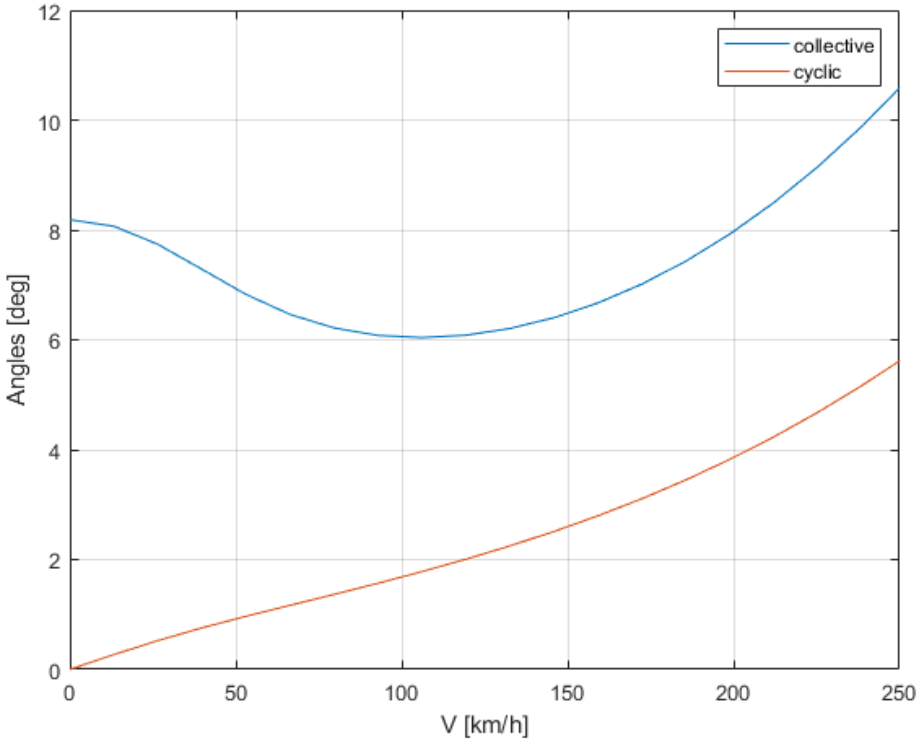

Figure 4.3: Trim curve of collective δ_{col} and cyclic δ_{lon} input at $h = 0\ [m]$ altitude for steady-state horizontal flight

Following the trimming and linearization, the derived linearized plant is shown in Equation 4.11. For these equations, the subscript zero (e.g., γ_0) denotes the trim conditions at the operating point using flight path γ_0, altitude h_0, and airspeed V_0 as input variables for trimming.

$$
G_{AF}: \quad
\begin{bmatrix} \dot{u} \\ \dot{w} \\ \dot{q} \\ \dot{\theta} \end{bmatrix} =
\begin{bmatrix} X_u & X_w & X_q - w_0 & -g\cos(\theta_0) \\ Z_u & Z_w & Z_q + u_0 & -g\sin(\theta_0) \\ M_u & M_w & M_q & 0 \\ 0 & 0 & 1 & 0 \end{bmatrix}
\begin{bmatrix} u \\ w \\ q \\ \theta \end{bmatrix} +
\begin{bmatrix} X_{\delta_{col}} & X_{\delta_{lon}} \\ Z_{\delta_{col}} & Z_{\delta_{lon}} \\ M_{\delta_{col}} & M_{\delta_{lon}} \\ 0 & 0 \end{bmatrix}
\begin{bmatrix} \delta_{col} \\ \delta_{lon} \end{bmatrix}
$$

$$
\begin{bmatrix} V_z \\ q \\ \theta \end{bmatrix} =
\begin{bmatrix} \sin(\theta_0) & -\cos(\theta_0) & 0 & u_0\cos(\theta_0) + w_0\sin(\theta_0) \\ 0 & 0 & 1 & 0 \\ 0 & 0 & 0 & 1 \end{bmatrix}
\begin{bmatrix} u \\ w \\ q \\ \theta \end{bmatrix}
\tag{4.11}
$$

The research focuses on the design of a Control Augmentation System (CAS) that tracks the attitude (ACAH) and vertical velocity command at a flight point specified by sea level altitude of $h = 0\,\mathrm{m}$ and an airspeed of $20\,\mathrm{m/s}$. In addition, to the application of the methodology to other flight points. The chosen outputs for the linear plant model are the vertical velocity velocity V_z $\mathrm{m/s}$, the pitch rate q $\mathrm{rad/s}$, and the pitch θ rad.

These outputs provide the basis for analyzing the system dynamics at the operating point described by Equation 4.12. The full linearization solution is shown in Appendix B for the unknowns in Table A.1.

$$G_{AF}: \quad \begin{bmatrix} \dot{u} \\ \dot{w} \\ \dot{q} \\ \dot{\theta} \end{bmatrix} = \begin{bmatrix} -0.025 & -0.0084 & 0.10 & -9.81 \\ 0.0016 & -0.99 & 20 & 0.15 \\ 0.0044 & 0.0036 & -0.29 & 0 \\ 0 & 0 & 1 & 0 \end{bmatrix} \begin{bmatrix} u \\ w \\ q \\ \theta \end{bmatrix} + \begin{bmatrix} -2.4 & 10.0 \\ -144.7 & 19.66 \\ 1.0 & -4.20 \\ 0 & 0 \end{bmatrix} \begin{bmatrix} \delta_{col} \\ \delta_{lon} \end{bmatrix} \tag{4.12}$$

$$\begin{bmatrix} V_z \\ q \\ \theta \end{bmatrix} = \begin{bmatrix} -0.015 & -1.0 & 0 & 20 \\ 0 & 0 & 1 & 0 \\ 0 & 0 & 0 & 1 \end{bmatrix} \begin{bmatrix} u \\ w \\ q \\ \theta \end{bmatrix}$$

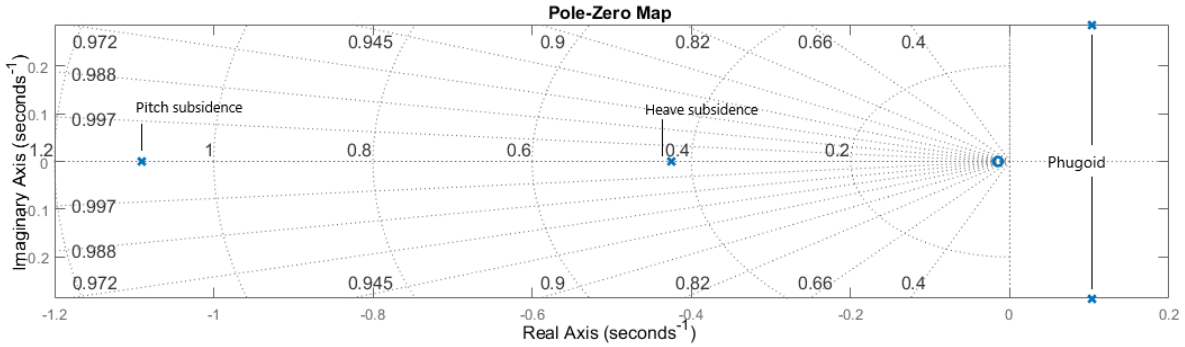

Figure 4.4: Open-loop pole-zero plot of longitudinal bare-frame helicopter model at $20\,\mathrm{m/s}$

The Bo-105 longitudinal helicopter was selected due to its well-known dynamic instability, which poses challenges and limitations to robustness in the design of control laws. An analysis of the Bo-105 bare airframe dynamics (Srinathkumar, 2015, 2019) shows that an unstable phugoid mode is present across most of the flight envelope. Additionally, there are local right-half-plane (RHP) zeros in the δ_{col} to V_z channel with zero pairs at $0.048 \pm 0.33i$, with the presence of a global zero near the marginal stability plane at -0.015 in all of the channels when linearizing, as shown Figure 4.4. This figure shows phugoid poles in the RHP at $0.1 \pm 0.29i$, as well as the vertical velocity and pitch subsidence in the stable left-half-plane at -0.43 and -1.1, respectively. The existence of these zeros and RHP poles introduces fundamental limitations on the level of performance and robustness that can be realized in the control system's design. RHP-zeros indicate an inverse initial input and output response characteristic observed in the time-domain step response. This characteristic of the system's initial reaction causes response delays or lag within the helicopter dynamics, which can be unfavorable from the perspective of a human operator due to its counterintuitive nature. It can impact the handling qualities and performance of the vehicle due to its control-disorienting properties. Therefore, control system design methodologies are applied to minimize their effect on the human operator with the addition of stabilising the system.

5

Flight Control Design

The application focuses on an attitude (ACAH) and vertical velocity control system using H_∞-based constraints for the multi-objective structured control synthesis. The inputs for the controller are vertical velocity and pitch errors, where pitch rate q is a regulated output. The commanded collective $\delta_{col,cmd}$ is the control signal for the vertical velocity V_z,channel, and the commanded longitudinal cyclic $\delta_{lon,cmd}$ is used for the pitch θ channel. To implement a linear design methodology, the nonlinear plant is linearized using Jacobian linearization from section 4.2. The linearization of the Bo-105 longitudinal model is based on an unstable open-loop steady-state equilibrium point.

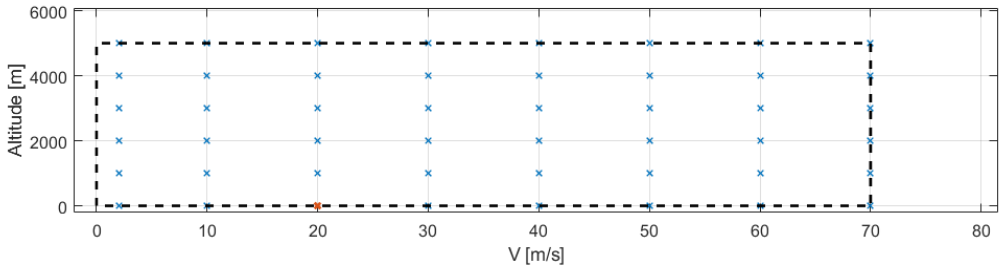

Figure 5.1: Linearized points in flight envelope (red: design point)

The flight dynamics of a helicopter change significantly with varying velocity and altitude through dynamic pressure and rotor dynamics. The most evident characteristic is the change in dynamics between hover to forward flight as indicated in Appendix B. Figure 5.1 shows the points in the flight envelope that are used for the design for which the $h = 0\,\mathrm{m}$ with $V = 20\,\mathrm{m/s}$ as the design point used as an example as the solution is both robust against the uncertainty and perform well in simulation. The structure of this chapter is as follows. The controller structure and design requirements are formalized and the resulting gain surfaces are shown in Figure 5.7 to Figure 5.9. In section 5.1, the general control structure and controller are discussed with the corresponding signals used for the structured H_∞ controller synthesis including constraints applied on signals for both hard stability constraints and soft optimisation constraints. The solution is discussed at the end of the section for which a linear analysis is done to assess the solution for the design point in section 5.2. Finally, the control solution at the design point is implemented for both linear and non-linear models to verify and compare the performance of the solution in section 5.3.

5.1. Structure, constraints and synthesis

This section is set up to explain controller design of using the control structure in subsection 5.1.1 with the hard constraints in subsection 5.1.2 and soft constraints in subsection 5.1.3 with the final control synthesis results are shown in subsection 5.1.4.

5.1.1. Control Structure

The transfer function I/O relationships used for decentralized control design are shown in Figure 5.2. The actuator model G_{act} consists of second-order transfer functions with $\omega_n = 50\,\mathrm{rad/s}$ and $\zeta = 0.95$, applied to both input channels. The two-degrees-of-freedom controller has two outputs and five inputs, since it includes both the reference and the measured signals of the controlled variables: vertical velocity, pitch rate, and pitch, respectively V_z^K, q^K, θ^K. The external signals are the disturbances at the input d_i composed of $d_{\delta_{col,cmd}}, d_{\delta_{lon,cmd}}$ and at the output d_o composed of d_{V_z}, d_q, d_θ as well as the sensor noise n composed of n_{V_z}, n_q, n_θ. Other signals involved in the controller design are the reference tracking signals $V_{z_{ref}}$ and θ_{ref}, the disturbed outputs y, composed of the measurements for V_z, q, θ and the actuator inputs, which are the commanded inputs u composed of $\delta_{col,cmd}, \delta_{lon,cmd}$ as the controller outputs.

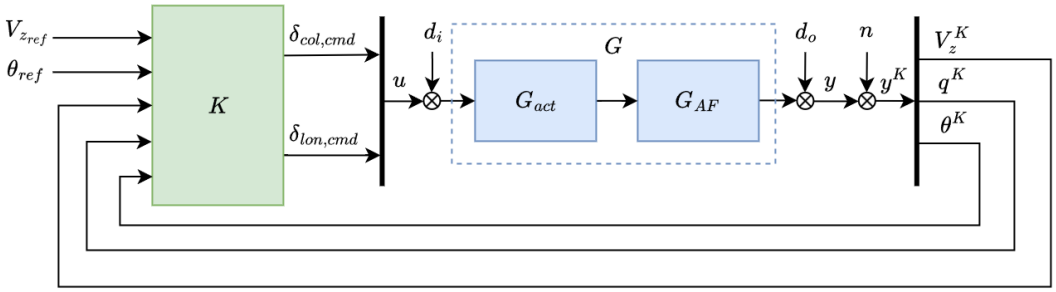

Figure 5.2: Longitudinal controller I/O layout

The autopilot structure used here is decentralized as shown Figure 5.3. This structure, consist of three key components. Firstly, the feed-forward injection K_{inj} using a second-order transfer functions to adjust the input signal u based on the reference signals $V_{z_{ref}}$ and θ_{ref}. The structure of K_{inj,V_z} and $K_{inj,\theta}$ is as follows:

$$K_{inj}(s) = \frac{z_1 s + z_0}{s^2 + p_1 s + p_0} \tag{5.1}$$

The second components are the first-order transfer functions K_c, which act as a PI-like controllers though the integrator with a low-pass filter with frequency of ω_c. This is used for tracking the reference signals $V_{z_{ref}}$ and θ_{ref} in the autopilot loop. The structure of K_{c,V_z} and $K_{c,\theta}$ is as follows:

$$\frac{K_c(s)}{s} = \frac{K}{s} \cdot \frac{s + z_0}{s + \omega_c} = \frac{K_p s + K_i}{s} \cdot \frac{\omega_c}{s + \omega_c} \tag{5.2}$$

Final component is the static output gain K_q which stabilizes the phugoid mode of the helicopter, improving the damping and transient response. The order of the components of the controller was determined after successive iterations in which the controller order was increased incrementally. These iterations revealed that the performance of the controller increased with increased order until the improvements in the robustness and handling qualities where small.

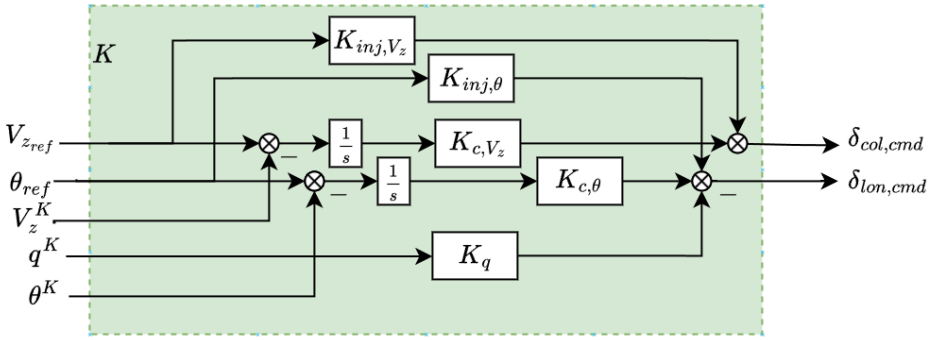

Figure 5.3: Longitudinal control structure

5.1.2. Hard Constraints

The flight control laws in the following sections are designed to fulfill a series of hard constraints using the signals in Figure 5.2 for the specified design points. The hard constraints involve the minimum necessary stability at the I/O of the plant, broken-loop-at-a-time, and pole placement constraints (Apkarian & Noll, 2007).

Stability Requirements

For the stability margin requirement, minimum robust disk-based stability margins are applied at each of the actuator inputs u for commanded collective $\delta_{col,cmd}$ and commanded longitudinal $\delta_{lon,cmd}$, and at each of the helicopter outputs y for vertical velocity V_z, pitch rate q, and pitch θ, broken loop-at-a-time. The margins can be assessed by breaking the loop at set points in the control loop to guarantee robustness to simultaneous gain and phase variations, unlike classical gain and phase margins (Seiler et al., 2020) as seen in Figure 5.4. These constraints can be written in terms of the open-loop transfer functions L associated with each of the five channels computed at each input or outputs. For the symmetric disk-based stability margins ($\sigma = 0$), the constraint is written as:

$$\begin{aligned} [\gamma_{min}, \gamma_{max}] &= \left[\frac{2-\alpha_{max}(1-\sigma)}{2+\alpha_{max}(1-\sigma)}, \frac{2+\alpha_{max}(1-\sigma)}{2-\alpha_{max}(1-\sigma)}\right] \\ \alpha_{max} &= \frac{1}{\left|\left|S+\frac{\sigma-1}{2}\right|\right|_\infty} \qquad \cos(\phi_m) = \frac{1+\gamma_{min}\gamma_{max}}{\gamma_{min}+\gamma_{max}} \end{aligned} \tag{5.3}$$

Given the parameters α_{max} which is the disk size for the guaranteed minimum gain $[\gamma_{min}, \gamma_{max}]$ and phase margins $[\phi_{min}, \phi_{max}]$ written as:

$$||S-T||_\infty = \left|\left|\frac{I-L}{I+L}\right|\right|_\infty = \frac{2}{\alpha_{max}} \tag{5.4}$$

The minimum required classical margins of $\pm 6\,\mathrm{dB}/\pm 45^\circ$ from a MIL document in (Anon, 2008) which are used as a standard for stability margins in flight control system design. With the minimum phase margins being the limiting parameter for the size of the disk $\alpha_{max} = 0.82$ in systematic case which results in $\pm 7.6\,\mathrm{dB}/\pm 45^\circ$ for the constraint as follows for i^{th} input/output:

$$H_{1,i} = \frac{||S-T||_\infty}{2.414} = \frac{\left|\left|\frac{I-L}{I+L}\right|\right|_\infty}{2.414} \leq 1 \tag{5.5}$$

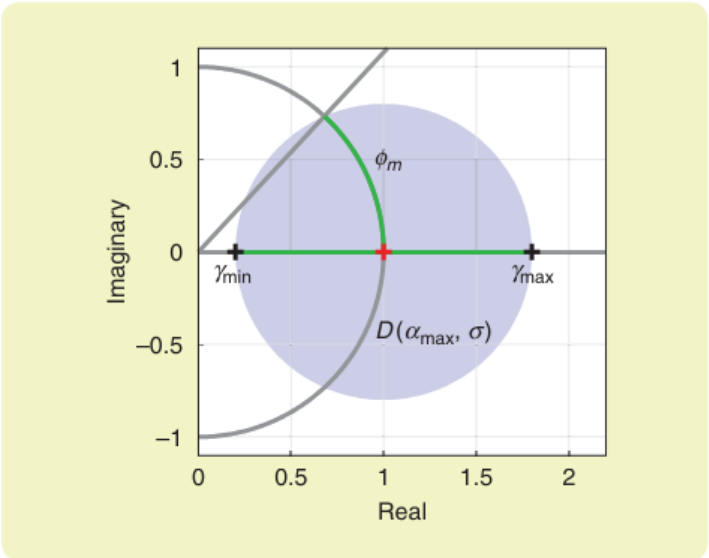

Figure 5.4: The guaranteed gain and phase margins from largest disk $D(\alpha, \sigma)$ maintaining stability (Seiler et al., 2020)

$\mathcal{D}$ - stability

This requirement which is also part of the ADS-33E handling quality guideline ensures the location of the closed poles of the system resides within a specific subset of the complex plane, defined as $\mathcal{D}$ for the specific design points. The damping ratio and the minimum decay rate are constrained which has a region defined in Equation 5.6 where $L = L^T$, M and L are real matrices that define a region on the complex plane. The damping ratio has been set to $\zeta = 0.35$. This results in the closed-loop pole locations as shown in Figure 5.5. In addition, the maximum frequency of the poles are bounded in the region of the complex plane to avoid dynamics of both plant and controller are too fast to detect and use respectively. Assuming that the variables are measured up to $100\,\mathrm{Hz}$ so the maximum frequency poles must be $\omega_{n_{max}} < 100\,\mathrm{rad/s}$.

$$H_{2,1} : \mathcal{D} = \{z \in \mathbf{C} : f_D(z) = L + zM + zM^T < 0\} \tag{5.6}$$

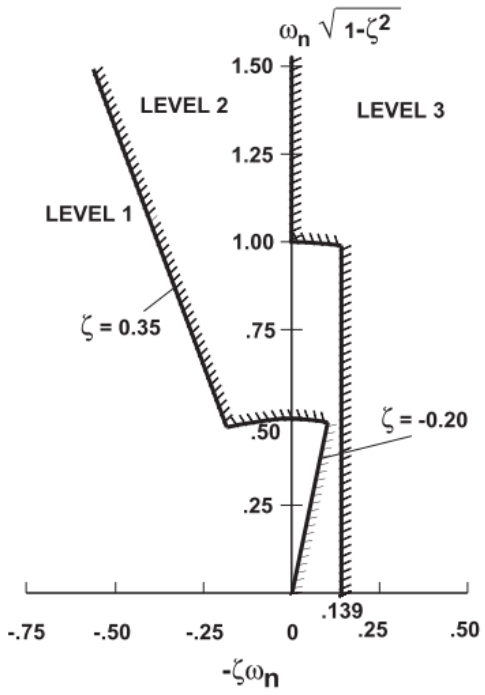

Figure 5.5: Limits on the pitch (roll) oscillations at hover and low speed (Anon, 2000)

5.1.3. Soft Constraints

The soft constraints involve a systematic process to bound frequency domain signals to obtain the various I/O disturbance rejection, control attenuation, and reference tracking for the vertical velocity and attitude control. The individual transfer functions are taken from Equation 5.7 and Equation 5.8 matrices, which are used to separately bound the vertical velocity and attitude control loops and optimize the robustness of the controller. The 4-block optimisation methods is taken from H_∞-loop shaping approaches for which a similar optimisation problem is posed to shape the open-loop by bounding closed-loop sensitivity functions in Equation 5.7. To simplify the H_∞ optimisation problem, a signal-based approach is used by looking at attitude (ACAH) and vertical velocity control systems separately ignoring the coupled dynamics in the control optimisation solution. For which only the direct reference tracking signal in Equation 5.8 is used to shape the T_o functions.

$$\begin{bmatrix} y \\ u \end{bmatrix} = \begin{bmatrix} S_o & S_oG \\ KS_o & T_i \end{bmatrix} \cdot \begin{bmatrix} d_o \\ d_i \end{bmatrix} \tag{5.7}$$

$$\begin{bmatrix} e_{V_z} \\ e_\theta \end{bmatrix} = (T_o - T_{ref}) \cdot \begin{bmatrix} V_{z_{ref}} \\ \theta_{ref} \end{bmatrix} \tag{5.8}$$

Output Disturbance Requirement

The disturbance rejection requirements involve rejecting plant I/O disturbances toward the measured output. The output disturbance rejection is defined by the output sensitivity transfer function S_o from the output disturbance d_o to the measured output y. These constraints are established based on the analysis in (Berger, Ivler, Berrios, et al., 2016) which uses HQ criteria and through experimentation establishing recommend guidelines for the output disturbance sensitivity. These guidelines are The disturbance rejection peak DRP and disturbance rejection bandwidth DRB are used to evaluate the handling and hold characteristics for each output channel. These parameters are defined as follows:

$$\omega\left(S_o = -3\,\mathrm{dB}\right) = DRB\ \mathrm{rad/s}, \quad ||S_o||_\infty = DRP\ \mathrm{dB} \tag{5.9}$$

The specifications on disturbance rejection are defined and enforced with the weighting function W_{S_o}. The transfer functions from $T_{d_{V_z}\to V_z}$ and $T_{d_\theta\to\theta}$ are subject to the required specifications for the vertical velocity and attitude channels, shown in Table 5.1 for the hold characteristics. This constraint concerns

Table 5.1: Disturbance rejection guidelines (Berger, Ivler, Berrios, et al., 2016)

	Pitch (θ)	Vertical velocity (V_z)
DRB rad/s $\geq$	0.5	1.0
DRP dB $\leq$	5.0	5.0

the rejection of plant output with respect to pitch attitude θ and vertical velocity V_z. Which is the transfer function from d_θ and d_{V_z} to the measured outputs θ and V_z respectively. The low-frequency gain must be reduced such that disturbances in this range are rejected for the respective hold-mode as well as limiting signal amplification. The constraint is denoted in Equation 5.10 and Equation 5.11 makes use of the weighting function W_{S_o}. The inverted weighting function $W_{S_o}^{-1}$ is chosen such that the low-frequency attenuation converges to $-40\,\mathrm{dB}$. The following constraints are written as:

$$S_{1,1} = \left|\left|W_{S_{V_z}} T_{d_{V_z}\to V_z}\right|\right|_\infty \tag{5.10}$$

$$S_{1,2} = ||W_{S_\theta} T_{d_\theta\to\theta}||_\infty \tag{5.11}$$

Control signal attenuation

The transfer functions from output disturbance d_o to control inputs u are to be restricted. This is needed to ensure that the actuator command signals are within the bandwidth of the actuators as well as to reduce high frequency control gains in the feedback path. This is because the KS_o function approximates to the controller $KS_o(\omega >> 1) \approx K$ at high frequencies. To align the system's I/O relationships across different operating points, the system's plant can be re-scaled, allowing the functions KS_o to be normalized. The re-scaling of the direct control gains in the open-loop system leads to specific results for the KS_o functions, ensuring that the transfer functions $T_{d_{V_z}\to\delta_{col,cmd}}$ and $T_{d_\theta\to\delta_{lon,cmd}}$ maintain a consistent value of $0\,\mathrm{dB}$ at a frequency of $0\,\mathrm{rad/s}$, as mentioned in (Skogestad & Postlethwaite, 2005). The plant re-scaling is achieved through a singular value decomposition (SVD) of the open-loop plant for the observed outputs σ_{V_z} and σ_θ written as:

$$\begin{bmatrix} d_{V_z} \\ d_\theta \end{bmatrix}_{re-scaled} = \begin{bmatrix} \sigma_{V_z} \cdot \frac{\sigma_\theta}{T_{\delta_{lon,cmd}\to\theta}} & 0 \\ 0 & \sigma_\theta \cdot \frac{\sigma_{V_z}}{T_{\delta_{col,cmd}\to V_z}} \end{bmatrix} \cdot \begin{bmatrix} d_{V_z} \\ d_\theta \end{bmatrix} \quad \text{at } \omega = 0\,\mathrm{rad/s} \tag{5.12}$$

For the control signal attenuation for the feedback loop is defined as KS_o, represented by $T_{d_{V_z}\to\delta_{col,cmd}}$ and $T_{d_\theta\to\delta_{lon,cmd}}$, the inverted weighting filters $W_{KS_o}^{-1}$ are adjusted so that the transfer functions are bounded, limiting the peak values and high frequency gains. The low frequencies are limited by gains of $10\,\mathrm{dB}$ for both channels to provide robustness to output multiplicative uncertainty for output related the corresponding disturbance input. With sufficient roll-off at frequencies of $10\,\mathrm{rad/s}$ and $20\,\mathrm{rad/s}$ for the control signal attenuation of the vertical velocity and attitude control channels, respectively. Furthermore, high-frequency gains are attenuated at $-40\,\mathrm{dB}$ in order to ensure reduced control effort at high frequencies limiting the effect of sensor noise on the controller. The following constraints are written as:

$$S_{2,1} = \left|\left|W_{KS_{V_z}} T_{d_{V_z}\to\delta_{col,cmd}}\right|\right|_\infty \tag{5.13}$$

$$S_{2,2} = \left|\left|W_{KS_\theta} T_{d_\theta\to\delta_{lon,cmd}}\right|\right|_\infty \tag{5.14}$$

Input disturbance rejection

The transfer functions from input disturbance d_i to measured output y are to be restricted. The reason this constraint had to be included was to enforce enough integral action to ensure that these transfer functions contain proper attenuation of low-frequency input disturbance signals. This is because the S_oG function approximates to the inverse of the controller $S_oG(\omega << 1) \approx K^{-1}$ at low frequencies. For input disturbance rejection, the re-scaling is inverted as the I/O relationships are reversed shown as follows:

$$\begin{bmatrix} d_{\delta_{col,cmd}} \\ d_{\delta_{lon,cmd}} \end{bmatrix}_{re-scaled} = \begin{bmatrix} \sigma_{V_z} \cdot \frac{\sigma_\theta}{T_{\delta_{lon,cmd} \to \theta}} & 0 \\ 0 & \sigma_\theta \cdot \frac{\sigma_{V_z}}{T_{\delta_{col,cmd} \to V_z}} \end{bmatrix}^{-1} \cdot \begin{bmatrix} d_{\delta_{col,cmd}} \\ d_{\delta_{lon,cmd}} \end{bmatrix} \quad \text{at } \omega = 0\,\mathrm{rad/s} \tag{5.15}$$

Additionally, due to normalization, similar weights can be applied for the input and output disturbance rejection. Although, for W'_{S_θ}, the roll-off is altered compared to W_{S_θ} to match the slope of the re-scaled S_oG function. The constraints are written as:

$$S_{3,1} = \left|\left| W_{S_{V_z}} T_{d_{\delta_{col,cmd}} \to V_z} \right|\right|_\infty \tag{5.16}$$

$$S_{3,2} = \left|\left| W'_{S_\theta} T_{d_{\delta_{lon,cmd}} \to \theta} \right|\right|_\infty \tag{5.17}$$

Input disturbance tracking

The input tracking is defined as T_i, the transfer function from input disturbance d_i to the controller output u. These transfer functions, represented by $T_{d_{\delta_{col,cmd}} \to \delta_{col,cmd}}$ and $T_{d_{\delta_{lon,cmd}} \to \delta_{lon,cmd}}$, are constrained to enforce low-frequency input open-loop crossover. The weighting functions limit the input tracking to provide robustness against uncertainties at the actuator input. For the weighting functions in the $\delta_{col,cmd}$ channel are $3\,\mathrm{rad/s}$ and for the $\delta_{lon,cmd}$ channel $15\,\mathrm{rad/s}$ are limited to $0\,\mathrm{dB}$. With high-frequency gains of $-40\,\mathrm{dB}$ in order to ensure a good attenuation of control disturbances at high frequencies at the input. The following constraints are written as:

$$S_{4,1} = \left|\left| W_{T_{\delta_{col,cmd}}} T_{d_{\delta_{col,cmd}} \to \delta_{col,cmd}} \right|\right|_\infty \tag{5.18}$$

$$S_{4,2} = \left|\left| W_{T_{\delta_{lon,cmd}}} T_{d_{\delta_{lon,cmd}} \to \delta_{lon,cmd}} \right|\right|_\infty \tag{5.19}$$

Model Following

ADS-33E guidelines are used to assess handling quality requirements for rotorcraft, focusing on desirable time/freqency-domain reference trajectory tracking. The transfer functions used are from the reference signal $V_{z_{ref}}, \theta_{ref}$ to the error between the measured output of the model and actual system e_{V_z}, e_θ. To ensure compliance with the handling quality requirements, low steady-state error is achieved through limiting the H_∞ norm of the weighted reference error signal W_{T_o}, using a model following architecture. This method promotes robust reference tracking in the time domain. The model following method is used to focus on time-domain transient responses. In which, a lower-order equivalent system (LOES) for the collective to height rate response from the HQ criteria in (Anon, 2000) is used to evaluate the vertical velocity response characteristics for desirable reference tracking performance, written as:

$$T_{ref,V_z} = \frac{K e^{-\tau_{V_{z_{eq}}} s}}{T_{V_{z_{eq}}} s + 1} \tag{5.20}$$

The parameters which meet the level 1 HQ criteria for the LOES for vertical velocity response are shown in Table 5.2 using the model following structure.

Table 5.2: Parameters for the model following of T_{ref,V_z}

Parameter	Description	Value
$\tau_{V_{z_{eq}}}$	Time delay	$5\,\mathrm{ms}$
$T_{V_{z_{eq}}}$	Time constant	$1.0\,\mathrm{s}$

The pitch control (ACAH) has reference following requirements for rise time and closed-loop shaping for level 1 handling qualities for T_o, the signal for the reference tracking performance. The LOES is formulated based on approximations seen in (Tischler et al., 2017), written as:

$$T_{ref,\theta} = \frac{\omega_n^2 e^{-\tau_{\theta_{eq}} s}}{s^2 + 2\zeta\omega_n s + \omega_n^2} \tag{5.21}$$

The parameters which meet the level 1 HQ criteria shown in Figure 5.6 are described in Table 5.3 using the model following structure, where the quickness requirement is the limiting constraint and the delay bounds phase-lag in the closed-loop bandwidth of the handling requirements.

Table 5.3: Parameters for the model following of $T_{ref,\theta}$

Parameter	Description	Value
$\tau_{\theta_{eq}}$	Time delay	$7.5\,\mathrm{ms}$
ζ	Damping ratio	1
ω_n	Natural frequency	$4.5\,\mathrm{rad/s}$

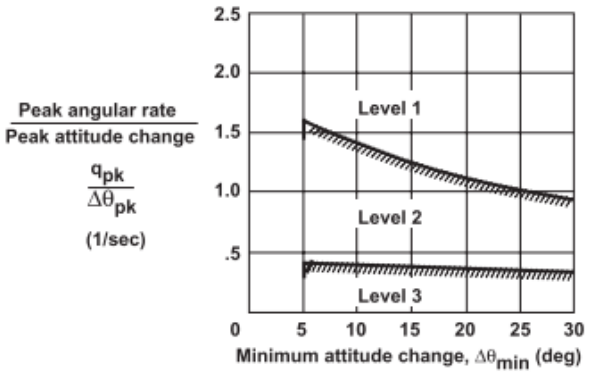

(a) Agility requirements for small/medium-amplitude attitude (Anon, 2000) (target Acquisition and Tracking)

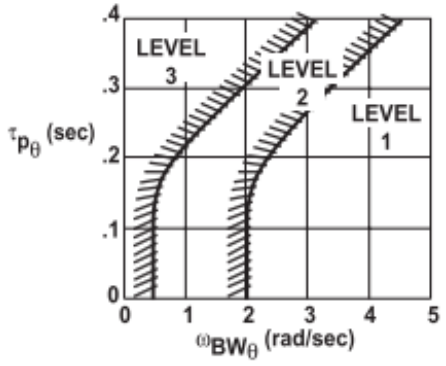

(b) Bandwidth requirements for moderate-amplitude attitude change (Anon, 2000) (target Acquisition and Tracking)

Figure 5.6: Closed-loop shaping and bandwidth requirements for ACAH system (Anon, 2000)

The targeted HQ criteria for the phase delay τ_{p_θ} is $0.05\,\mathrm{s}$ with a bandwidth ω_{BW_θ} of $6.3\,\mathrm{rad/s}$ and the response speed $\frac{q_{pk}}{\theta_{pk}}$ of $1.6\,\mathrm{s}^{-1}$. The delay's for both channels can be linearized using a first-order Padé approximation for the constraint, which is modified limiting the non-minimum phase behavior in the time-domain for the constraint described as follows:

$$e^{-\tau s} \approx \frac{-\frac{2\tau}{6}s + 1}{\frac{2\tau}{3}s + 1} \tag{5.22}$$

To ensure compliance with HQ criteria, low steady-state error is achieved through limiting the H_∞ norm of the weighted reference error signal at low frequencies, bounding the transfer functions $T_{V_{z_{ref}} \to V_z}$ and $T_{\theta_{ref} \to \theta}$. Furthermore, to ensure that the frequency domain response are followed at low to mid-frequencies, attenuation is required of $-40\,\mathrm{dB}$ at $1\,\mathrm{rad/s}$ applied to both channels with a roll-off relaxing the constraint at higher frequencies where matching is less critical. The following constraints are written as:

$$S_{5,1} = \left|\left| W_{T_{V_z}} (T_{V_{z_{ref}} \to V_z} - T_{ref,V_z}) \right|\right|_\infty \tag{5.23}$$

$$S_{5,2} = \left|\left| W_{T_\theta} (T_{\theta_{ref} \to \theta} - T_{ref,\theta}) \right|\right|_\infty \tag{5.24}$$

5.1.4. Control Gains

The synthesised controller after tuning the five control gains $K_{inj,V_z}, K_{inj,\theta}, K_{c,V_z}, K_{c,\theta}, K_q$ against the soft and hard design specifications described above. The solution was obtained using the *systune()* function in the MATLAB Control Design Toolbox, which can handle multi-objective design problems (Apkarian & Noll, 2006; Apkarian, 2013; Apkarian et al., 2014). In this approach, the soft design constraints $S_{i,j}$ are minimized under the condition that the hard constraints $H_{i,j}$ are satisfied, as detailed in (Authié, 2023; Theodoulis & Proff, 2021).

To investigate controller solutions for variations in speeds and altitudes, 48 flight points are designed throughout the flight envelope shown in Figure 5.1, between which the controller parameters are linearly interpolated as shown in the Figure 5.7 to Figure 5.9. For which, the results for the chosen design point $h = 0\,\mathrm{m}, V = 20\,\mathrm{m/s}$ is the focus of research looking at the 2-DoF controller design in the linear analysis in section 5.2. The controller gains, the function returns two scalar values, denoted by $\max(H_{i,j}) = 1$ and $\max(S_{i,j}) = 0.9$, which indicate whether the constraints are satisfied by the controller for the design point. The synthesized structured H_∞ controller for the design point are written as follows taken from Figure 5.7 to Figure 5.9:

$$\begin{aligned} K_{inj,V_z} &= \frac{0.056s - 0.30}{s^2 + 12.24s + 54.04} \quad K_{inj,\theta} = \frac{-46.87s + 26.46}{s^2 + 11.36s + 46.16} \\ K_{c,V_z} &= \frac{0.064(s + 1.03)}{s + 5.45} \quad K_{c,\theta} = \frac{-11.09(s + 0.51)}{s + 4.87} \quad K_q = -1.97 \end{aligned} \tag{5.25}$$

The results of the sub-optimal H_∞-norm for each flight point are presented in Appendix B. The resulting non-smooth gain surfaces are illustrated in Figure 5.7 through Figure 5.9. These figures show that the feedback controller gains K_c have higher magnitudes at specific points in the flight envelope, indicating that the system requires greater control effort at these points to meet the design objectives described in this section.

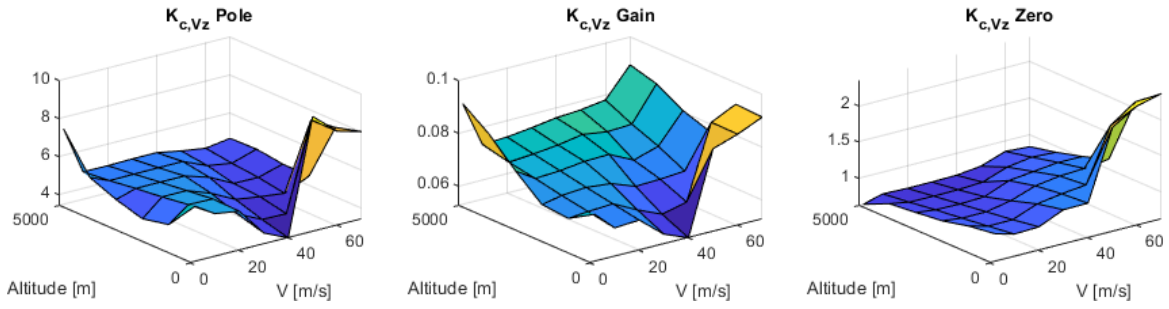

(a) The controller design solution K_{c,V_z} for points in flight envelope

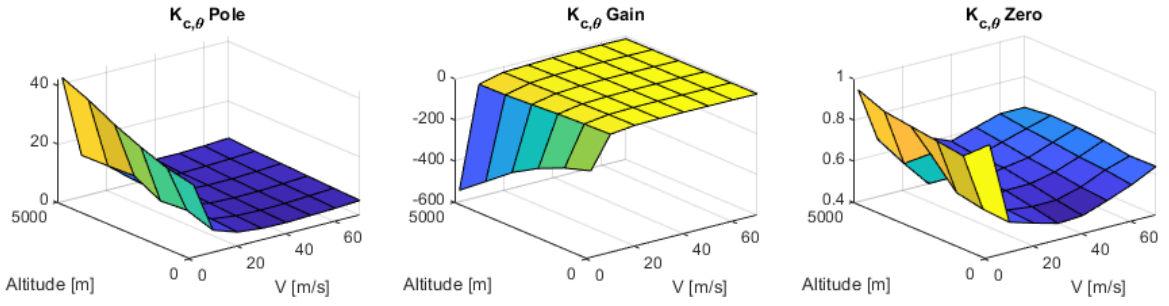

(b) The controller design solution $K_{c,\theta}$ for points in flight envelope

Figure 5.7: The controller design solution K_c for points in flight envelope

For vertical velocity control using the collective command $\delta_{col,cmd}$, as shown in the trim point solution in Figure 4.3, $\delta_{col,cmd}$ is most effective at mid-velocities. It has low open-loop gains at hover and higher forward flight speeds, necessitating higher control gains to stabilize and meet the same objectives. This effect is seen at the central plot of Figure 5.7a for the range of velocities at altitude $h = 0\,\mathrm{m}$. Combined with lower control effectiveness proportional to altitude caused by a decrease in air density, results in a general trend of higher gains with increase in altitude, as seen in Figure 5.7a.

This indicates around $h = 0\,\mathrm{m}, V = 70\,\mathrm{m/s}$ in Figure 5.7a, to maintain consistent performance to meet the controller design objectives as shown in Appendix C results in an increase of the gain and lead-lag terms (pole/zero). This non-smooth irregularity can be the caused by tighter or a change in the solutions limiting constraints at that point.

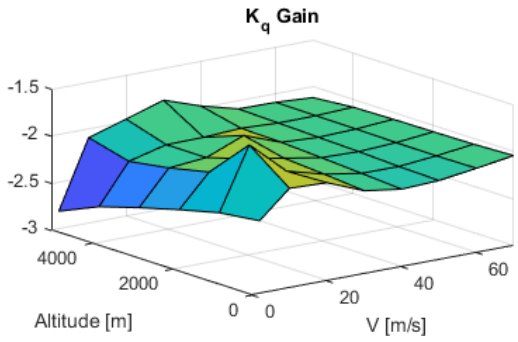

Figure 5.8: The controller design solution K_q for points in flight envelope

The pitch control channel is most effective during forward flight, as gains required increase near hover. This increase is larger relative to the loss of effectiveness due to altitude changes, as seen in Figure 5.7b. The rate stabilization gain K_q in Figure 5.8 shows a similar pattern but is less sensitive during the transition between hover to forward flight compared to the pitch control gains $K_{c,\theta}$. These non-smooth inconsistencies in Figure 5.7 and by extension Figure 5.9, shown in for the pitch controller Figure 5.7b close to hover are the result of trade-off performed during the optimisation process shown in Appendix C as a trade-off between stability, robustness, and tracking performance. In these cases, the cause is due to a large changes in the helicopter dynamics between hovering and forward flight illustrated in Figure B.4. These model characteristics can be caused by the assumptions when deriving the longitudinal helicopter model. The neglected dynamics pertain to the inaccuracies of the main rotor modelled which includes ignoring rotor tilt, blade-twist and higher order flapping dynamics which can have a parametric sensitive affect on pitch attitude control during hover. Their are other assumptions made for the helicopter model such as ignoring rotor drag forces as well as contribution of the horizontal tail but these affects are more relevant during forward flight.

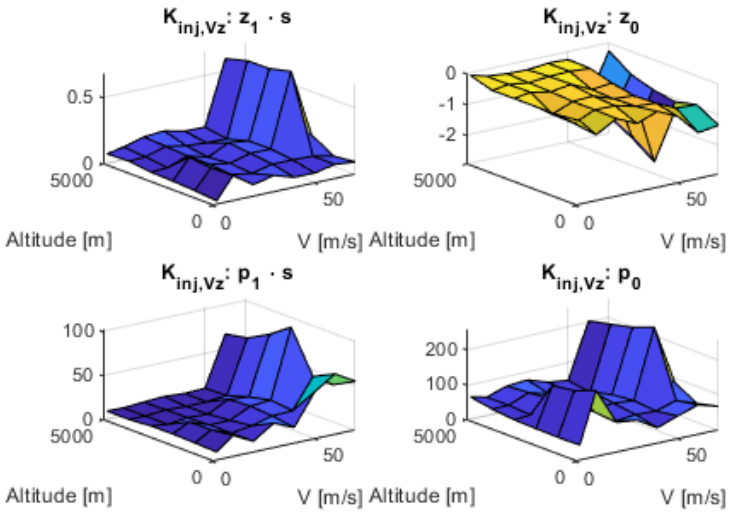

(a) The controller design solution K_{inj,V_z} for points in flight envelope

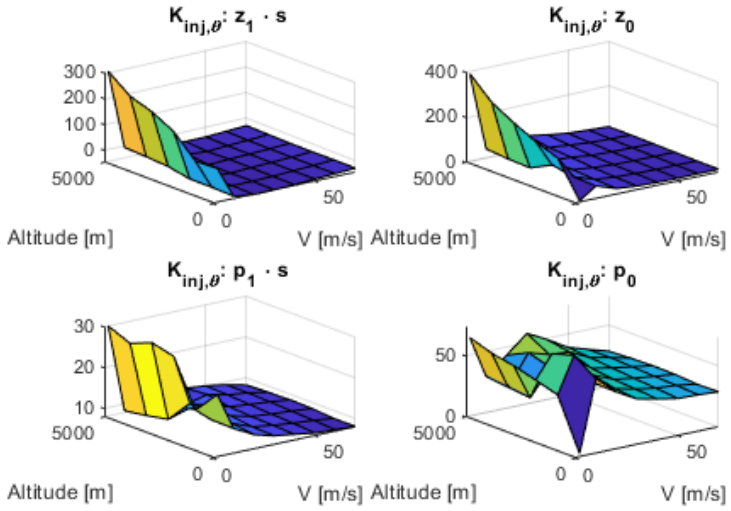

(b) The controller design solution $K_{inj,\theta}$ for points in flight envelope

Figure 5.9: The controller design solution K_{inj} for points in flight envelope

The feedforward control gains K_{inj} are influenced by model matching constraints. As the only signal path with a feedforward component, K_{inj} is limited by the properties of feedback control, such as the reduction of steady-state error at lower frequencies. This represents a trade-off between stability, robustness, and tracking performance. The feed-forward controller perform poorly in a gain-scheduled format largely due to the relatively high order and due to some regions of the gain surface not being smooth enough as shown in Figure 5.9, a similar case can be made for the feedback control shown in Figure 5.7 and Figure 5.8. However, it is clear that the gains are highly similar for large portions of the flight envelope with a few clear velocity and altitude based distinctions.

5.2. Linear Analysis

In this section a linear analysis describes the stability margins and pole placement requirements set by the hard constraints in subsection 5.2.1. In addition to, the closed loop transfer function which have soft optimisation constraints in subsection 5.2.2. In subsection 5.2.3, the handing qualities design objectives are assessed. This analysis is extended in subsection 5.2.4 for the flight envelop showing key results for the controller described in subsection 5.1.4 with the constraints.

5.2.1. Stability Requirements

In Figure 5.10, the disk-based gain and phase margins as functions of frequency are shown for each of the helicopter inputs and outputs. The minimum classical gain margins are approximately $\pm 12\,\mathrm{dB}$ or greater for all inputs and outputs, which is well above the $6\,\mathrm{dB}$ objective. In contrast, the minimum classical phase margins are $\pm 45\,^\circ$ or greater that are on target, as the hard constraint only guarantees $\pm 7.6\,\mathrm{dB}$ and $\pm 45\,^\circ$ of classical margins. As shown in the figure the exclusion regions are highlighted in which the broken open-loop transfer functions are avoided indicating robustness against perturbations for combinations of phase and gain margins, meeting the disk based stability requirements set. Additionally, Figure 5.11 shows the hard requirement on the pole-location for $\mathcal{D}$-stability, ensuring that all poles in the closed-loop system are stable with sufficient damping in accordance with the HQ criteria. Thus, the remaining degrees of freedom for the controller design could be used to optimize for the remaining 10 soft objectives.

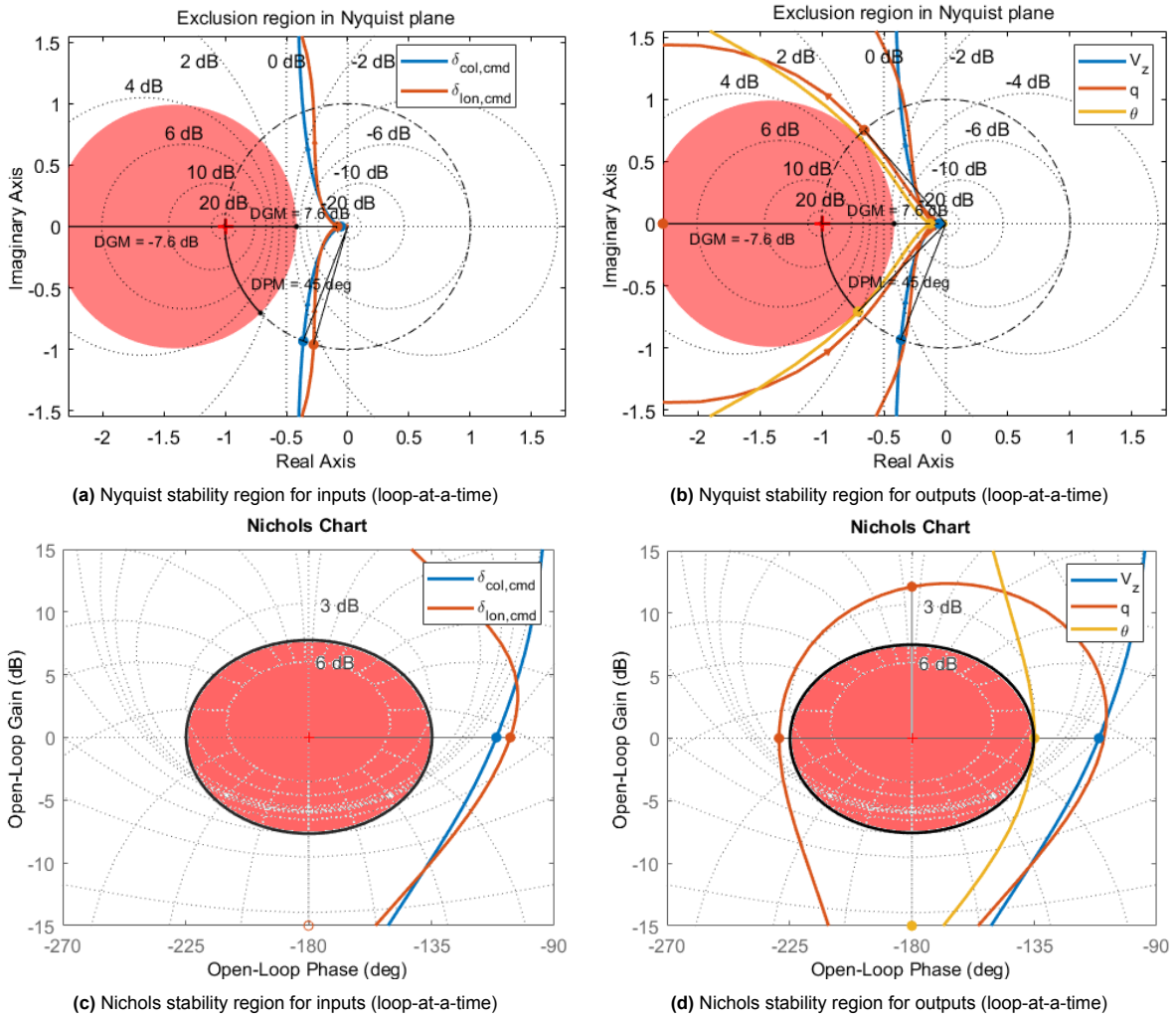

(a) Nyquist stability region for inputs (loop-at-a-time)

(b) Nyquist stability region for outputs (loop-at-a-time)

(c) Nichols stability region for inputs (loop-at-a-time)

(d) Nichols stability region for outputs (loop-at-a-time)

Figure 5.10: Nyquist and Nichols plots with symmetric stability regions for the inputs/outputs (loop-at-a-time) of open loops for the design point

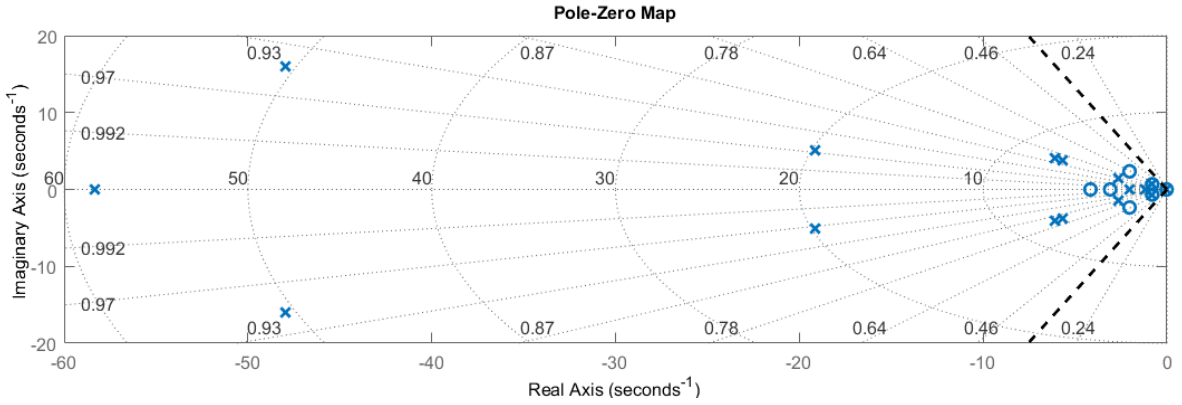

Figure 5.11: Closed-loop pole-zero plot at design point

5.2.2. Closed-loop Transfer Functions

The five closed-loop transfer functions that are constrained to assess the frequency-domain characteristics of the closed-loop system are shown in Figure 5.12 and 5.13 for the 2-DoF controller. To attenuate I/O disturbances acting on both the plant input and output, S_o and S_oG signals are minimized at low frequencies. Furthermore, it can be seen that the KS_o, T_i and T_o signals have adequate roll-off at high frequencies to attenuate the high frequency measurement noise.

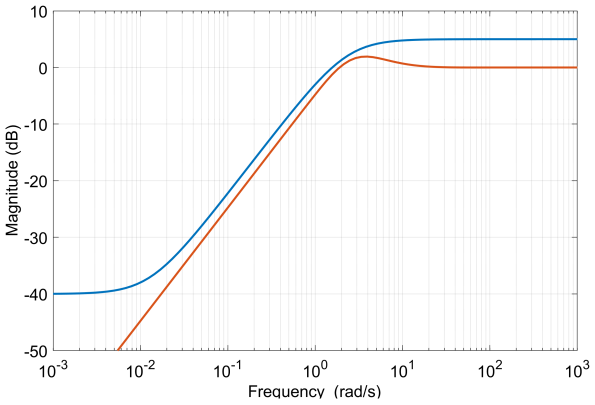

(a) Soft constraint on $T_{d_{V_z} \to V_z}$ (output disturbance sensitivity on V_z)

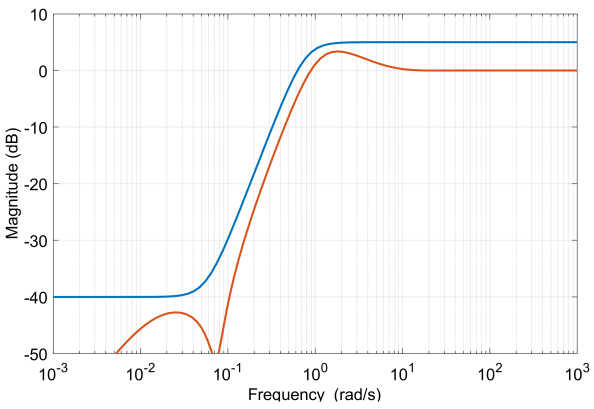

(b) Soft constraint on $T_{d_\theta \to \theta}$ (output disturbance sensitivity on θ)

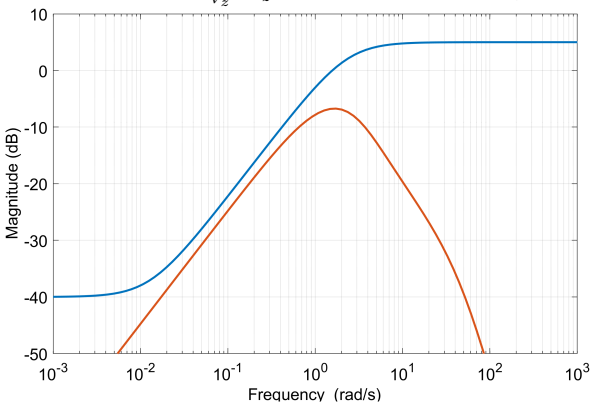

(c) Soft constraint on $T_{d_{\delta_{col,cmd}} \to V_z}$ (input disturbance sensitivity on V_z)

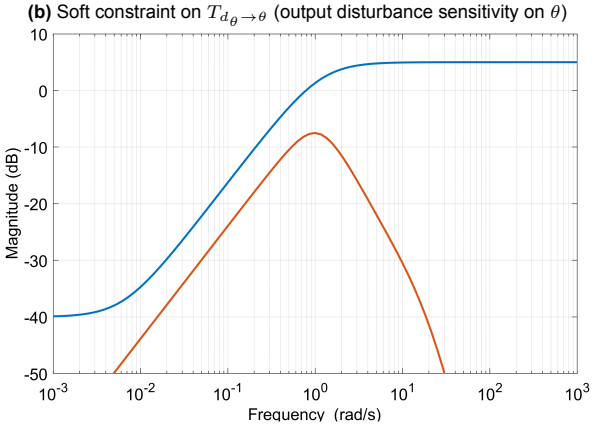

(d) Soft constraint on $T_{d_{\delta_{lon,cmd}} \to \theta}$ (input disturbance sensitivity on θ)

Figure 5.12: Overview of the designs of soft constraints related to disturbance rejection and signal attenuation frequency responses for the design point (blue: inverted weights W^{-1}, red: designed solution)

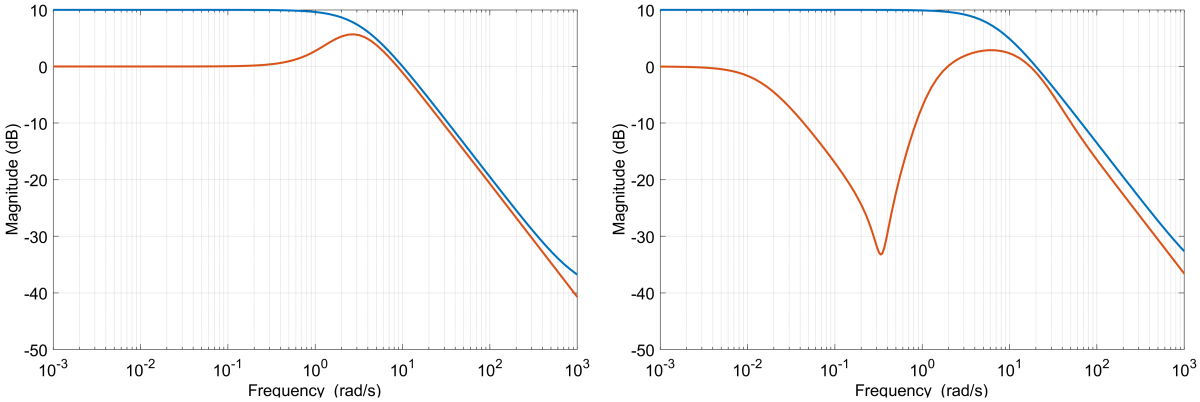

(a) Soft constraint on $T_{d_{V_z} \to \delta_{col,cmd}}$ (output disturbance sensitivity on $\delta_{col,cmd}$)

(b) Soft constraint on $T_{d_\theta \to \delta_{lon,cmd}}$ (output disturbance sensitivity on $\delta_{lon,cmd}$)

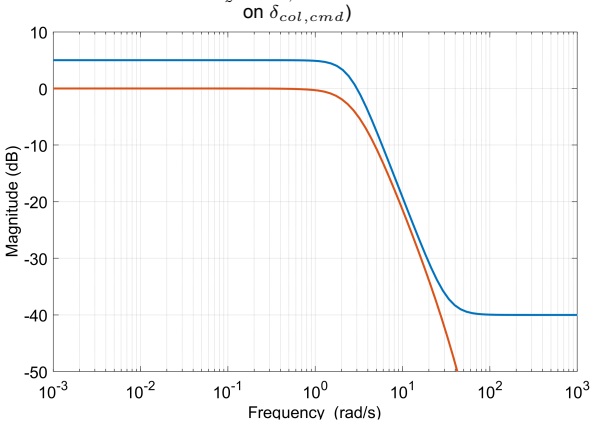

(c) Soft constraint on $T_{d_{\delta_{col,cmd}} \to \delta_{col,cmd}}$ (input disturbance sensitivity on $\delta_{col,cmd}$)

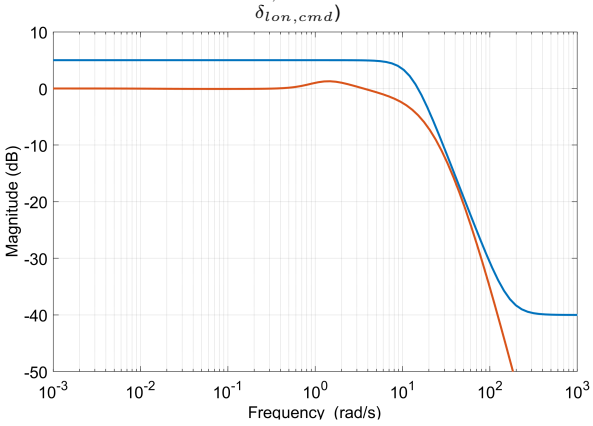

(d) Soft constraint on $T_{d_{\delta_{lon,cmd}} \to \delta_{lon,cmd}}$ (input disturbance sensitivity on $\delta_{lon,cmd}$)

Figure 5.13: Overview of the designs of soft constraints related to disturbance rejection and signal attenuation frequency responses for the design point, cont. (blue: inverted weights W^{-1}, red: designed solution)

The closed-loop transfer functions of the 2-DoF controller design are shown in Figure 5.14. It can be seen that $T_o - T_{ref}$ has a high peak in the mid-frequency range and is low in the low-frequency which results in low steady-state error from sufficient integral action of the controller. This peak is reshaped with the feedforward controller, leading to the controlled system requiring more control effort in this frequency range without affecting the robustness of the feedback control. Furthermore, bounding the $T_o - T_{ref}$ function in Figure 5.14 to be small at lower frequencies will reduce the error between the reference model and the output of the system at lower to mid-frequencies. A trade-off takes place where the peak of $T_o - T_{ref}$ is limited as much as possible in the mid-frequency range, while minimizing functions KS_o the required control effort in the from the reference tracking and T_i the input tracking so the signals have adequate roll-off at higher frequencies.

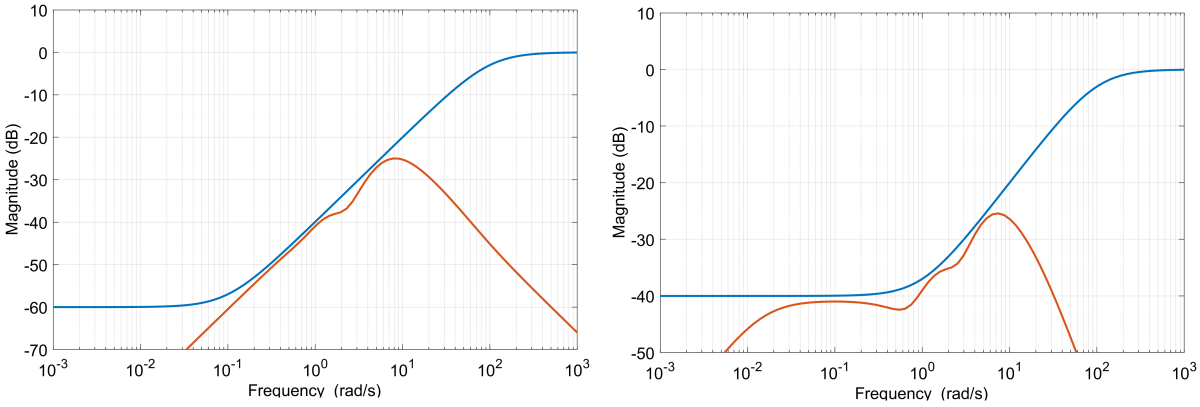

(a) Soft constraint on $T_{V_{z_{ref}} \to V_z} - T_{ref,V_z}$ (reference tracking)

(b) Soft constraint on $T_{\theta_{ref} \to \theta} - T_{ref,\theta}$ (reference tracking)

Figure 5.14: Overview of the designs of soft constraints related model following frequency responses for the design point (blue: inverted weights W^{-1}, red: designed solution)

5.2.3. Handling Quality Requirements

he performance of the resulting design is evaluated against the quickness and bandwidth of the attitude response which are the requirements that are enforced using a model following approach for the longitudinal helicopter model. The quickness criterion, defined by ADS-33, uses amplitude step inputs to assess the rate at which the controller converges to the target attitude while minimising overshoot using the peaks as metrics $\frac{q_{pk}}{\theta_{pk}}$. Figure 5.15 shows the results obtained using the designed system in the time domain, which can be compared with the theoretical performance of the reference model. As can be seen, responses remain close to the targets defined by the reference models. This indicates that the combination of the reference model tracking approach leads to a consistent response of the flight control system solution in the time domain. Furthermore, the responses exhibit inter-axis decoupling between the channels, despite the absence of constraints directly associated with decoupling requirements. However, the risk of actuator saturation remains, which is a problem for the attitude quickness requirement. As shown in Figure 5.15b, the attitude command quickness is $\frac{q_{pk}}{\theta_{pk}} = 1.8\,\mathrm{s}^{-1}$ meeting level 1 required for mission task elements (MTE) and attitude target acquisition ($> 1.6\,\mathrm{s}^{-1}$) requirement for $1\,^\circ$ attitude changes (Anon, 2000).

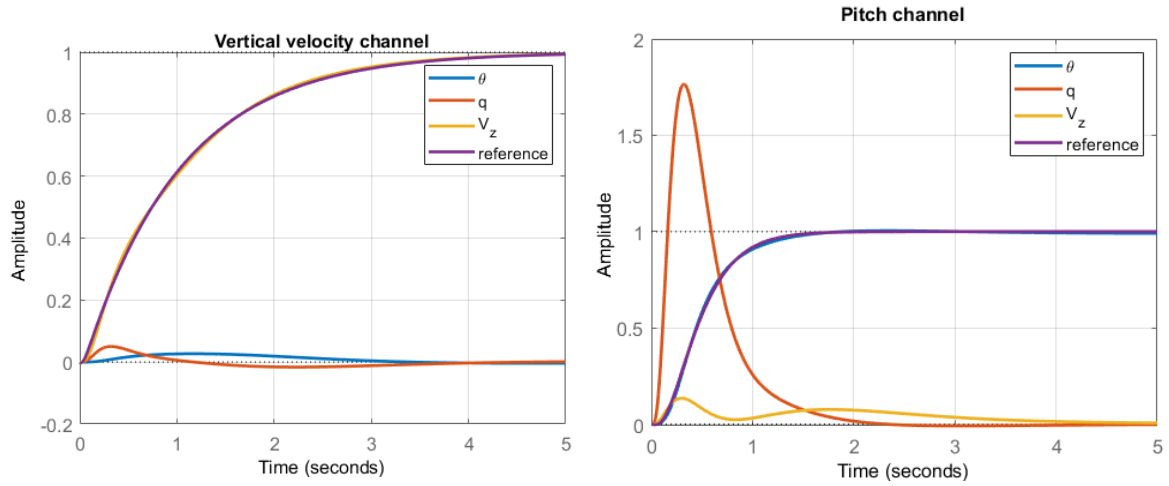

(a) $1.0\,\mathrm{m/s}$ step response of $V_{z_{ref}}$

(b) $1.0\,^\circ$ step response of θ_{ref}

Figure 5.15: Step responses in the time domain

The bandwidth handling criteria assess the accuracy of the reference tracking in the frequency domain using two parameters: the phase delay τ_{p_θ} and bandwidth ω_{BW_θ}. The bandwidth of the ACAH response types is the minimum between the frequency at which the phase is at $-135\,^\circ$ and the frequency

at which the gain is $6\,\mathrm{dB}$ greater than at the crossover frequency ω_{180}. The phase delay τ_{p_θ} is defined according to Equation 5.26 in terms of the crossover frequency ω_{180} and the phase shift at twice the crossover frequency $\Delta\phi_{2\omega_{180}}$. The application of this criterion to the designed flight control system from reference models is shown in Figure 5.16, meeting level 1 handling requirements and closely matching the reference point.

$$\tau_{p_\theta} = \frac{\Delta\phi_{2\omega_{180}}}{57.3(2\omega_{180})} \tag{5.26}$$

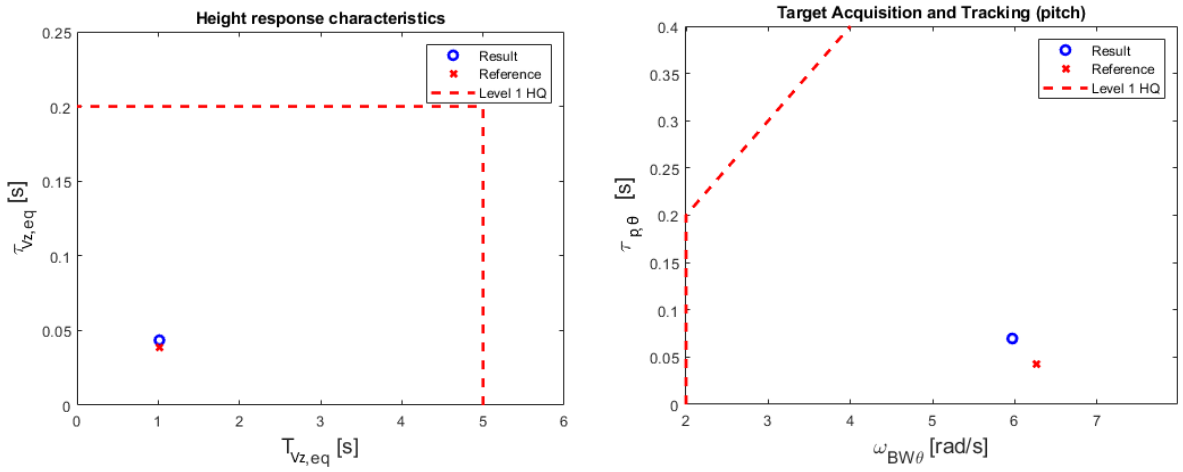

(a) Vertical velocity LOES response requirements

(b) Bandwidth requirements for small-amplitude attitude

Figure 5.16: Model following frequency domain HQ requirement

5.2.4. Results for the flight envelope

For the flight envelope using the controller in Figure 5.7 through Figure 5.9 applied to the set linearised plants shown in Appendix B, the hard stability constrains are shown in Appendix C. The loop-at-a-time $S - T$ based disk margins at the input and output are summarized in Table 5.4. At all inputs and outputs, the disk-based gain margins are larger than $\pm 6\,\mathrm{dB}$, and the disk-based phase margins are larger than $\pm 45\,^\circ$. The 10 soft constraints for the flight envelope are shown in Figure 5.17 which

Table 5.4: Minimum gain/phase based stability margins for the flight envelope

Parameter	Gain Margin dB	Phase Margin °
$\delta_{cmd,col}$	24	45
$\delta_{cmd,lon}$	18	45
V_z	15	45
q	10	45
θ	11	45

describes $\max(S_{i,j})$, taken from the closed-loop transfer functions shown in Appendix C. In addition, it can be seen that where this methodology work well at the design point $h = 0\,\mathrm{m}, V = 20\,\mathrm{m/s}$ which is in the mid-velocities at sea level altitudes.

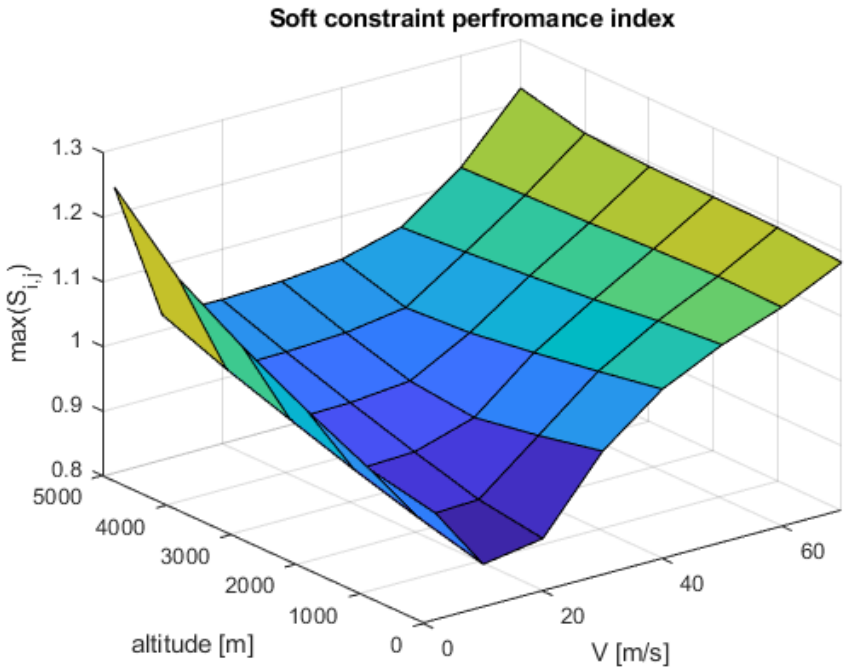

Figure 5.17: The soft optimisation constraints $\max(S_{i,j})$

The application of this criterion to the designed flight control system from reference models is shown in Figure 5.18, meeting level 1 handling requirements for the flight envelope and closely clustered around the reference point. In Figure 5.19 shows the results obtained using the designed system in the time domain for the entire flight envelope, which can be compared with the theoretical performance of the reference model. As can be seen, response are consistent with the reference model. Furthermore, the responses exhibit greater levels of inter-axis decoupling between the channels than the design point. Despite the absence of constraints directly associated with decoupling requirements, the effect of cross-coupling is limited. The figure also shows that level 1 quickness requirements are achieved for most of the flight envelope expect for low speed, high altitude flight which is due to a reduction in control authority.

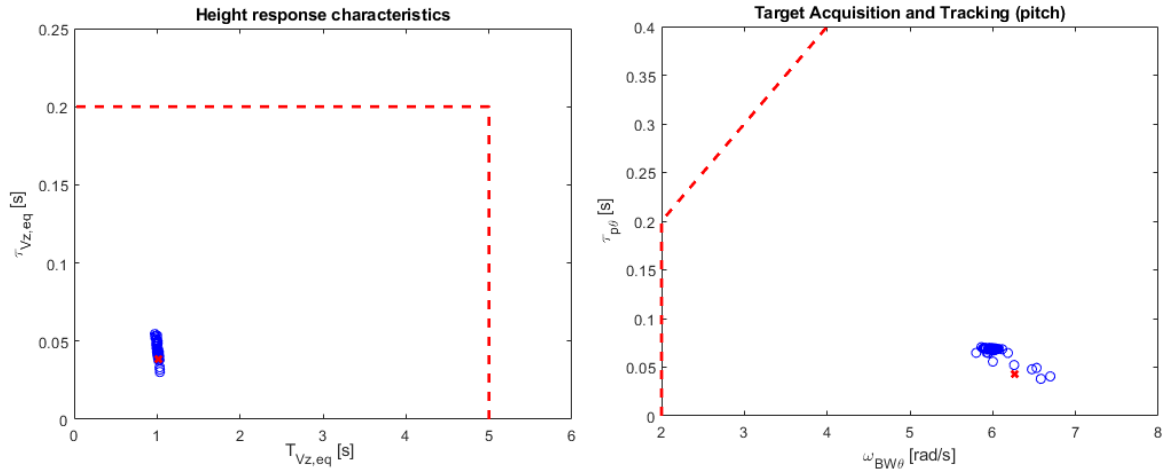

(a) Vertical velocity LOES response requirements

(b) Bandwidth requirements for small-amplitude attitude

Figure 5.18: Model following frequency domain HQ requirement for the flight envelope

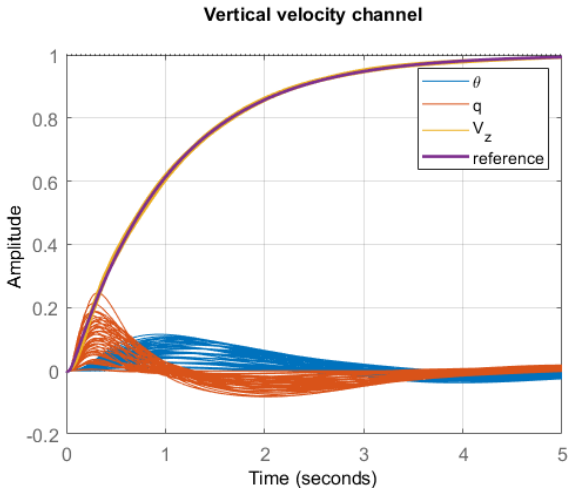

(a) $1.0\,\mathrm{m/s}$ step response of $V_{z_{ref}}$

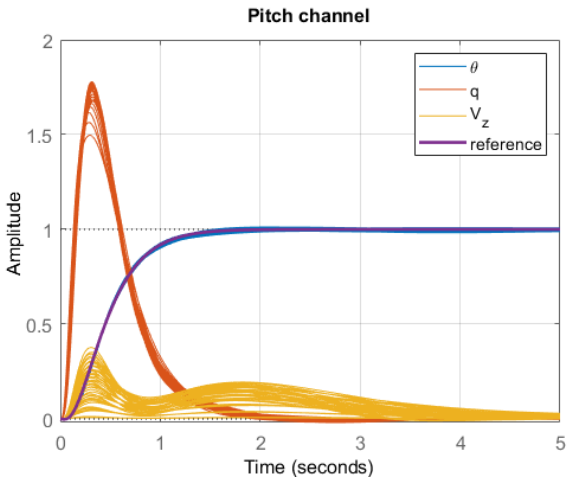

(b) $1.0\,^\circ$ step response of θ_{ref}

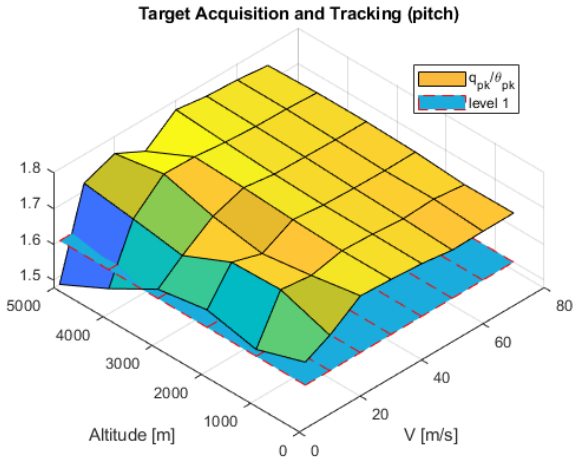

(c) Attitude quickness for $\Delta\theta_{ref} = 1.0\,^\circ$

Figure 5.19: Step responses in the time domain

5.3. Non-linear implementation

The following simulations in Figure 5.20 and Figure 5.21 use a series of step-wise reference signals in which the altitude is $h = 0\,\mathrm{m}$ to compare linear and non-linear performance. The reference signal profiles allow for flight coverage around the design point. The commanded maneuvers were filtered using Equation 5.27 to stay within the limitations of actuators as shown in Table 4.1. It can be seen that even for large vertical velocity changes and pitch angles, the control effort is small, and the response accurately follows the reference signal. In addition, the tracked and control signal closely match for linear and non-linear cases when near when near the designed operating point. Although, deterioration is seen in the non-linear case in the vertical velocity control at high pitch angles as steady state error compared to the linear case.

$$H_{\theta_{cmd},filter} = \frac{\omega_n^2}{s^2 + 2\zeta_n\omega_n s + \omega_n^2} \quad \omega_n = 4\,\mathrm{rad/s} \quad \zeta_n = 1 \tag{5.27}$$

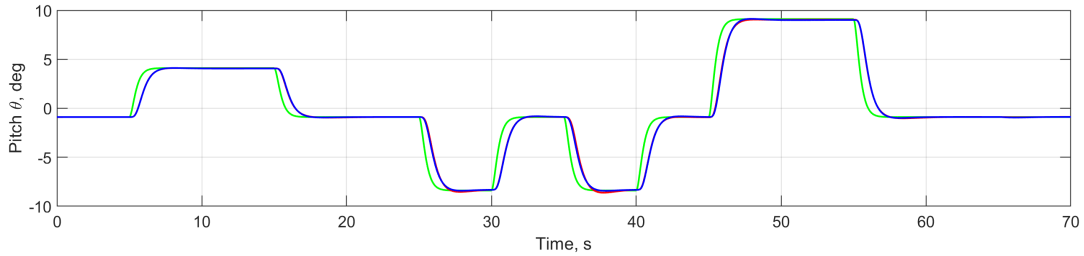

(a) Tracked output signal θ (pitch attitude)

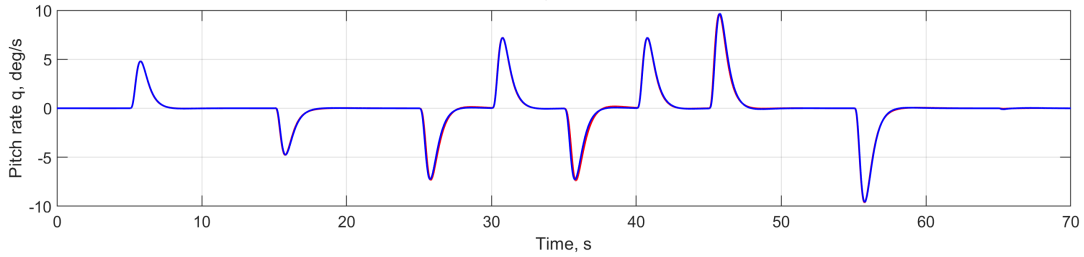

(b) State output signal q (pitch rate)

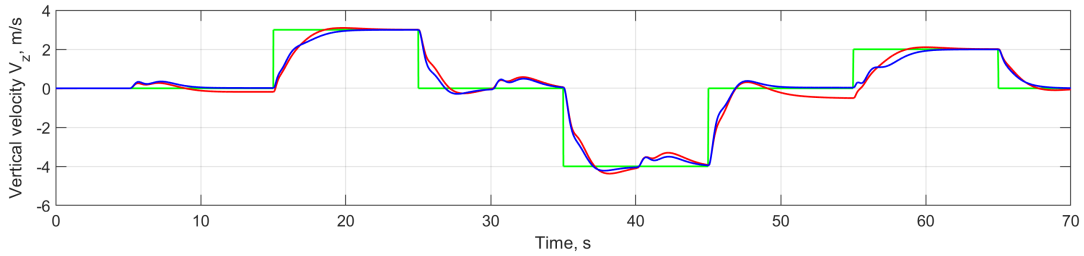

(c) Tracked output signal V_z (vertical velocity)

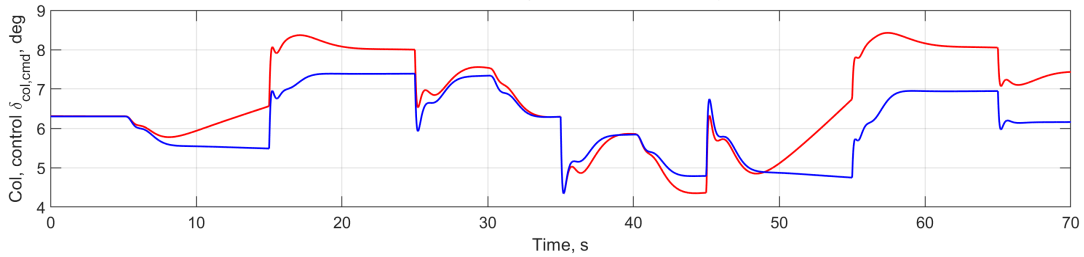

(d) Control signal $\delta_{col,cmd}$ (desired collective)

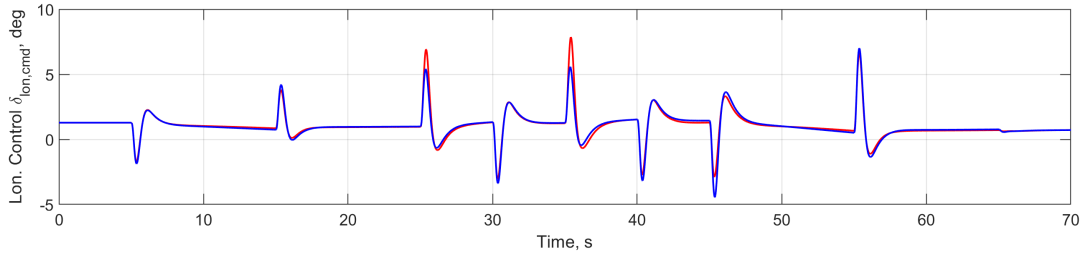

(e) Control signal $\delta_{lon,cmd}$ (desired longitudinal)

Figure 5.20: Simulation part 1 (green: reference, red: non-linear, blue: linear)

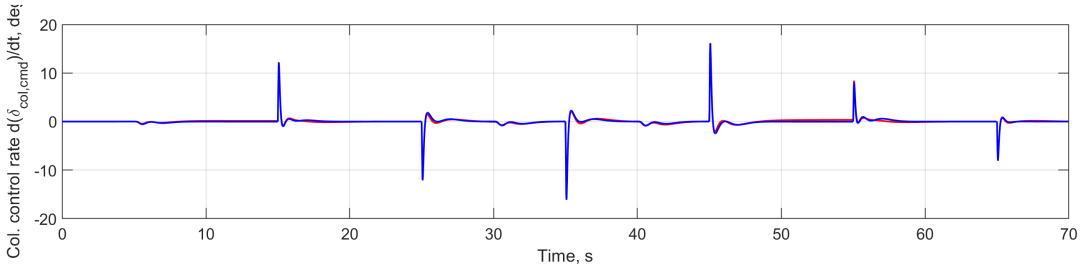

(a) Control rate signal $\dot{\delta}_{lon,cmd}$ (longitudinal rate)

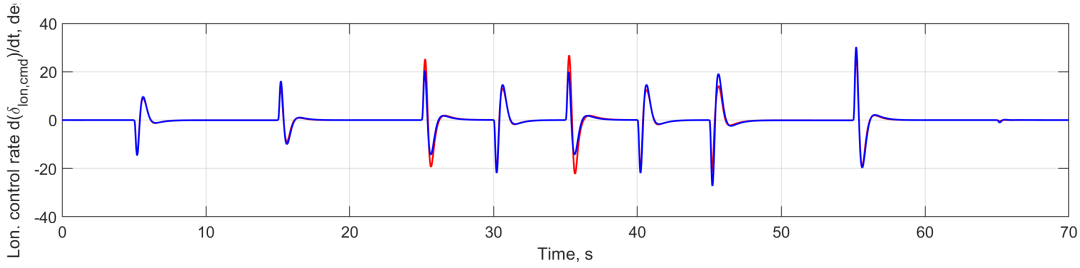

(b) Control rate signal $\dot{\delta}_{lon,cmd}$ (longitudinal rate)

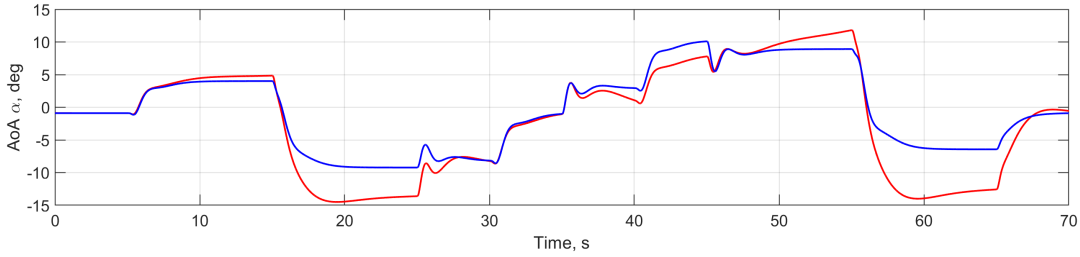

(c) Model output signal α (angle of attack of the helicopter airframe)

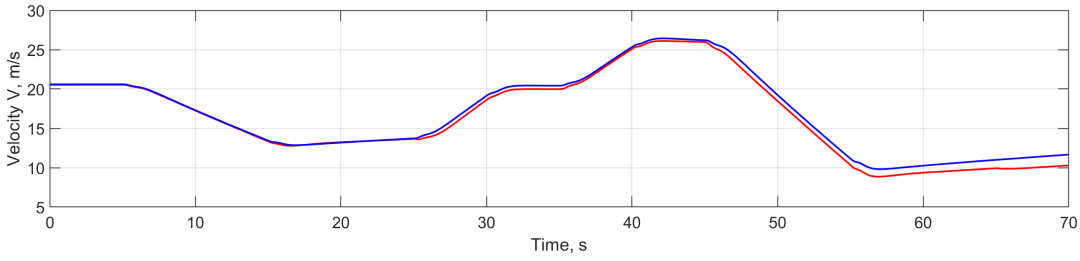

(d) Model output signal V (velocity)

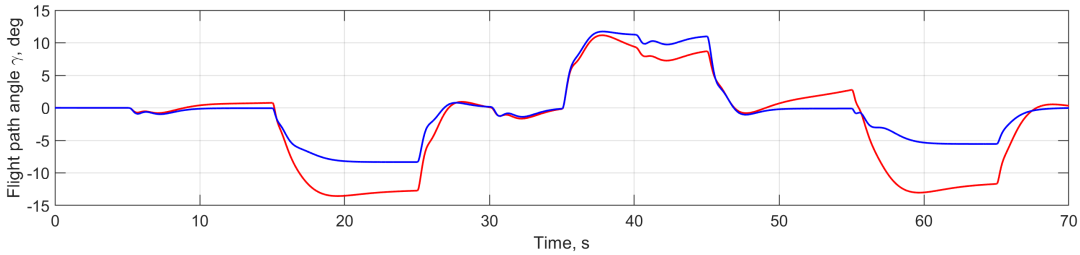

(e) Model output signal γ (flight path angle)

Figure 5.21: Simulation part 2 (green: reference, red: non-linear, blue: linear)

6

Uncertainty Analysis

To investigate the robustness of the controller and to verify the stability shown in the simulation of non-linear implementation in Figure 5.20 and Figure 5.21 across a subset of the flight envelop around the design point and to show robustness against uncertainty. The theoretical background behind this is explained in section 6.1. Then, using these tools an analysis can be performed to assess the stability and robustness across flight envelop in section 6.2, section 6.3 and section 6.4 as using structured singular value analysis.

6.1. Stability and Robustness analysis tools

In this section, stability analysis of the controller is explained used in section 6.2 and robustness of the controller analysis is explained used in section 6.3 and section 6.4. For the stability analysis focusing on examining aspects such as gain and phase uncertainties by introducing a complex perturbation at the model inputs and outputs which can be done loop-at-a-time or simultaneously used to assess multi-variable stability margins. This makes the stability margins reasonable method of measuring the robustness against neglected or inaccurately modelled dynamics used in the design process as shown in chapter 5. Additionally, using a multi-model approach, the closed-loop stability can be check across various flight conditions by linearising the non-linear model at different operating points for a controller. In which, the key states affecting the dynamics during nominal helicopter operation are air density from change in altitude ρ, speed V and angle of attack (AoA) α. Their are also other design parameters linked to the configuration of the helicopter which are the mass m, moment of inertia I_{yy}, center of gravity position Z_{CG}, X_{CG} with the variation in the aerodynamic forces/moments and their derivatives can be assessed using structured singular value (SSV) analysis.

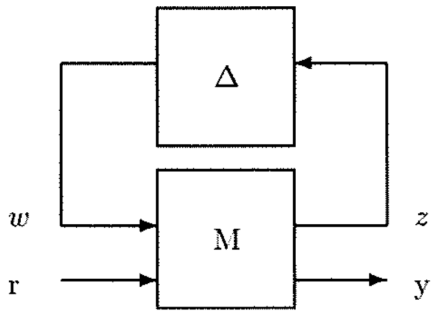

Figure 6.1: $M(s) - \Delta(s)$ configuration for robust stability

The robustness of the controller analysis is explained as follows, used in section 6.3 and section 6.4. The method to test the robustness of a system against uncertainties using real parameters and their combinations can be added to the closed-loop in an $M(s) - \Delta(s)$ configuration.

In these models, uncertainties within the system are typically separated from the system models, with $\Delta(s)$ representing the variation from nominal values (e.g., $X_u = X_{u_{nom}} + \Delta_{X_u}$). This is commonly used in modern control theory for robust control design to assess the stability of the system when real parameters change. This creates an uncertain model to capture the different types of dynamics that uncertainties impact in a dynamic system. This structure, shown in Figure 6.1, comprises two components: the nominal system, $M(s)$, which is the combination of the plant and the controller, and the uncertainty $\Delta(s)$. In this configuration, SSV can be derived and be applied to provide an estimate for the stability of the system against uncertainty. Robust stability is achieved in a system with no uncertainties if the matrix $I - M\Delta(s)$ is not singular, given that $\det(I - M\Delta(s)) \neq 0 \forall \omega$, in terms of normalized uncertainty $\overline{\sigma}(\Delta(s)) \leq 1$ with $\overline{\sigma}$ indicating the largest singular value. However, this condition is logical (yes or no) as a robustness indicator because the determinant $\det(I - M\Delta(s))$ is not a quantitative indicator of the singularity of $I - M\Delta(s)$. To obtain a scalar estimate of the uncertainty the system can tolerate without being destabilized, it is required to calculate the smallest $k_m = \frac{1}{\mu}$ with which the uncertainty can be scaled to make the matrix $I - k_m M\Delta(s)$ singular. Therefor, for a given complex matrix M, a set of complex matrices denoted by $\Delta = \text{diag}(\Delta_i)$, with $\overline{\sigma}(\Delta(s)) \leq 1$ in the block structure, the real non-negative function $\mu(M)$ (SSV) is defined as stated in (Skogestad & Postlethwaite, 2005):

$$\mu(M) \triangleq \frac{1}{\min k_m | \det(I - k_m M\Delta(s)) = 0 \text{ for structured } \Delta, \sigma(\Delta(s)) \leq 1} \tag{6.1}$$

This calculation is solved by *robstab()* in which the the lower/upper bounds can estimated. Additionally, the estimate can be improved by complexifying the uncertainty using *complexify()* which adds a relatively small imaginary component without changing the magnitude (e.g., $\Delta_{X_u} = (100\%)\Delta_{X_u,real} + (5\%)\Delta_{X_u,imag}$) as described by (Packard & Pandey, 1993) to eliminate discontinuities in robust stability margin as a function of frequency for the computation of μ. The SSV can be smoothed to eliminate such jumps by adding a small amount of uncertain imaginary component in the dynamics to every uncertain real parameter. This combination covers the original uncertainty and adds a 5% conservative estimate to the complex uncertainty to obtain a more reliable estimate of μ.

6.2. Stability analyses

To investigate the stability of the closed-loop system around the design point against variations in flight which includes steady-state horizontal flight shown in Figure 6.2a and steady-state climbing/descending flight shown in Figure 6.2b. In Figure 6.2 shows that loop-at-a-time stability margins degrade slightly when the flight state is close to hover. In addition, to the degradation seen at higher and lower AoA while increasing with velocity due to the phugoid mode becoming more unstable at the lower velocities, vise versa. Subsequently, this indicates robustness against trim point uncertainty as during the two flight conditions are assessed to be stable under variations in both model and trim point uncertainty across a subset of the flight envelope specified in Appendix B for the horizontal flight.

This is supported by the simultaneous disk margins at the design point, which are also an indicator of robustness against input and/or output uncertainty shown in Figure 6.3. These disk margins do not adhere to the $6\,\text{dB}$, $45\,^\circ$ MIL guidelines (Anon, 2008). Although, it does show controller as a whole also displays very robust stability margins especially at the inputs with margins at the output being the limiting factor with the worst gain of $3.2\,\text{dB}$ and phase of $21\,^\circ$ for simultaneous all input and outputs.

6.3. Uncertainly in the stability and control derivatives

To investigate robustness against uncertainties in the dynamics, an uncertain model of the helicopter was derived from the design model by defining a $\pm 20\,\%$ uncertainty for all stability and control derivatives in matrices Equation 4.11. In Figure 6.4 shows a breakdown of the uncertain derivatives with the most significant contributions to the robust stability of the controller at the design point. The upper bound peak value is equal to 0.9988 at a critical frequency of $0\,\text{rad/s}$ at the design velocity when all of the uncertainty is applied, indicating that robust stability for the uncertainty is guaranteed. This corresponds to the controller being capable of handling $100/(0.9988) = 100.12\,\%$ of the uncertainty. Therefore, for values less than 1, the controller is robustly stable against the specified parametric uncertainty. The uncertainty in the longitudinal X and moment M derivatives significantly affect the phugoid dynamics, which are the major contributing factors towards the robustness limitations at $0\,\text{rad/s}$.

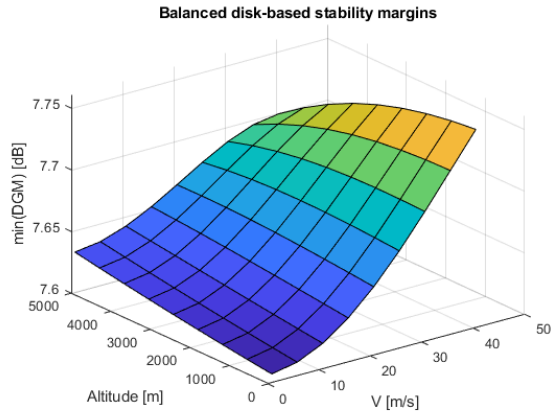

(a) The minimum balanced disk-based gain margins (DGM) at the inputs and outputs loop-at-a-time for steady-state horizontal flight in a altitude-velocity grid

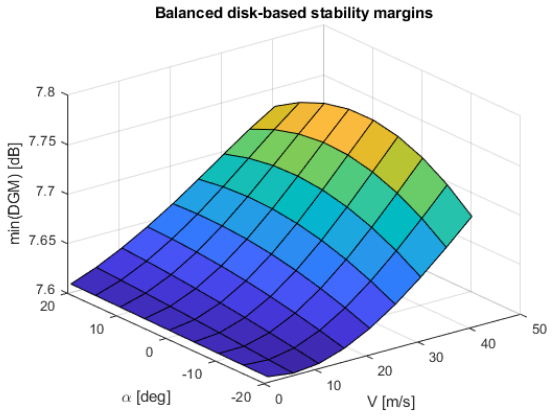

(b) The minimum balanced disk-based gain margins (DGM) at the inputs and outputs loop-at-a-time for steady-state climbing/descending flight in a AoA-velocity grid

Figure 6.2: The minimum balanced disk-based gain margins (DGM) at the inputs and outputs loop-at-a-time for different flight conditions around the design point $h = 0\,\mathrm{m}, V = 20\,\mathrm{m/s}$

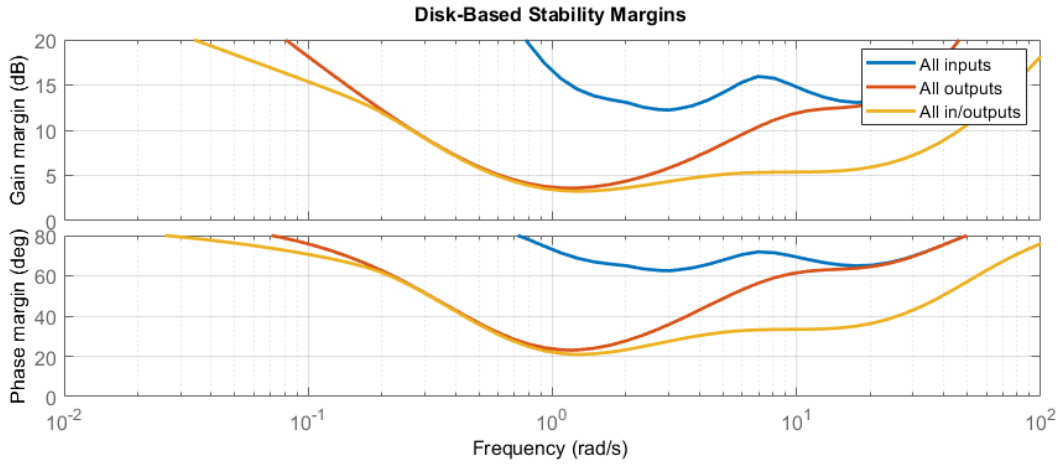

Figure 6.3: The disk-based margins for simultaneous inputs/outputs at the design point $h = 0\,\mathrm{m}, V = 20\,\mathrm{m/s}$

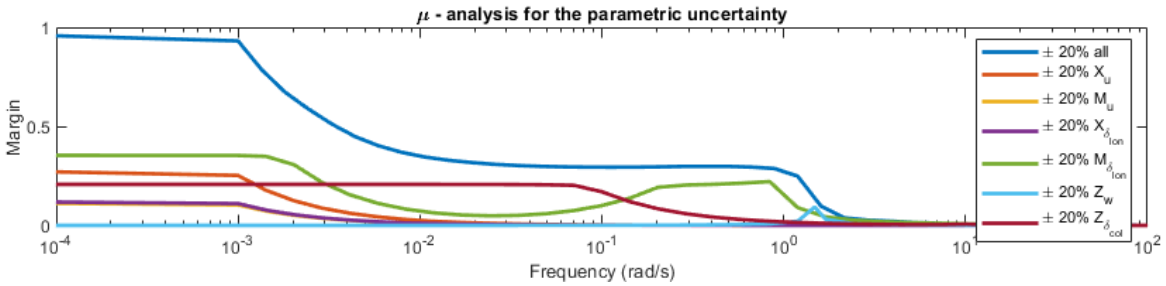

Figure 6.4: SSV analysis as a function of frequency for at the design point $h = 0\,\mathrm{m}, V = 20\,\mathrm{m/s}$ (stability and control derivatives)

In contrast, the normal Z derivatives affecting the vertical velocity subsidence, which is already stable in the open loop and has a less significant cumulative contribution to robust stability. In Figure 6.6 shows the full solution in Figure 5.7 to 5.9 using the entire flight envelope for the corresponding operating points in the linearised models found in Appendix B. A similar pattern can be seen in Figure 6.6, in which uncertainty in the stability and control derivatives linked to the phugoid mode limits the robust stability at low velocities.

In addition, for higher velocities the X_u and $M_{\delta_{lon}}$ with the normal stability and control derivatives are the significant limiting contributions to robust stability.

In the figure, it can be seen that the methodology used for the flight control design has limitations in terms of the robustness against uncertainty in the stability and control derivatives close to hovering flight. This is linked to the limited control authority seen in the model which causes high gains in feedback the controller in Figure 5.7 for the pitch control.

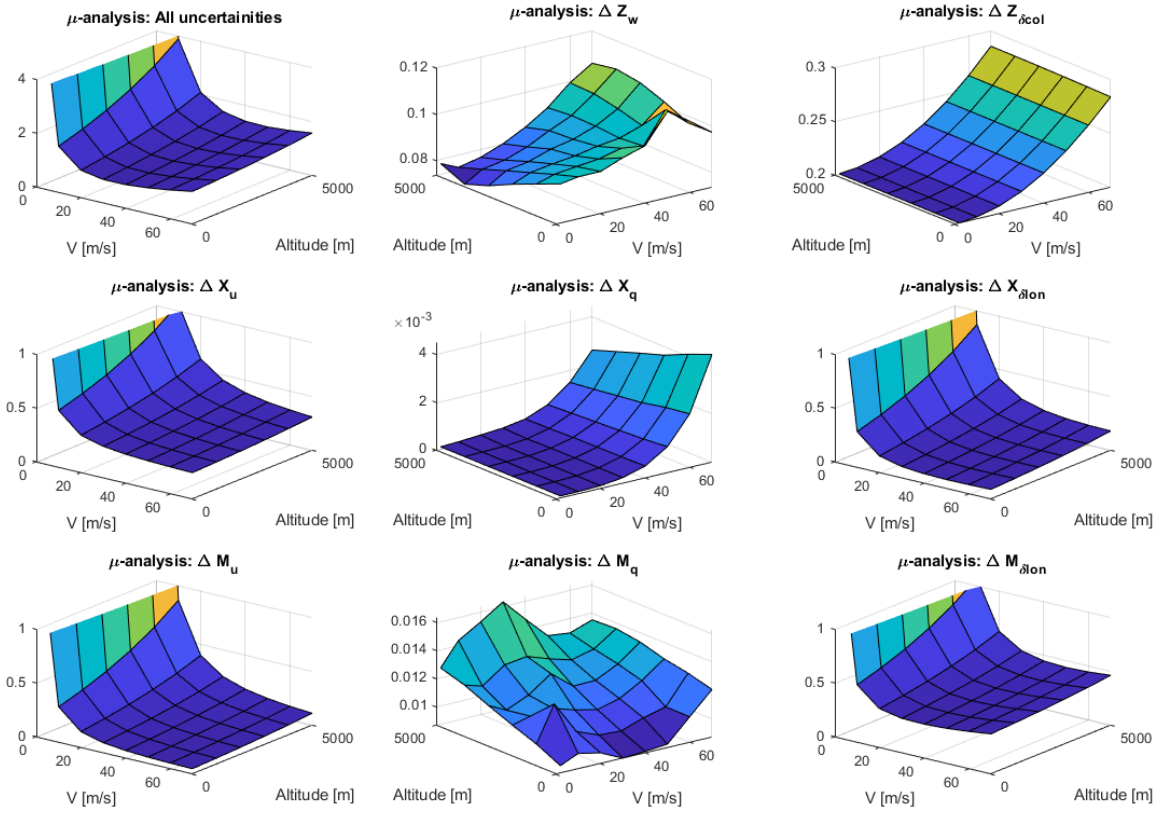

Figure 6.5: Peak SSV analysis for the design solution across the flight envelope (stability and control derivatives)

6.4. Uncertainty in the flight configuration and aerodynamics forces

To investigate robustness against uncertainties in the flight configuration and aerodynamics forces, parametric uncertainties can be added directly into the nonlinear model using *ureal()* and linearized using *ulinearize()* to obtain an uncertain linear model for variations in mass and moment of inertia ($m \pm 10\,\%$, $I_{yy} \pm 10\,\%$) combined with variations in the center of gravity position both normally and longitudinally ($Z_{CG}, X_{CG} \pm 0.05\,\mathrm{m}$) from the nominal model. Additionally, multiplicative uncertainties in the aerodynamic forces and moments were added ($F_x \pm 20\,\%$, $F_z \pm 20\,\%$, $M_y \pm 20\,\%$). This introduces uncertainties in the force/moment derivatives and operating points, which allows for the robustness of the resulting controller to be assessed at various flight configurations using SSV analysis. The μ analysis, shown in Figure 6.6, demonstrating that the system is robustly stable against the parametric changes in the configuration and the uncertainty in the aerodynamic forces and moments, with a tolerance up to $100/(0.238) = 420\,\%$.

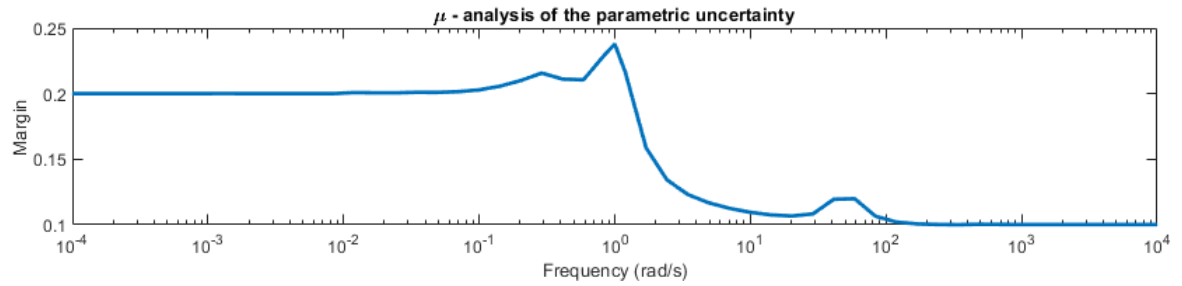

Figure 6.6: Structured singular value analysis for at the design point $h = 0\,\mathrm{m}, V = 20\,\mathrm{m/s}$ (configuration and forces/moments)

To showcase the robustness of the controller, nonlinear Monte Carlo simulations were performed, as shown in Figure 6.7, by varying uncertain parameters used for Figure 6.6, which corresponds to the μ analysis. The following simulations use a series of step-wise reference signals where the altitude is $h = 0\,\mathrm{m}$ to assess the non-linear performance. The reference signal profiles allow for flight coverage around the design point. In the simulation, uncertainties in the force/moment derivatives and operating points were introduced in the nonlinear 3-DoF longitudinal helicopter model. The commanded maneuvers were designed to stay within the limitations of actuators for the nominal model described in Table 4.1 using the same stepping scheme and command filter as shown in Figure 5.20.

It can be seen that even for large vertical velocity changes and pitch angles, the control effort is small, and the response accurately follows the reference signal. This is evident in the first 25 seconds when the step functions were individually applied. Both steps converge to the reference signal, but as seen, the parametric uncertainty introduces notable variations in the vertical velocity response in terms of overshoot, with consistent rise times. Although the ACAH response remains consistent throughout the simulation, including the uncertainty. Furthermore, although uncertainties influence the response, the controller is still able to accurately track the reference signal with a noticeable degradation in performance as uncertainty increases. This degradation is primarily seen in the vertical velocity control during simultaneous reference commands with the pitch channel for $5\,^\circ$ steps. The steady-state error is approximately around the order of $0.1\,\mathrm{m/s}$, which is a relatively small steady-state error. However, due to the non-linear coupling dynamics, greater levels of variation are introduced in the final 30 seconds of the simulation for $15\,^\circ$ steps reference inputs.

To conclude, the simulation verified in the time domain the results of the μ analysis performed, given that changes in the stability of the model are assumed to be negligible as a function of velocity.

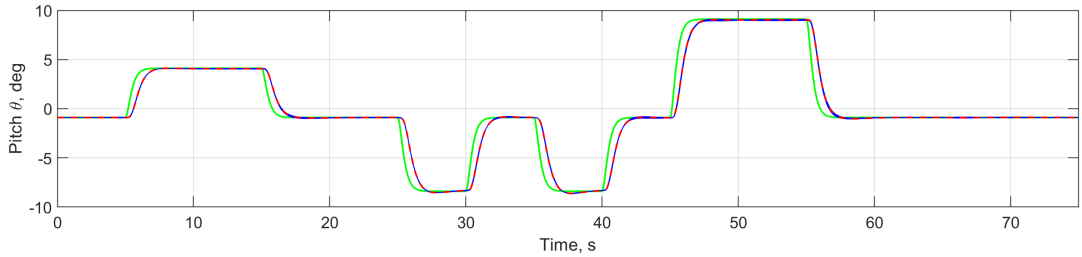

(a) Tracked output signal θ (pitch attitude)

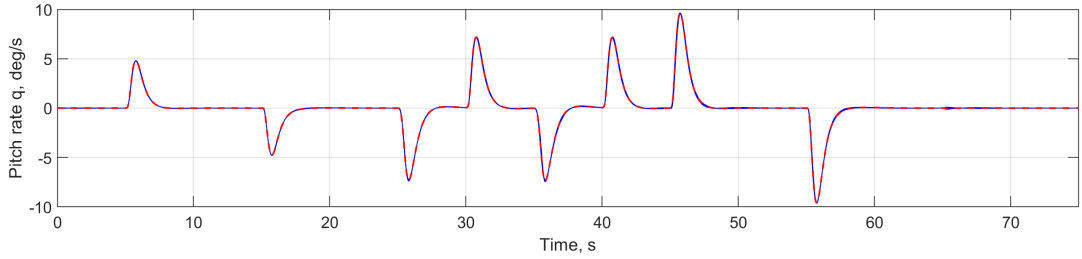

(b) State output signal q (pitch rate)

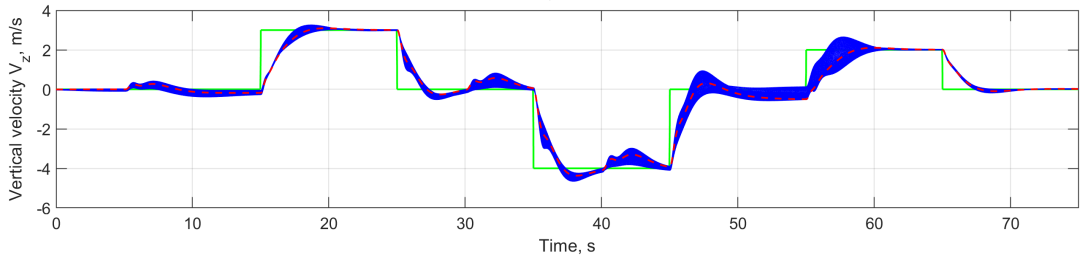

(c) Tracked output signal V_z (vertical velocity)

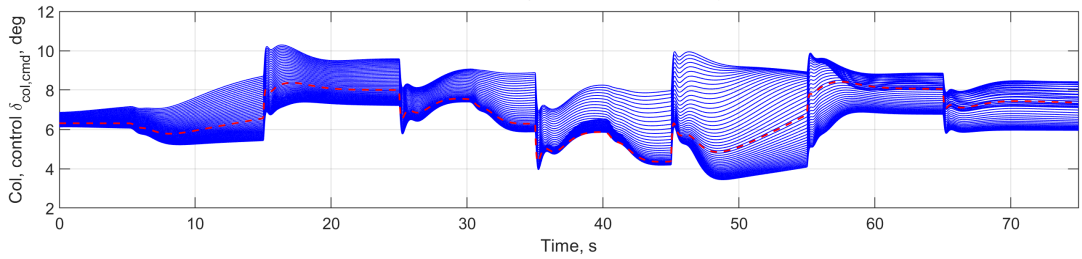

(d) Control signal $\delta_{col,cmd}$ (desired collective)

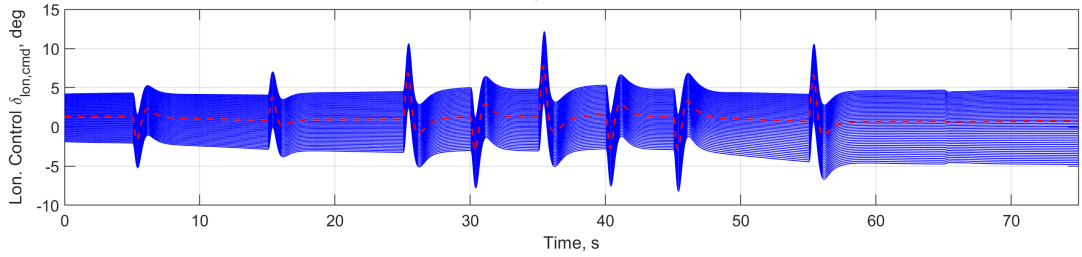

(e) Control signal $\delta_{lon,cmd}$ (desired longitudinal)

Figure 6.7: Nonlinear simulation (green: reference, red: nominal parameter run, blue: 50 uncertain parameter runs)

7

Conclusion & Recommendations

This final chapter concludes the research. The problem statement is examined and the extent to which this question could be addressed is summarized. Thereafter, topics that were touched upon during this research and could be of interest in further research are discussed.

The objective of this thesis was to obtain more insights into the performance and robustness of helicopters in which a multi-objective methods is developed to obtain both, through a structured control synthesis methods in the H_∞ framework.

Research Objective

To investigate the effects of uncertainties in the rotor dynamics onto longitudinal helicopter dynamics and control by explicitly modelling the model uncertainty of the rotor dynamics on the helicopter model and analysing the robustness of the synthesised controller.

A robust 2-DoF autopilot is designed for an MBB Bo-105 helicopter, which was selected for due to it open-loop instability, robustness limitations, its imposed requirements on the handling characteristics making it a challenging control problem. The model non-linear dynamics are analysed and verified, after which trimming and point-linearization at steady-state horizontal flight applied for the flight envelop. This paper introduced a transparent flight control architecture combining robust control theory as a method for tuning controllers to meet HQ requirements. The design methodology adopts a multi-objective approach to balance trade-offs between robustness and performance in the controller design. The proposed methodology uses simple structured controllers that can be gain-scheduled and/or applied in multi-model methods to obtain robust controllers. Various soft and hard constraints were systematically applied, resulting in a 2-DoF longitudinal controller with desired properties for reference tracking, disturbance rejection at the plant inputs and outputs, sensor noise attenuation, control signal attenuation, and disk-based stability margins.

In general, there are several ways to model uncertainty but given that the rotor dynamics affect the stability and control forces/moments of the helicopter. The easiest method is to apply the uncertainty directly in the the linear model thought stability and control derivatives of the state-space model. Using μ analysis, resulted that the most influential is the phugoid mode which means for robust control an accurate estimation of the longitudinal forces and moments are required. In addition, the uncertainty can also be applied a multiplicative way affecting the resulting control forces and other parameters of interest which is a more forgiving way to model uncertainty looking at the results (answering RQ-1). Furthermore, the uncertainties in the dynamics affect controller design to a point which comes down to limited control authority and resulting trade-off against performance seen close to hover for this low-fidelity longitudinal model. Although, the feed-forward controller handling quality are met while maintaining robustness through the feedback controller. It can also be seen in the time domain that the a handling quality requirements are impacted by the uncertainties and do degrade slightly but not by sufficient notable margins, despite this the actuator saturation is a key limiting component of the problem for which is still not addressed which can be at topic of further research (answering RQ-2).

Research Questions

- **RQ-1:** How can the uncertainties within the rotor dynamics be modelled?
  - **RQ-1.1:** Which parameters within the rotor dynamics are uncertain?
    Their are uncertainties in the flight configuration as mass m, moment of inertia I_{yy} and center of gravity position Z_{CG}, X_{CG} change during flight. In addition, to flight envelope during nominal helicopter operation in which the air density from change in altitude ρ, speed V and angle of attack (AoA) α. Their are also inaccuracies linked to the variation in the aerodynamic forces/moments and their derivatives modelled like for in the unstable phugoid mode.
  - **RQ-1.2:** What is the uncertainty bound of these parameters?
    The mass $m \pm 10\,\%$, moment of inertia $I_{yy} \pm 10\,\%$ and center of gravity position $Z_{CG}, X_{CG} \pm 0.05\,\mathrm{m}$ are approximated based on the MBB Bo-105 specification in terms of in-flight variation. The variation in the aerodynamics force/moments with there derivatives $F_x \pm 20\,\%$, $F_z \pm 20\,\%$, $M_y \pm 20\,\%$ are approximated based data available from the literature study.
  - **RQ-1.3:** How does the uncertainty in the rotor dynamics affect the helicopter dynamics?
    The effect on the uncertainty on the rotor dynamics is investigated using 3 different. The SSV analysis, multi-variable disk based stability margins and disk based stability margins around the trim point of the model. In which, the key conclusion drawn that uncertainty of the unstable phugoid has the most significant impact on the stability of the autopilot which can be caused by a change in flight conditions and/or uncertainty in the model dynamics.
- **RQ-2:** Does the uncertain rotor dynamics affect the robustness and performance of the synthesised robust controller?
  - **RQ-2.1:** Which elements of the controller are affected by the uncertain rotor dynamics?
    The feedback control design impacts the uncertainty in the stability of the which can be analysis using SSV analysis. Additionally, the feed-forward design impacts the uncertainty in the meeting HQ requirements as shown by the variation in the non-linear simulations.
  - **RQ-2.2:** How do the uncertain rotor dynamics affect the handling qualities of the helicopter?
    The feed-forward controller is sufficient to meet handling quality in the nominal case while maintaining robustness through the feedback controller. It can also be seen in the time domain that the handling quality requirements are impacted by the uncertainties and do degrade caused by changes in the sensitivity of the system especially noticeable for the vertical velocity responses. Although, margins can be designed taking this into account.
  - **RQ-2.3:** How do the uncertain rotor dynamics affect the robustness of the controller?
    The uncertainties in the dynamics affect controller design to a point which comes down to limited control authority and resulting trade-off against performance seen close to hover for pitch control in this low-fidelity longitudinal model. Although, their are inaccuracies in the low-fidelity longitudinal model which can be taken into account to allow for smaller uncertainties and/or higher fidelity modeling at the hovering flight condition.

For the main research objective it can be concluded that the given structured control design procedure combining loop-shaping methodologies with structured robustification is very powerful as it can be automated while yielding desirable robustness and performance results despite its complexities. The described control synthesis is effective for its application against various types of uncertainty, completing main research objective. Although, the design methodology worked for the design point their were issues raised when the method was applied through out the flight envelope.

As controller have non-smooth inconsistencies in the gain surfaces due variation in the model dynamics between hover and high speed horizontal flight. In addition, to the risk of actuator saturation which can alter both stability and handling qualities of the rotorcraft. Finally, the non-linear implementation shows signs of deterioration in the from of steady-state error for simultaneous reference command inputs in an off-equilibrium state which the solution can be through gain scheduling to take into account input trim variations.

This methodology is limited by the designer's experience in handling the trade-offs between robustness and performance to meet HQ requirements and ensure the constraint parameters are properly tuned. Despite this limitation, the methodology simplifies the design process. Future work could focus on better understanding the connection between helicopter design limitations and control law design in terms of robustness and performance in meeting HQ requirements. In addition, to looking at anti-windup models to investigate the performance and robustness during actuator saturation. Further looking at higher degree of freedom models to verify it effectively while introducing more handling requirements and modeling more complex flow/rotor bending phenomena which the helicopter is subject to.

References

Anon. (2000). Ads-33e-prf-handling qualities requirements for military rotorcraft. https://www.roberthefley.com/docs/HQs/ADS-33E-PRF.pdf

Anon. (2008). Detailed specification: Flight systems—design, installation, and test of piloted aircraft, general specification for mil-dtl-9490e. http://everyspec.com/MIL-SPECS/MIL-SPECS-MIL-DTL/MIL-DTL-9490E_10979/

Antonioli, J.-C., Taghizad, A., Rakotomamonjy, T., & Ouladsine, M. (2014). Towards the development of a methodology for designing helicopter flight control laws by integrating handling qualities requirements from the first stage of tuning. *40th European Rotorcraft Forum (ERF 2014)*.

Apkarian, P., & Noll, D. (2006). Nonsmooth h∞ synthesis. *IEEE Transactions on Automatic Control*, *51*(1), 71–86. https://doi.org/10.1109/TAC.2005.860290

Apkarian, P. (2013). Tuning controllers against multiple design requirements. *2013 American Control Conference*, 3888–3893. https://doi.org/10.1109/ACC.2013.6580433

Apkarian, P., Gahinet, P., & Buhr, C. (2014). Multi-model, multi-objective tuning of fixed-structure controllers. *2014 European Control Conference (ECC)*, 856–861. https://doi.org/10.1109/ECC.2014.6862200

Apkarian, P., & Noll, D. (2007). Nonsmooth optimization for multiband frequency domain control design. *Automatica*, *43*(4), 724–731. https://doi.org/https://doi.org/10.1016/j.automatica.2006.08.031

Authié, P. (2023). A multi-model and multi-objective approach to the design of helicopter flight control laws. *CEAS Aeronautical Journal*, 1–15.

Ayush, Prabha, H., & Kumar, R. (2020). Robust h∞ control approach for trajectory tracking of twin rotor mimo system. *2020 International Conference on Emerging Trends in Communication, Control and Computing (ICONC3)*, 1–4. https://doi.org/10.1109/ICONC345789.2020.9117352

Balas, G. J. (2003). Flight control law design: An industry perspective. *European Journal of Control*, *9*(2), 207–226. https://doi.org/https://doi.org/10.3166/ejc.9.207-226

Bates, D., & Postlethwaite, I. (2002). *Robust multivariable control of aerospace systems*. DUP Science.

Berger, T., Ivler, C., Berrios, M., Tischler, M., & Miller, D. (2016). Disturbance rejection handling qualities criteria for rotorcraft. *AHS 72nd Annual Forum West Palm Beach, FL, USA*.

Berger, T., Ivler, C., Berrios, M. G., Tischler, M. B., & Miller, D. (2016). Disturbance rejection handling qualities criteria for rotorcraft. *72nd Annual Forum of the American Helicopter Society, West Palm Beach, USA*.

Biannic, J.-M., Taghizad, A., Dujols, L., & Perozzi, G. (2017). A multi-objective h∞ design framework for helicopter pid control tuning with handling qualities requirements. *7th European Conference for Aeronautics and Space Science (EUCASS), Milan, Italy*, 89.

Bouwer, G., & Hilbert, K. B. (1986). A piloted simulation of a model following control system. *Journal of the American Helicopter Society*, *31*(2), 27–32.

Civita, M. L., Papageorgiou, G., Messner, W. C., & Kanade, T. (2003). Integrated modeling and robust control for full-envelope flight of robotic helicopters. *2003 IEEE International Conference on Robotics and Automation (Cat. No.03CH37422)*, *1*, 552–557 vol.1. https://doi.org/10.1109/ROBOT.2003.1241652

Cooper, G. E., & Harper, J., R. P. (1969, April). *The use of pilot rating in the evaluation of aircraft handling qualities* (NASA Technical Note). NASA. Ames Research Center Moffett Field, CA, United States. https://ntrs.nasa.gov/api/citations/19690013177/downloads/19690013177.pdf

Dai, J., Ying, J., & Tan, C. (2014). A novel particle swarm optimization based robust h-infinity control for rotorcrafts. *Engineering Computations*, *31*(4), 726–741. https://doi.org/10.1108/ec-07-2012-0148

Dehkordi, V. R., & Boulet, B. (2011). Robust controller order reduction. *International journal of control*, *84*(5), 985–997.

Du Val, R. W., & He, C. (2018). Validation of the flightlab virtual engineering toolset. *The Aeronautical Journal*, *122*(1250), 519–555. https://doi.org/10.1017/aer.2018.12

Gribble, J. J. (1993). Linear quadratic gaussian/loop transfer recovery design for a helicopter in low-speed flight. *Journal of Guidance, Control, and Dynamics*, *16*(4), 754–761.

Gu, D. W., Petkov, P. H., & Konstantinov, M. M. (2013). Robust control design with matlab®. https://doi.org/10.1007/978-1-4471-4682-7

Guarnizo, M. J. G., Trujillo, R. C. L., & Guacaneme, M. J. A. (2010). Modeling and control of a two dof helicopter using a robust control design based on dk iteration. https://doi.org/10.1109/iecon.2010.5675183

Heffley, R. (1979). Analysis of helicopter handling qualities data, volume one: Data compilation. *NASA Contractor Report*, *3145*.

Horn, J. F., Guo, W., & Ozdemir, G. T. (2012). Use of rotor state feedback to improve closed-loop stability and handling qualities. *Journal of the American Helicopter Society*, *57*(2), 1–10. https://doi.org/10.4050/JAHS.57.022001

Hu, J., & Gu, H. (2017). Survey on flight control technology for large-scale helicopter. *International Journal of Aerospace Engineering*, *2017*, 1–14. https://doi.org/10.1155/2017/5309403

Jeong, D.-Y., Kang, T., Dharmayanda Hardian, R., & Budiyono, A. (2012). H-infinity attitude control system design for a small-scale autonomous helicopter with nonlinear dynamics and uncertainties. *Journal of Aerospace Engineering*, *25*(4), 501–518. https://doi.org/10.1061/(ASCE)AS.1943-5525.0000176

Ji, S., & Wu, A. (2011). Study on dual-loop controller of helicopter based on the robust h-infinite loop shaping and mixed sensitivity. *2011 International Conference on Electrical and Control Engineering*, 1291–1294. https://doi.org/10.1109/ICECENG.2011.6057783

Khalid, M. U., Saleem, F., Shaikh, I. U. H., & Ali, A. (2017). Decentralized 2 degree of freedom loop shaping h∞ controller for twin rotor aerodynamic system. *2017 13th International Conference on Emerging Technologies (ICET)*, 1–6. https://doi.org/10.1109/ICET.2017.8281728

Kumar, M. V., Sampath, P., Suresh, S., Omkar, S., & Ganguli, R. (2008). Design of a stability augmentation system for a helicopter using lqr control and ads□33 handling qualities specifications. *Aircraft Engineering and Aerospace Technology*, *80*(2), 111–123.

Luo, C.-C., Liu, R.-F., Yang, C.-D., & Chang, Y.-H. (2003). Helicopter h∞ control design with robust flying quality. *Aerospace Science and Technology*, *7*(2), 159–169. https://doi.org/https://doi.org/10.1016/S1270-9638(02)00012-3

Ma, Y., Huang, B., Xiang, C., Wang, W., & Huang, N. (2015). Forward flight attitude control of unmanned small-scaled gyroplane based on μ-synthesis. *2015 International Conference on Unmanned Aircraft Systems (ICUAS)*, 1338–1345. https://doi.org/10.1109/ICUAS.2015.7152428

Marantos, P., Dritsas, L., & Kyriakopoulos, K. J. (2013). Robust h2/h∞ position tracking control of an unmanned helicopter for near-hover flights. *21st Mediterranean Conference on Control and Automation*, 161–166. https://doi.org/10.1109/MED.2013.6608715

Maurer, M. (2023). Helicopter sonar control: Cable control for helicopter dipping sonar operations in hover using incremental nonlinear dynamic inversion. http://resolver.tudelft.nl/uuid:5835a215-66bc-467b-9db5-6cb4457aedbd

P. Apkarian, D. N. (2017). The h∞ control problem is solved. *AerospaceLab*, (13). https://doi.org/10.12762/2017.al13-01

Packard, A., & Pandey, P. (1993). Continuity properties of the real/complex structured singular value. *IEEE Transactions on Automatic Control*, *38*(3), 415–428. https://doi.org/10.1109/9.210140

Padfield, G., & Safari, a. O. M. C. (2018). Helicopter flight dynamics, 3rd edition. https://login.proxy.bib.uottawa.ca/login?url=https://learning.oreilly.com/library/view/-/9781119401056/?ar&orpq&email=%5Eu

Padfield, G. D. (2008). Helicopter flight dynamics : The theory and application of flying qualities and simulation modelling. http://www.123library.org/book_details/?id=23094

Panza, S., & Lovera, M. (2014). Rotor state feedback in helicopter flight control: Robustness and fault tolerance. *2014 IEEE Conference on Control Applications (CCA)*, 451–456. https://doi.org/10.1109/CCA.2014.6981387

Pavel, M. D. (1996). *Six degrees of freedom linear model for helicopter trim and stability calculation*. Delft University of Technology, Faculty of Aerospace Engineering.

Phillips & H., W. (1949, January). *Appreciation and prediction of flying qualities* (NACA Technical Report). National Advisory Committee for Aeronautics. Langley Aeronautical Lab. Langley Field,

VA, United States. https://ntrs.nasa.gov/api/citations/19930091992/downloads/19930091992.pdf

Prempain, E., & Postlethwaite, I. (2005). Static h∞ loop shaping control of a fly-by-wire helicopter. *Automatica*, *41*(9), 1517–1528. https://doi.org/https://doi.org/10.1016/j.automatica.2005.04.001

SAE. (2008). Aerospace - flight control systems - design, installation and test of piloted military aircraft, general specification for sae-as94900. https://publishers.standardstech.com/content/military-dod-sae-as94900

Saetti, U., & Horn, J. (2017). Use of harmonic decomposition models in rotorcraft flight control design with alleviation of vibratory loads. *43rd European Rotorcraft Forum, ERF 2017*, 391–400.

Seiler, P., Packard, A., & Gahinet, P. (2020). An introduction to disk margins [lecture notes]. *IEEE Control Systems Magazine*, *40*(5), 78–95. https://doi.org/10.1109/MCS.2020.3005277

Silva, L. R. T. d., Campos, V. A. F. d., & Potts, A. S. (2020). Robust control for helicopters performance improvement: An lmi approach. *Journal of Aerospace Technology and Management*, *12*. https://doi.org/10.5028/jatm.v12.1179

Skogestad, S., & Postlethwaite, I. (2005). *Multivariable feedback control: Analysis and design*. john Wiley & sons.

Srinathkumar, S. (2015). Eigenstructure control: A rotorcraft handling qualities engineering tool. *Journal of the American Helicopter Society*, *60*. https://doi.org/10.4050/JAHS.60.022010

Srinathkumar, S. (2019). Rotorcraft precision hover control in atmospheric turbulence via eigenstructure assignment. *Journal of the American Helicopter Society*, *64*(1), 1–12. https://doi.org/10.4050/JAHS.64.012005

Takahashi, M. D. (1994). H-infinity helicopter flight control law design with and without rotor state feedback. *Journal of Guidance, Control, and Dynamics*, *17*(6), 1245–1251. https://doi.org/10.2514/3.21340

Theodoulis, S., & Proff, M. (2021). Robust flight control tuning for highly agile missiles. In *Aiaa scitech 2021 forum*. https://doi.org/10.2514/6.2021-1568

Tijani, I. B., Akmeliawati, R., Legowo, A., Budiyono, A., & Abdul Muthalif, A. G. (2011). Robust controller for autonomous helicopter hovering control. *Aircraft Engineering and Aerospace Technology*, *83*(6), 363–374. https://doi.org/10.1108/00022661111173243

Tischler, M. B., Berger, T., Ivler, C. M., Mansur, M. H., Cheung, K. K., & Soong, J. Y. (2017). *Practical methods for aircraft and rotorcraft flight control design: An optimization-based approach*. ARC.

Toscano, R. (2013). Structured controllers for uncertain systems : A stochastic optimization approach. https://doi.org/10.1007/978-1-4471-5188-3

Trentini, M., & Pieper, J. K. (2001). Mixed norm control of a helicopter. *Journal of Guidance, Control, and Dynamics*, *24*(3), 555–565. https://doi.org/10.2514/2.4746

Voskuijl, M., Padfield, G. D., Walker, D. J., Manimala, B. J., & Gubbels, A. W. (2010). Simulation of automatic helicopter deck landings using nature inspired flight control. *The Aeronautical Journal*, *114*(1151), 25–34. https://doi.org/10.1017/s000192400000350x

Walker, D. (2003). Multivariable control of the longitudinal and lateral dynamics of a fly-by-wire helicopter. *Control Engineering Practice*, *11*(7), 781. https://doi.org/10.1016/S0967-0661(02)00189-2

Walker, D. J., & Postlethwaite, I. (1996). Advanced helicopter flight control using two-degree-of-freedom h(infinity) optimization [doi: 10.2514/3.21640]. *Journal of Guidance, Control, and Dynamics*, *19*(2), 461–468. https://doi.org/10.2514/3.21640

A

Helicopter Data MBB Bo-105

Table A.1: Bo-105 Simulation parameters

Parameters	Value	Unit	Description
Ω	44.4	rad/s	Rotational speed
R	4.91	m	Rotor radius
N	4	$-$	Number of blades
c	0.27	m	Equivalent blade chord
C_{l_α}	6.11	rad^{-1}	Blade lift curve slope
I_b	231.7	$kg \cdot m^2$	Blade moment of inertia about flapping hinge
Z_{CG}	0.94468	m	Vertical position w.r.t helicopter CG
X_{CG}	0.0	m	Longitudinal position w.r.t helicopter CG
σ	0.07	$-$	Rotor solidity
F_0	1.3	m^2	Parasite drag area
m	2200	kg	Helicopter mass
I_{yy}	4973	$kg \cdot m^2$	Moment of inertia about pitch-axis

B

Full Linearisation Solution

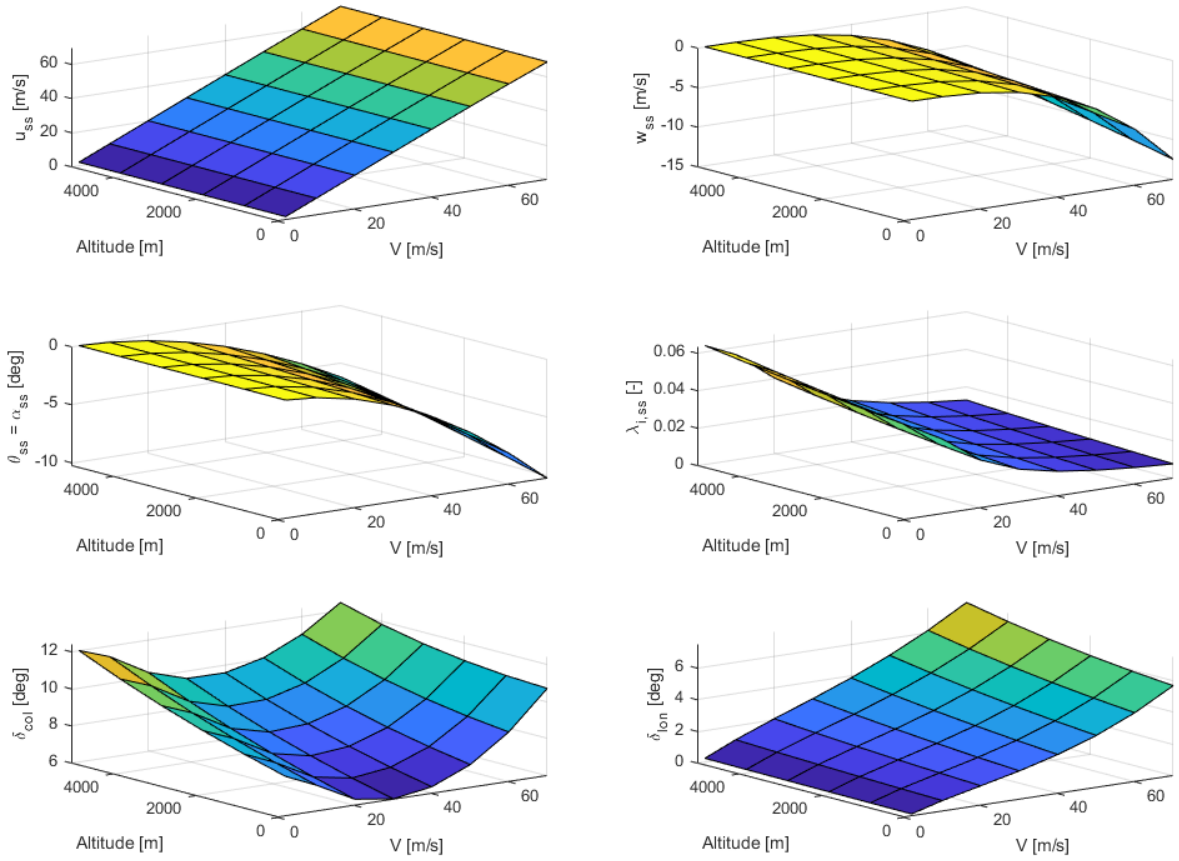

Figure B.1: Full linearisation solution of the steady-states ranging from $0 \leq V \leq 70\,\mathrm{m/s}$ and $0 \leq h \leq 5000\,\mathrm{m}$

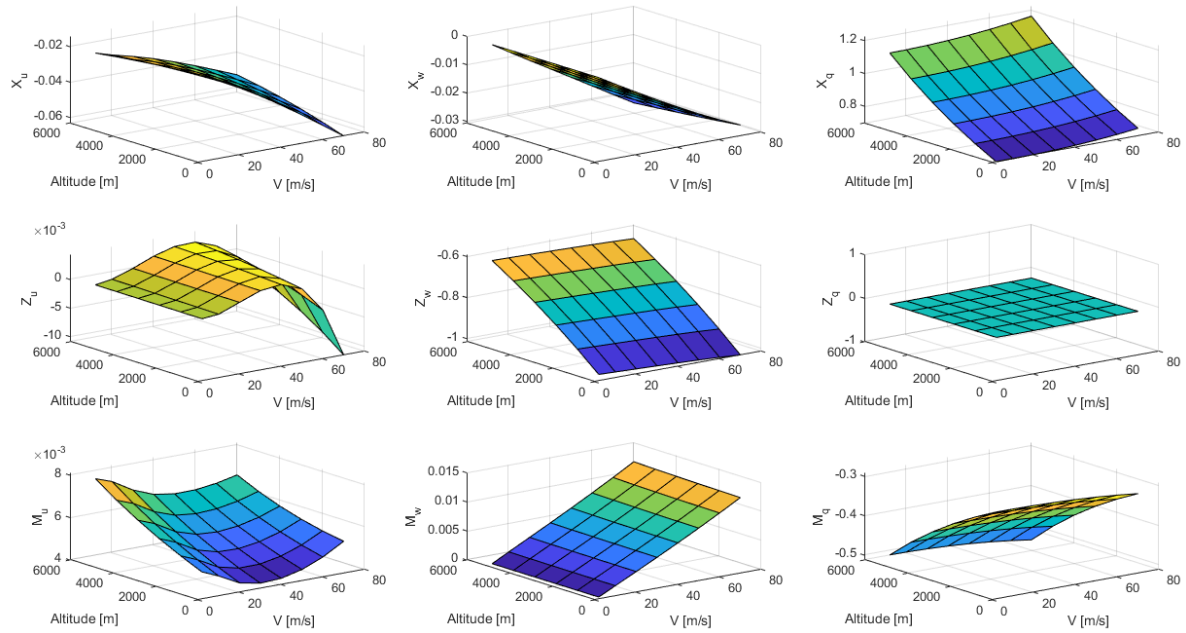

Figure B.2: Full linearisation solution of the normalised force/moment stability derivatives ranging from $0 \leq V \leq 70\,\mathrm{m/s}$ and $0 \leq h \leq 5000\,\mathrm{m}$

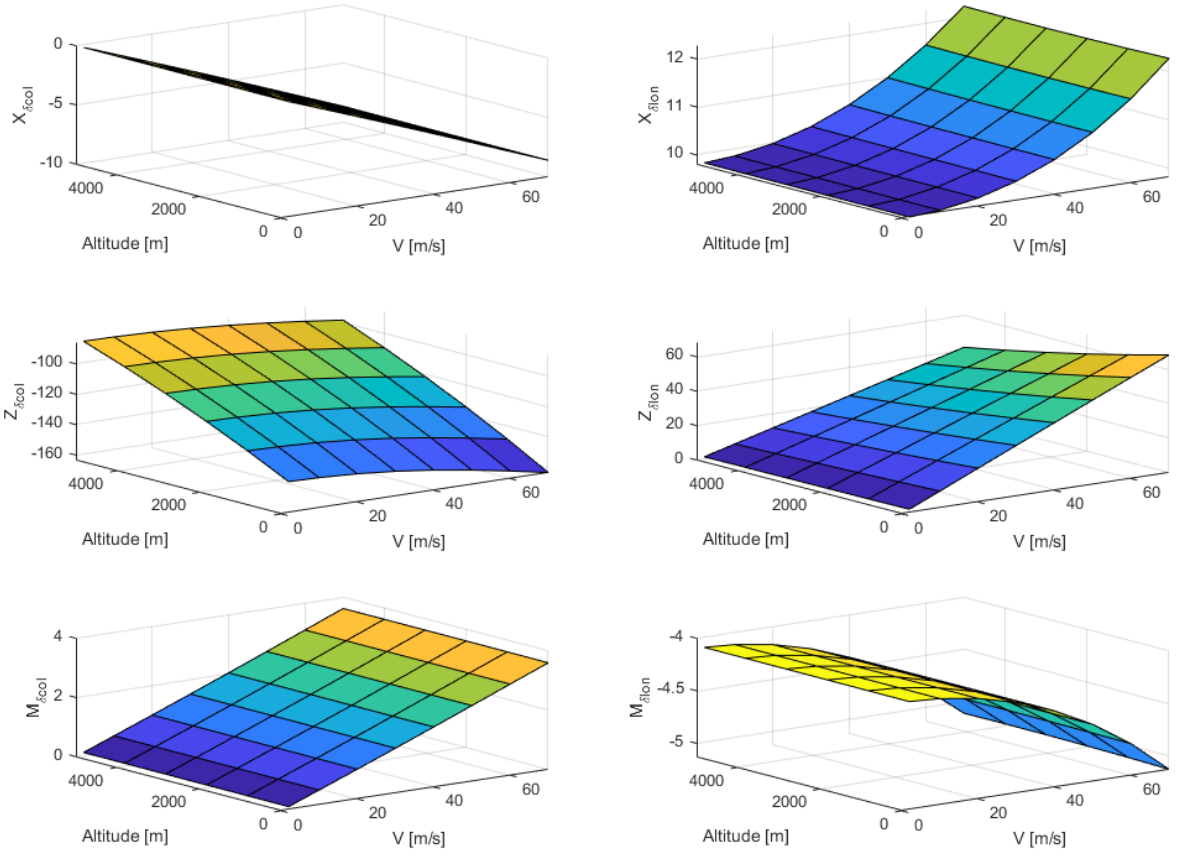

Figure B.3: Full linearisation solution of the normalised force/moment control derivatives ranging from $0 \leq V \leq 70\,\mathrm{m/s}$ and $0 \leq h \leq 5000\,\mathrm{m}$

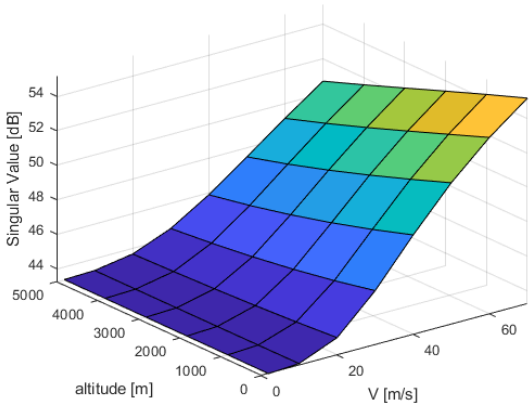

(a) Singular value decomposition of G for σ_{V_z} at $\omega = 0\,\mathrm{rad/s}$ across the flight envelope

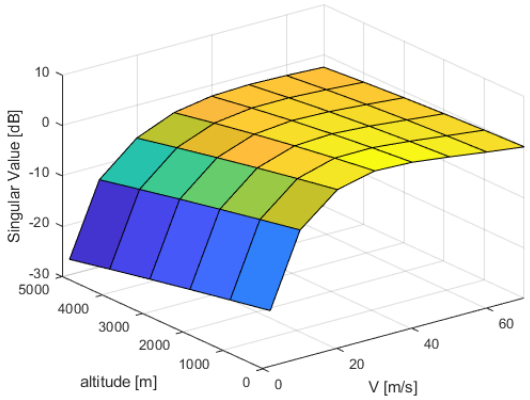

(b) Singular value decomposition of G for σ_θ at $\omega = 0\,\mathrm{rad/s}$ across the flight envelope

Figure B.4: Results for the SVD of the open-loop model G at $\omega = 0\,\mathrm{rad/s}$ across the flight envelope

C

Additional Results

In Figure C.1, the disk-based gain and phase margins as functions of frequency are shown for each of the helicopter inputs and outputs for the controller design across the flight envelope. The minimum classical gain margins are approximately $\pm 10\,\mathrm{dB}$ or greater for all inputs and outputs, which is well above the $6\,\mathrm{dB}$ objective. The minimum classical phase margins are $\pm 45\,\mathrm{deg}$ or greater that are on target, as the hard constraint only guarantees $\pm 7.6\,\mathrm{dB}$ and $\pm 45\,\mathrm{deg}$ of classical margins. As shown in the figure the exclusion regions are highlighted in which the broken open-loop transfer functions are avoided indicating robustness against perturbations for combinations of phase and gain margins, meeting the disk based stability requirements set.

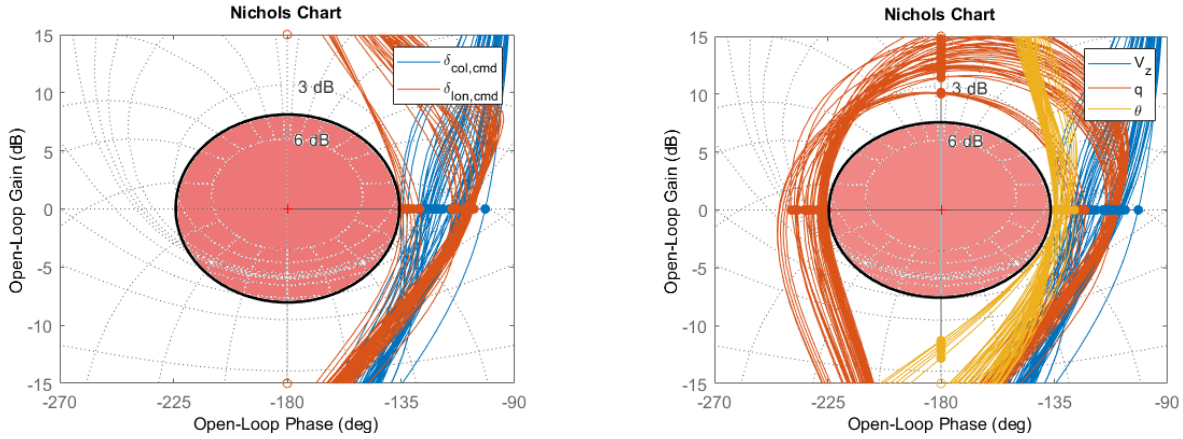

(a) Nichols stability region for inputs (loop-at-a-time)

(b) Nichols stability region for outputs (loop-at-a-time)

Figure C.1: Nichols plots with symmetric stability regions for the inputs/outputs (loop-at-a-time) of open loops for the flight envelope

In Figure C.2 shows the hard requirement on the pole-location for $\mathcal{D}$-stability for the controller design across the flight envelope, ensuring that all poles in the closed-loop system are stable left-hand plane with sufficient damping in accordance with the HQ criteria. The same can be said for the zero locations which indicate minimum-phase behaviors and no RHP cancellations.

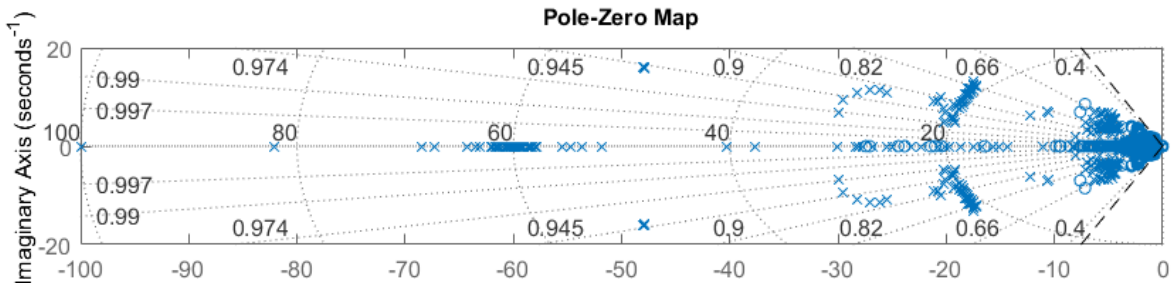

Figure C.2: Closed-loop pole-zero plot for the flight envelope

The five closed-loop transfer functions that are constrained to assess the frequency-domain characteristics of the closed-loop system are shown in Figure C.3 and C.4 for the 2-DoF controller. To attenuate I/O disturbances acting on both the plant input and output, S_o and S_oG signals are minimized at low frequencies. Furthermore, it can be seen that the KS_o, T_i and T_o signals have adequate roll-off at high frequencies to attenuate the high frequency measurement noise. The 10 soft constraints for the flight envelope are shown in Figure 5.17 which describes $\max(S_{i,j})$, taken from the closed-loop transfer functions shown in Figure C.3 and C.4. As shown, the $\max(S_{i,j})$ is minimised in the optimisation of the structured control solution, the trade-off between the soft constrains results in overshoot as the $\max(S_{i,j}) > 1$ for hover and higher velocities. This indicates that the weights or trade-off are more strict during in specific areas of the flight envelope. This variation in meeting with constrains has an impact on the robustness and performance of the control solution, although slight deterioration can be seen in Figure 5.18 still meeting level 1 handling requirements for most of the flight envelope and with relatively small variation in the μ analysis shown in Figure 6.6 for the higher velocities.

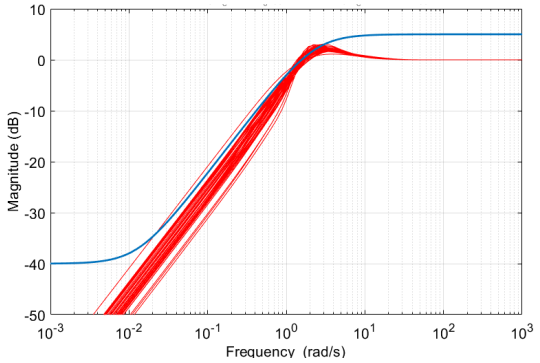

(a) Soft constraint on $T_{d_{V_z} \to V_z}$ (output disturbance sensitivity on V_z)

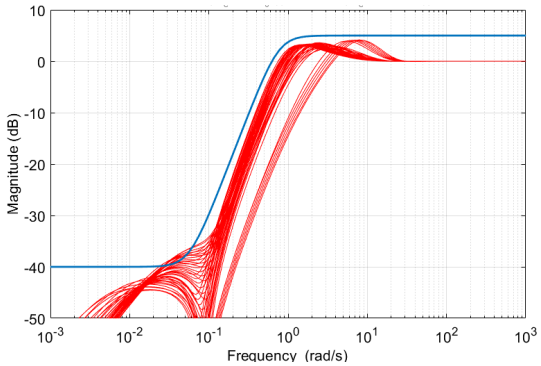

(b) Soft constraint on $T_{d_\theta \to \theta}$ (output disturbance sensitivity on θ)

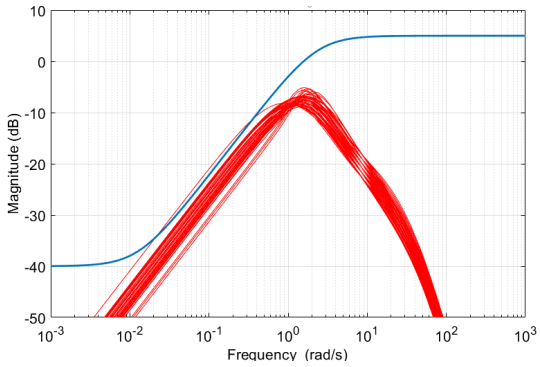

(c) Soft constraint on $T_{d_{\delta_{col,cmd}} \to V_z}$ (input disturbance sensitivity on V_z)

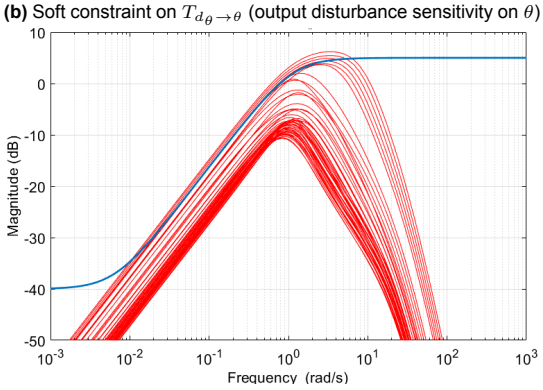

(d) Soft constraint on $T_{d_{\delta_{lon,cmd}} \to \theta}$ (input disturbance sensitivity on θ)

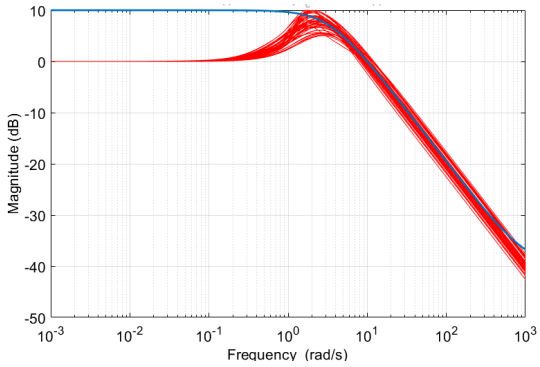

(e) Soft constraint on $T_{d_{V_z} \to \delta_{col,cmd}}$ (output disturbance sensitivity on $\delta_{col,cmd}$)

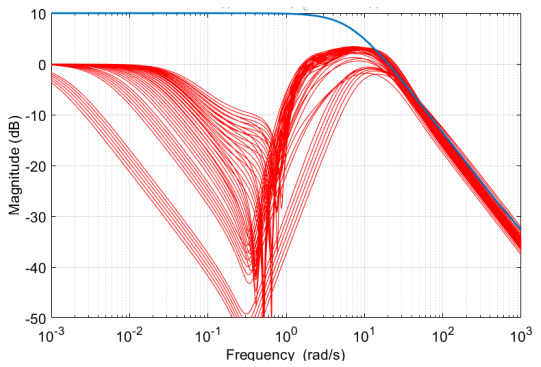

(f) Soft constraint on $T_{d_\theta \to \delta_{lon,cmd}}$ (output disturbance sensitivity on $\delta_{lon,cmd}$)

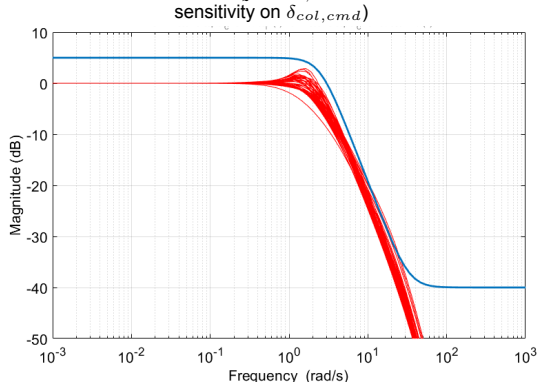

(g) Soft constraint on $T_{d_{\delta_{col,cmd}} \to \delta_{col,cmd}}$ (input disturbance sensitivity on $\delta_{col,cmd}$)

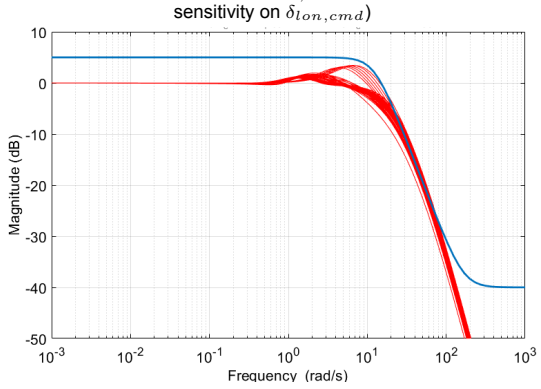

(h) Soft constraint on $T_{d_{\delta_{lon,cmd}} \to \delta_{lon,cmd}}$ (input disturbance sensitivity on $\delta_{lon,cmd}$)

Figure C.3: Overview of the designs of soft constraints related to disturbance rejection and signal attenuation frequency responses for the flight envelope (blue: inverted weights W^{-1}, red: designed solution)

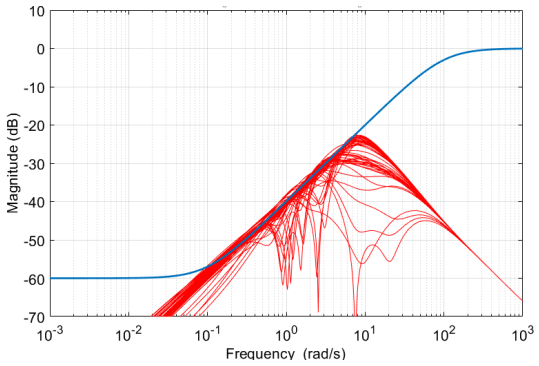

(a) Soft constraint on $T_{V_{z_{ref}} \to V_z} - T_{ref,V_z}$ (reference tracking)

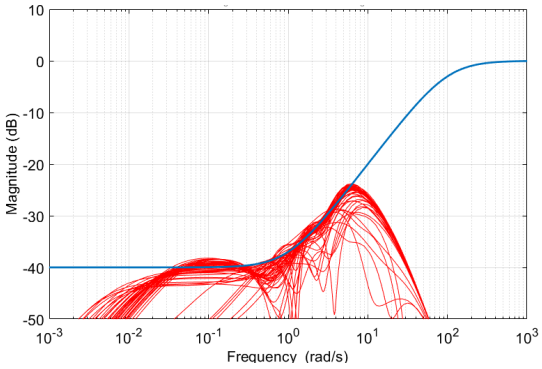

(b) Soft constraint on $T_{\theta_{ref} \to \theta} - T_{ref,\theta}$ (reference tracking)

Figure C.4: Overview of the designs of soft constraints related model following frequency responses for the flight envelope (blue: inverted weights W^{-1}, red: designed solution)